University of Alberta

Loading Rate Effects and Sulphate Resistance of Fibre Reinforced Cement-based Foams

by

Muhammad Mamun

A thesis submitted to the Faculty of Graduate Studies and Research
in partial fulfillment of the requirements for the degree of

Master of Science
in
Structural Engineering

Department of Civil and Environmental Engineering

Fall 2010
Edmonton, Alberta

Examining Committee

Dr. Vivek Bindiganavile, Department of Civil and Environmental Engineering

Dr. Qingxia Chad Liu, Department of Chemical and Materials Engineering

Dr. Mohamed Al-Hussein, Department of Civil and Environmental Engineering

Abstract

This study describes the strength, toughness and strain-rate sensitivity of fibre-reinforced cement-based foams subjected to variable loading rates. Drop-weight impact tests were conducted on beams with cast density between 475 - 1200 kg/m^3. The study shows that under quasi-static loading, the compressive strength, elastic modulus and the modulus of rupture of plain mixes scale with the square of the relative density. On the other hand, the flexural toughness factor scaled linearly with it. Fibres were seen to increase the flexural strength at all rates of loading, regardless of cast density. Further, cement based foams were seen to be strain-rate sensitive.

The resistance of cement-based foams to sulphate exposure was also investigated. Heavier cement-based foams are more susceptible to sulphate attack and perform poorly with an increase in the duration of exposure when compared to the lightest mix which showed improved responses up to 30 days of exposure due to self-healing.

Acknowledgment

This research work would not have existed without the support of my supervisor Dr. Vivek Bindiganavile. I would like to take the opportunity to thank him for his invaluable guidance throughout this study. I am very grateful to him for the financial assistance given to me, which helped me concentrate on this research program. I wish to thank Dr. Jim Li (Cematrix, Canada, Inc.) for the hands-on training to prepare test specimens and his continued assistance with documentation of cellular materials. I am thankful to Mr. Md Toihidul Islam, who has made available his support during the past two years.

I would like to express my gratitude to Mr. Rizaldy Mariano for his continuous support during my laboratory activities. I am indebted to Mr. Greg Miller and Mr. Sean Watt for helping me conduct the tests. I owe my deepest gratitude to Ms. Arlene Oatway for her assistance with Scanning Electron Microscopy. I am also thankful to Ms. Diane Caird for her painstaking effort to carry out X-ray Diffraction analysis. I also thank Ms. Joanna Klimowicz for the editorial review.

Last, but not the least, I am grateful to my parents and other family members for their moral and emotional support throughout this research program.

Table of Contents

List of Tables

List of Figures

List of Symbols

Chapter 2

a	Fly ash content
A	Air content
B_d	Base mix density
B_m	Mass of base mix
f_{cu}	Cube compressive strength
f_{cy}	Cylinder compressive strength
f_c, f'_c	Compressive strength
E_c	Modulus of elasticity
F_d	Foam density
F_m	Mass of foam
l	Edge length of cell
p	Porosity
$P_i(t)$	Initial load at time t
RD_f	Relative density of foam
RD_c	Relative density of cement
RD_a	Relative density of fly ash
RD_s	Relative density of sand
s	Sand content
t	Thickness of cell wall
T	Age of concrete
T_d	Target density
$\ddot{u}_0(t)$	Acceleration at time t
V_f	Volume of foam
w	water content
w_c	Water-cement ratio
W_d	Air-dry density

x	Cement content
$\dot{\epsilon}$	Strain rate
$\dot{\varepsilon}_s$	Quasi-static strain rate
ρ_{cast}	Cast density
ρ_{dry}	Oven-dry density
ρ^*	Density of cellular composite
ρ_s	Density of cell wall material
ρ_m	Target cast density
σ	Compressive strength of foamed concrete
σ_p	Compressive strength of cement paste
σ_f	Stress at final condition
σ_i	Stress at initial condition
$\dot{\sigma}$	Stress rate

Chapter 6

C	Calcite
E	Ettringite
f_r	Modulus of rupture
G	Gypsum
P	Portlandite
ρ, ρ_f	Density of foamed composite
ρ_s	Density of Cement paste (material in cell wall)

Chapter 1

INTRODUCTION

1.1 General

Cement-based foams are a lightweight mixture of cementitious material, fine aggregates, water and a stable pre-formed foam. In recent years their use has increased noticeably mainly due to their low density, favourable thermal properties, ease of manufacturing, demolition and relatively low production cost in comparison to other materials used for the same purpose. Cement-based foams are used in many sectors of infrastructure mostly as an engineered non-structural fill, precast panels, thermal and acoustic insulation and refractory materials.

The honeycomb like air void network formed internally allows the material to be used as an impact energy absorber. But not much is known about its mechanical characteristics including modulus of elasticity, Poisson's ratio and toughness is known. While the impact resistance of structural lightweight composites has been utilized in sandwich structures, there exists no report in the literature describing the strain-rate sensitivity of low-density fibre-reinforced cement-based foams at high rates of loading. This lack of information inhibits their development for shock absorbing cores and crash cushions.

Due to the active nature of hydrated cement paste, the properties of cement-based foams evolve with time and are sensitive to the chemical environment. In the

context of their use in geothermal and geostructural applications in Canada, the sulphate resistance of cement-based foams remains a concern. Performance of this material largely depends on how efficiently it can resist the severe chemical action from exposure to an extreme environment. A question also remains surrounding its long term performance as an insulator. Existing research data is not capable of answering any of these issues. Experimental investigation is needed to develop this material for higher efficiency.

Generally it is well established that the mechanical response of cellular material can be expressed as a function of its relative density. Empirical models are available for polymeric cellular solids to predict the mechanical response. However, a lack of research data prevents the development of such response prediction models to study the behaviour under different loading configuration. Innovative use of cement-based foams demands information regarding material behaviour under extreme conditions. Experimental investigations were carried out in this study in an attempt to enrich the existing knowledge base regarding cement-based foamed material.

1.2 Objectives and Scope

The cellular nature allows cement-based foams to be used in a variety of applications. Existing studies are not capable of describing the behaviour of cement-based foams when subjected to varying rate of loading. Further, the conventional method of assessing the performance of cement-based foams does

not reflect the distress suffered due to sulphate exposure. To investigate the use of this material in shock absorbing and sulphate resistant system, the objectives of this project were set as follows:

- To study the response of low-density cement-based foams under quasi-static compression and flexure.
- To investigate the performance of polypropylene microfibre in cellular cementitious composites under various loading configurations.
- To examine the strain rate sensitivity of cement-based foams.
- To study the sulphate resistance of cement-based foams in terms of mechanical strength and changes to their internal structure.

The scope of this thesis comprises the following aspects of building construction materials:

- Characterization of controlled low density material.
- Material response when subjected to high rate of loading.
- Response of cellular cementitious material when exposed to severe environment.

1.3 Presentation

This thesis is divided into 7 Chapters. The topics are introduced and the objectives and scope are presented in Chapter 1. A comprehensive literature survey relevant to this study is provided in Chapter 2. An overview of constituent materials of cement-based foams including their effects on fresh and hardened properties is

provided. In particular, the two most widely used mix design methods are reviewed in this Chapter as well. A brief description of several experimental techniques that were developed over the years to study material response under impact loading is included here. It also contains an outline of the most commonly used empirical models to predict mechanical response of cement based composites. This Chapter concludes with a description of the mechanism of sulphate attack on concrete and a review of some existing reports on sulphate attack on cement-based foams. The detailed experimental program for this study is described in Chapter 3. Various aspects of mix design and specimen preparation along with details of quasi-static tests and impact tests are presented in this Chapter. Chapter 4 contains the data from the test programs. Response under quasi-static category was studied for two loading configurations - compression and flexure. Compression tests were carried out to get the stress-strain response as well as the Poisson's ratio. The flexural load-deflection response under third point loading was recorded for both plain and fibre-reinforced specimens. The impact response included data from two impact rates. Chapter 5 presents analysis and discussion of results obtained from the experimental program. The mechanical properties derived from test data are discussed on the basis of theoretical concepts and other published data. Chapter 6 focuses entirely on the sulphate resistance of cement-based foams. The study evaluates changes in mechanical properties at various durations of sulphate exposure in a range of cast densities. The effect of such exposure on the internal microstructure is discussed with the aid of advanced microscopic imaging and

mineralogical analysis. Finally, a summary of conclusions and recommendations for further study are provided in Chapter 7. A detailed bibliography is attached at the end of this thesis.

Chapter 2

LITERATURE REVIEW

2.1 General

Cement-based foam is a controlled low-strength mixture of Portland cement, fine aggregate, water and entrained air. The air can be entrained either by adding pre-formed foam or a surfactant to the base mix constituents. The air voids in cement-based foam consist of more than 20% of the total volume which makes it distinguishable from highly air entrained concrete (Aldrige, 2005). The material is also called cellular concrete because of its cellular microstructure (ACI 523.1R, 1996). Cement-based foams also weigh substantially less than regular concrete. The cast density of cement-based foam ranges from 300 - 1600 kg/m^3. Cast density not exceeding 800 kg/m^3 is primarily used in non-structural applications. Such low-density foam is typically made of cement mortar and pre-formed foam. Cast densities ranging from 800 - 1600 kg/m^3 are considered as semistructural materials. And their application depends on the strength and density requirements (Fouad, 2006). A small amount of fine aggregates or very lightweight aggregates may be added to impart strength and other desired properties. Density may be further controlled by adding a predetermined amount of foam to the base mix.

Macroscopic air voids are formed internally and uniformly distributed with the cell size varying from 0.1–1 mm (Legatski, 1994). The mechanical and thermal properties of cellular materials depend on the shape and structure of the cell

(Gibson and Ashby, 1999). The most important structural characteristic of a cellular solid is its relative density, which is defined as the ratio of the density of the cellular material to that of the material from which the cell walls are made. The relative density is an indirect way of relating material behaviour to porosity. The mechanical behaviour of a cellular solid is usually expressed as a function of its relative density.

Depending on the foaming agent used, two types of internal structure can be achieved namely, open-cell and closed-cell. In the case of an open-cell structure, the individual cells are connected to the neighbouring cells through open faces. In the closed-cell structure, each cell is completely sealed off from the neighbouring one (Gibson and Ashby, 1999). The relative density for both open-cell and closed-cell structure can be mathematically expressed in terms of the ratio of cell wall thickness to edge-length of the cell. For open-cell structure, the relative density is linearly varied, whereas for closed-cell structure the relationship is parabolic as shown below:

$$\frac{\rho^*}{\rho_s} \propto \frac{t}{l} \qquad \text{(open-cell foam)} \qquad \text{Equation 2.1(a)}$$

$$\frac{\rho^*}{\rho_s} \propto \left(\frac{t}{l}\right)^2 \qquad \text{(closed-cell foam} \qquad \text{Equation 2.1(b)}$$

Where, $\frac{\rho^*}{\rho_s}$ = relative density; t = cell wall thickness; and l = edge-length.

Characteristics of foamed cementitious materials vary depending on their mix constituents. Regardless of the variation due to mix design criteria, a good number

of general properties can be achieved, namely high strength-to-weight ratio, low permeability, low water absorption, favourable freeze-thaw resistance, relatively higher modulus of elasticity, low shrinkage, better load distribution capacity and shock absorption properties (Aldrige, 2005). Industrial by-products, like fly ash, ground granulated blast furnace slag and bottom ash can be utilized as raw materials for cement-based foams and in the process they help reduce the environmental cost. Besides these above mentioned properties, lightweight and cement-based foam is widely used in a large number of applications due to its ease of handling. Typical application includes thermal insulation, acoustic dampening, low-density engineered fill, etc. It is also used as protective systems in military applications such as advanced military weapons, fragmentation shields, blast attenuating walls, void filling in nuclear vessels and tunnel lining (Fouad, 2006). As a floor-filling material it is very effective for the rehabilitation of old buildings. The subset with a cast density of 450 - 650kg/m^3 is typically used for roof deck filling. As an engineered fill, it can be an economical solution to many geotechnical problems. A cast density of 480 kg/m^3 can reduce overburden pressure up to four times when existing soil is replaced with foamed material. For uses as a precast structural material, typically autoclaved aerated concrete is employed to provide the material with improved structural properties and dimensional stability. In Canada, especially in colder regions of the Canadian Prairies and Northern Territories, use of cement-based foams is preferred due to their thermal insulating properties. Foamed concrete is also used as road sub-base to prevent frost heaves and as backfill to reduce surcharge.

2.2 Materials

Cement-based foam is produced by incorporating air voids in a base mix of cementitious material, water and fine aggregates. Portland cement is the primary cementitious component of the foamed material. The dosage of Portland cement can be as high as 1400 kg/m^3, but usually between 300 – 500 kg/m^3 (British Cement Association, 1994; Jones and McCarthy, 2005). Besides ordinary Portland cement, other types such as high early-strength cement, high-alumina cement and calcium-sulphoaluminate cement have also been used to achieve lower setting time and rapid strength development (Jones and McCarthy, 2005). The use of alkaline cement and geocement has also been reported (Krivenko *et al.*, 2005).

2.2.1 Supplementary Cementitious Materials

Portland cement can be blended with fly ash (classified or unclassified). Research indicates that a large volume of cement can be replaced with fly ash. Although the early-strength development is affected by high fly ash content, considering the long term improvement up to 75% of cement can be successfully replaced (Kearsley and Wainwright, 2001). A research on the effect of fly ash on the air void system shows that the addition of fly ash to foamed cement as filler renders more uniform distribution of air voids than fine sand for cast densities ranging 600–1200 kg/m^3 (Nambiar and Ramamurthy, 2007). Further, the use of fly ash helps to reduce the water demand for a given consistency (Mehta and Monteiro,

1993). It is reported that partial replacement of cement with fly ash also helps to prevent autogenous shrinkage (Lee *et al.*, 2003). Other research on fly ash utilization indicates that the use of fly ash with high carbon content may require more foam to maintain desired plastic density, due to significant foam collapse in the fresh state as a result of adsorption onto carbon content (Jones and McCarthy, 2004). Ground granulated blast furnace slag has also been used as partial replacement of cement at levels between 30 to 50%. Silica fume has been used up to 10% by mass of cement and is reported to be effective in improving compressive strength without affecting the stability of the air void system when foam volume is less than 30% (Jones and McCarthy, 2005). In the quest for utilizing by-products, researchers are investigating the use of solid waste such as rice husks as pozzolanic admixture, paper sludge as fibre and recycled expanded polystyrene as lightweight aggregate in foamed concrete as alternatives to typical constituents (Lee and Hung, 2005). As pozzolanic admixture, 40% of cement can be replaced by rice husk ash with no loss in compressive strength. Lee *et al.* (2005) also reported that the use of expanded polystyrene as lightweight aggregates results in lower absorption and better chemical resistance.

2.2.2 Aggregates

Fine aggregates with maximum particle size up to 5mm can be used in cement-based foam only when desired cast density is more than 1200 kg/m^3. For materials below this limit the fine aggregates are usually replaced by fly ash, lime, chalk, crushed concrete, granite dust, recycled glass and materials from demolition

(Jones and McCarthy, 2005). It is usual practice to not use coarse aggregates in the production of foamed concrete. However low-density lightweight aggregates such as perlite or vermiculite are sometimes used to replace fine aggregates partially or completely. This type of replacement is done in order to enhance the strength–density ratio for structural application (ACI 213R, 2003).

2.2.3 Foaming Agent

Historically, air entrainment was accomplished by generating hydrogen gas from the reaction of aluminum powder with calcium hydroxide and water. The hydrogen gas in turn produced foam bubbles in the raw mix. These days, air bubbles in foamed concrete are incorporated by using a foaming surfactant. Based on the source, the surfactant can be either synthetic or protein-based. Synthetic foaming agents are made of amine and amine oxides, naphthalene sulphonate formaldehyde condensates, etc. (Bindiganavile and Hoseini, 2008). On the other hand, protein-based foaming agents are made from animal products. A protein based surfactant results in a more stable and strong bubble structure whereas a synthetic type provides better expansion resulting in lower density (Tikalsky *et al.*, 2004). The synthetic type can also be stored longer (12months) than the protein type (6 months). Besides the source-based classification, foaming agents can be further categorized into two types, where the respective type is capable of producing predominantly an open-cell or a closed-cell internal air void network.

2.2.4 Fibre Reinforcement

Fibre reinforcement can be used in foamed concrete to help control shrinkage cracking. Usually short fibres of glass, carbon or polymeric type are used. Since plain foamed concrete is brittle in nature, the addition of fibres helps mitigate this by imparting post-crack strength and toughness to the material (Jones and McCarthy, 2005). It has been reported that the use of microfibre improves the shear resistance of cement-based foams. The behaviour of cement-based foams with fibre reinforcement is significantly influenced by fibre types and internal void networks. A typical dosage of polymer or glass microfibre is 1 kg/m^3. The preferred fibre length is 13–38 mm (1/2"–1 ½"). The upper limit of the length depends on the increasing difficulties arising from fibre dispersion (Fouad, 2006). Microfibre of length 19 mm has been found to be effective for cement-based foams.

2.3 Mix Design

There is no standardized method available for proportioning ingredients required to make cement-based foams. Mix design criteria for cementitious foam differ from that of regular concrete. As for foamed concrete mix proportioning depends not only on a specified strength, but also on the required cast density (Bindiganavile and Hoseini, 2008). Many factors affect the behaviour of foamed concrete such as air content, cast density, composition of cementitious materials, as well as the water-binder ratio. The type of the foaming agent used affects both

fresh and hardened behaviour of the material. Use of fly ash, ground granulated blast furnace slag and silica fume also results in a significant change in material properties (Wee *et al.*, 2006).

Mix proportioning begins by selecting a target cast density of foamed concrete, cement content and water-binder ratio. The choice of these parameters depends on the strength and thermal conductivity requirements. A slurry mixture is then proportioned using the absolute volume method. This method estimates the volume of air required for a unit volume of concrete by calculating the sum of the absolute volume of the cement, water and aggregates (ACI 523.3R, 1993). Based on the air volume required, foam volume can easily be estimated by taking the foam-air ratio as 1.05 to 1.07. ACI 523.3R (2010), a draft document, proposed a mix design method based on required cast density (greater than 800 kg/m^3) of cement based foams.

Kearsley and Mostert (2005) proposed a method of mix design by taking input parameters such as the target cast density, the water-cement ratio, the water–fly ash ratio, the water–sand ratio, the fly ash–cement ratio and the sand–cement ratio. They proposed following two equations, which calculate the cement content and the foam volume based on a selected value of input parameters:

$$\rho_m = x + x\left(\frac{w}{c}\right) + x\left(\frac{a}{c}\right) + x\left(\frac{s}{c}\right) + x\left(\frac{a}{c}\right)\left(\frac{w}{a}\right) + x\left(\frac{s}{c}\right)\left(\frac{w}{s}\right) + RD_f V_f \qquad \text{Eq. 2.2(a)}$$

$$1000 = \frac{x}{RD_c} + x\left(\frac{w}{c}\right) + \frac{x\left(\frac{a}{c}\right)}{RD_a} + \frac{x\left(\frac{s}{c}\right)}{RD_s} + x\left(\frac{a}{c}\right)\left(\frac{w}{a}\right) + x\left(\frac{s}{c}\right)\left(\frac{w}{s}\right) + V_f \qquad \text{Eq. 2.2(b)}$$

Where,

ρ_m	= target cast density (kg/m^3)	*s/c*	= sand–cement ratio
x	= cement content (kg)	*w/a*	= water–ash ratio
w/c	= water–cement ratio	*w/s*	= water–sand ratio
a/c	= fly ash–cement ratio	V_f	= volume of foam (*l*)
RD_c	=relative density of cement (specific gravity)	RD_a	= relative density of fly ash
		RD_s	= relative density of sand
RD_f	= relative density of foam		

Wimpenny (1996) proposed a method of calculating the required foam volume based on the density of the base mix using the following equation:

$$F_m = F_d B_m \left(\frac{1}{T_d} - \frac{1}{B_d}\right) \qquad \text{Equation 2.3}$$

Where,

F_m	= mass of foam (kg)	T_d	= target density (kg/m^3)
B_m	= mass of base mix (kg)	B_d	= Base mix density (kg/m^3)
F_d	= foam density (kg/m^3)		

2.4 Production of Cement-based Foam

The production process of cement-based foams can be divided into three stages: i) Generation of foam, ii) Preparation of base mix (cement-sand slurry) and iii) Addition of foam to the base mix.

There are two principal methods of production of foamed concrete, namely the mixing foam method and the pre-formed foam method. In mixing foam method,

the foaming surfactant is directly mixed with base constituents (Aldrige, 2005). The pre-formed foam method is further divided into two categories such as the wet foam method and the dry foam method. In the wet foam method, the foam is produced by spraying a solution of foaming agent and water over a fine mesh which results in bubble formation with size ranging from 2 mm to 5 mm in diameter. Foam thus formed has a loose bubble structure but is relatively stable. This type of foam is not suitable for foamed concrete with a cast density less than 1100 kg/m^3. This method is also not recommended for pumping concrete over a long distance. In the dry foam method, the foam is produced by forcing a foaming agent and water through a series of chambers whilst at the same time forcing compressed air into the mixing chamber. The action of forcing this pressurized air into the solution expands the solution into thick, tight foam that is similar to shaving foam in appearance. The diluted foaming agent expands in volume up to about 30 times with density ranging from 26–60 kg/m^3. The bubble size thus formed is typically 1 mm in diameter. The production of foamed concrete is most commonly done by the pre-formed foam method.

2.5 Fresh Properties

2.5.1 Flow Characteristics

The water-binder ratio plays an important role during production of foamed material. If the water-binder ratio is very low (less than 0.35) then the cement will extract water from the foam bubbles resulting in a loss of volume and an increase in composite density because of instability of the foam bubble (Jones and

McCarthy, 2005). Again too high a water content results in bleeding and lower strength in the final mix. A typical range of water–binder ratio is 0.4–0.8. Factors affecting the selection of water-binder ratio are the mix composition, required flow characteristics and type of foaming surfactant. Kearsley and Mostert (2005) found that the addition of a small amount (less than 25% of fly ash) of fine sand to the base mix does not require additional water for satisfactory workability. But utilizing sand above 25% (by weight of fly ash) changes the water demand significantly.

Fresh cement-based foams cannot be subjected to compaction or vibration because of air bubble stability issues. The foamed material has to be free flowing, self-levelling and self-compacting, so it will be easy to place even in areas where placement is difficult with regular concrete (Jones and McCarthy, 2005). Since foamed cementitious material is handled in fluid consistency, a slump cone test to measure flow characteristics is meaningless (Fouad, 2006). Instead a Marsh Cone test is performed to ensure that the material has an appropriate level of consistency. A Marsh cone flow value (carried out after mixing the foam) below 20 seconds was found satisfactory for the material to be placed without any mechanical disturbance (Nambiar and Ramamurthy, 2008). The consistency of the base mix was found to be an important factor for the stability of the mix. This consistency was reduced after adding foams to the base mix. The reduction was attributed to the loss of weight and increased cohesion due to presence of air

bubbles (Nambiar and Ramamurthy, 2008). The increased cohesion is likely due to the adhesion between the bubbles and solid particles.

2.5.2 Mixing Time

The duration of mixing pre-formed foam with the base mix is very important. In general, the greater the mixing time the more the entrained air content in the final composite. A study on the effect of mixing time on air void characteristics revealed that after reaching a critical limit, further mixing results in a drop in entrained air content (Beningfield *et al.*, 2005). This is because prolonged mixing leads to instability of the air bubble network.

2.5.3 Density

The oven dry density of cement-based foams can be as low as 48 kg/m^3 and as high as 1800 kg/m^3 (Kearsley and Wainwright, 2001). The change in the density due to air drying is a function of change in temperature, duration of drying, humidity, cast density, water–cement ratio and surface area for the material. Expressing dry density in terms of all the controlling factors is very difficult. Cast density usually drops by 80 kg/m^3 due to air drying (Fouad, 2006). Oven-dry density is used to relate physical properties with relative density of the material. Oven-dry density can be estimated by the following equation:

$$D = 1.2C + A \quad \text{kg/m}^3 \qquad \text{Equation 2.4}$$

Where,

D = oven-dry density, kg/m^3

C = weight of cement, kg

A = weight of aggregate, kg

Kearsley and Mostert (2005) proposed a relationship between the oven-dry density and the cast density for different mixes, which included various levels of fly ash replacement, as follows:

$$\rho_{cast} = 1.034\rho_{dry} + 101.96 \qquad \text{Equation 2.5}$$

2.5.4 Curing

During the cement paste hydration process, foam bubbles release trapped moisture, which is absorbed by the cement matrix. This phenomenon not only aids in the hydration process, but also contributes to the air void network (Bindiganavile and Hoseini, 2008). Higher strengths have been obtained with air curing in comparison to sealed or water cured specimens (Jones and McCarthy, 2005). On the other hand, long-term strength gain is observed to be higher for well-cured specimens containing fly ash (Kearsley and Wainwright, 2001). A study on the effect of high temperature curing on strength development shows that curing under high temperatures can substantially increase the rate of strength gain of mixes containing high-volume fly ash, but it resulted in a lower ultimate strength (Kearsley and Mostert, 2005).

2.5.5 Heat of Hydration

Cement-based foams to be used for semi-structural application require higher cement content compared to those for non-structural use. Foamed concrete in semi-structural applications could potentially results in significant temperature rise up to 62°C in excess of ambient temperature. The resulting core–surface temperature differential could exceed the strain capacity of foamed concrete (Jones and McCarthy, 2006). The study showed that the use of fly ash as partial replacement of cement helps to reduce this heat of hydration. Figure 2.1 shows a significant attenuation of peak temperature due to cement replacement by fly ash. Temperature development in cement-based foams was found to be influenced by greater parameters than regular concrete. Thus the existing temperature prediction models for conventional concrete may not be used with this material.

2.6 Hardened Properties

2.6.1 Porosity

The pore structure of foamed concrete consists of gel pores, capillary pores and air voids. Air voids contain a very small portion of entrapped air because of the self- compacting nature of foamed concrete. Several researchers proposed different porosity models to predict the strength of cement-based foams. A study on the air void network shows that volume, size and spacing of voids influence the density and mechanical properties of foamed concrete. It is found that the shape of these voids, however, does not affect strength (Nambiar and

Ramamurthy, 2007). Additionally concrete with higher air content has a tendency to form larger voids (Figure 2.2), especially when air content is more than 42% (Babu *et al.*, 2005). Another study found that filler material like fly ash and fine sand influence the air void network. Use of fly ash is reported to result in more uniform air void distribution than fine sand (Nambiar and Ramamurthy, 2007). Wee *et al.* (2006) proposed a relationship between cube compressive strength and porosity of foamed concrete at a given water–cement ratio as:

$$\sigma = 1.262\sigma_p(1 - A)^{2.962} \qquad \text{Equation 2.6}$$

Where: σ, σ_p and A are cube compressive strength of foamed concrete, compressive strength of cement paste and air content, respectively. Similarly, Kearsley and Wainwright (2002) proposed a porosity model as follows:

$$f_c = 981e^{-7.43p} \qquad \text{Equation 2.7}$$

Where: f_c is the cube compressive strength (MPa) of foamed concrete and p is the porosity of the material.

2.6.2 Shrinkage

Cement-based foam will shrink more than regular concrete because of relatively higher cement paste content. No plastic shrinkage has been reported in foamed concrete, but drying shrinkage is ranges from 0.1% to 0.35% depending on the density (Jones and McCarthy, 2005). The lower the density, the higher the shrinkage strain (British Cement Association, 1994). ACI 523.2R (1996) limits

the average drying shrinkage of cementitious foam to 0.2%. The drying shrinkage of relatively higher density foamed concrete with a sand–cement ratio of 2 was reported to be less than 0.09% (Lee and Hung, 2005). In a study of foamed concrete with high-calcium fly ash, it was found that cement replacement by this particular type of fly ash decreased the drying shrinkage from 1800 microstrain to 1200 microstrain by reducing the fly ash content from 70% to 60% (Figure 2.3). It was also observed that the higher the strength of the material the lower the drying shrinkage (Papayianni and Milud, 2005). Another study found that use of coarse-grained fly ash helped reduce drying shrinkage (Kearsley, 1999).

2.6.3 Thermal Conductivity

Thermal conductivity is measured as the rate of heat transferred by conduction through unit thickness, across a unit area, for a unit difference of temperature. The principal parameter controlling thermal conductivity of cellular material is its oven-dry density. Figure 2.4 shows the relationship of thermal resistance to oven-dry density as found by Steiger *et al.* (1978). They found that the thermal conductivity is influenced by moisture content in cement-based foam. They recorded approximately a 5% increase in thermal conductivity for every 1% increase in density directly attributed to moisture content.

2.7 Mechanical Response under Quasi-static Load

2.7.1 Compressive Strength

The compressive strength of cement-based foams is primarily affected by density. The compressive strength decreases with a decrease in the density. Typical values are observed to vary from 0.5 MPa to 20 MPa (Aldrige, 2005; Kearsley and Wainwright, 2001; Jones and McCarthy, 2005; Wee *et al.*, 2006; Nambiar and Ramamurthy, 2006). Compressive strength as high as 50 MPa can be achieved by using pozzolanic admixtures such as fly ash in foamed concrete for cast density more than 1500 kg/m^3 (Kearsley and Wainwright, 2001). One of the most desired material properties is a high strength to weight ratio. Figure 2.5 shows typical variation of compressive strength with density.

Compressive strength of foamed concrete is a function of its density; the other parameters, like cement replacement with pozzolans, filler type and cement content, do not seem to affect compressive strength significantly (Kearsley and Mostert, 2005; Kearsley and Wainwright, 2001). However, research data has shown that fineness of sand has a noticeable effect (Figure 2.6) on compressive strength (Nambiar and Ramamurthy, 2006). Mixes with coarse sand have a much lower compressive strength compared to those with fine sand especially at higher densities. Figure 2.6 shows strength variation of mixes with the variation of fineness of sand.

As for the effect of pozzolans, results from several studies show that the use of fly

ash as filler material has a significant effect on compressive strength: an increase in fly ash content (up to a certain limit) results in higher strength (Kearsley and Wainwright, 2002; Nambiar and Ramamurthy, 2006). Papayianni and Milud (2005) showed that high-calcium fly ash replacement of cement up to 70% increased the compressive strength of foamed concrete. The results indicated that with an increase in the fly ash content, the compressive strength increased compared to the reference foamed concrete with no fly ash. This effect continued even at 90 days. They concluded that the higher water retention in fly ash, in combination with its pozzolanic reactivity, may contribute to the excellent performance of fly ash as cement replacement in cement-based foams. Research on fly ash has also shown that coarser and higher fly ash content results in a decrease in the early strength, while improving long-term strength (Kearsley and Wainwright, 2002). The study reported a 60% fly ash content as the optimum level of cement replacement for maximum strength after one year. Higher compressive strength can be achieved for a given density of foamed concrete by reducing the volume of voids. This can be done by using lightweight ingredients (Kearsley and Mostert, 2005). However, use of other types of fine aggregates such as lime or recycled glass appears to have little or no effect on the compressive strength of cement-based foams (Jones and McCarthy, 2005). Another way of increasing the compressive strength of lower-density foamed concrete is by increasing the cement content (Hamidah *et al.*, 2005). On the other hand, it is reported that higher sand–cement ratios result in a lower compressive strength (Wee *et al.*, 2006).

Usually, water-reducing chemical admixtures are not used in foamed concrete because of their effect on foam stability. In addition, in foamed concrete, small changes in the water–cement ratio do not influence the strength in the way expected for normal weight concrete. Foamed concrete is characterized by its cast density (Jones and McCarthy, 2006). In other words, the volume of the voids is an important determinant of strength, as well as the water–cement ratio and it is often the defining parameter. This is particularly true in the case of the more highly air entrained mixes. Moreover, it has been observed that increasing the water content increases the strength as long as there is a reduction in the air–cement ratio. In other words, the effect of void content seems to counteract the effect of the water–cement ratio on the strength of foamed concrete (Nehdi *et al.*, 2003). Thus, the strength-controlling factor shifts from the water–cement ratio to the air–cement ratio.

The compressive strength of foamed concrete is influenced by the type of foaming agent used. It is observed that protein-based surfactants increase the compressive strength of foamed concrete more than synthetic surfactants (Jones and McCarthy, 2005), primarily through the creation of a closed-cell air void network. Thus, when comparing specimens, the type of foaming agent used to manufacture them should be considered and only those mixes with the same type of foaming agents should be compared.

A study of their freeze-thaw resistance showed that cement-based foamed material with a 28-days compressive strength of more than 1 MPa is durable in freezing

and thawing cycles, whereas specimens with a compressive strength less than 1 MPa are not resistant to freeze-thaw cycles.

Kearsley and Wainwright (2001) developed a strength prediction model for foamed concrete. This model considers two input parameters, age of the concrete and its water–cement ratio, as follows:

$$f_c(T, w_c) = 88.04 + 6.596 \ln(T) - 130(w_c) \quad \text{Equation 2.8}$$

Here, f_c = cube compressive strength (MPa); T = age of the concrete (days); and w_c = water–cement ratio.

Nehdi *et al.* (2001) developed an artificial neural network model for cement-based foam to predict density and compressive strength. They considered four key variables to develop the model: cement content, water-cementitious material ratio, foam–cementitious material ratio and sand–cementitious material ratio. This model seems to be efficient in predicting the properties of foamed material. However, it does not account for the other cementitious materials, chemical admixtures and fibre reinforcement. The stress-strain behaviour of brittle cellular solids is characterized first by a linear elastic behaviour followed by a plateau, which in turn is ultimately followed by a rapid rise due to densification as shown in Figure 2.7 (Gibson and Ashby, 1999).

Research on autoclaved, unreinforced cellular concrete showed that the stress-strain under quasi-static compression does not follow the same trend as for regular

concrete (Valore, 1954). Figure 2.8 shows the abrupt failure of the specimen under compression. No post-peak response was observed. However, the strain corresponding to peak stress was very similar to that of regular concrete. This exhibition may be attributed to the thin cell walls of cement-based foams. Based on this study (Valore, 1954), it is interesting to note that the cement-based cellular material does not follow the typical response pattern as expected for brittle cellular solids shown in Figure 2.7.

Babu *et al.* (2005) investigated foamed concrete with or without aggregates to find a relationship of cube compressive strength and cylinder compressive strength. They found a conversion factor of 1.06 (f_{cu}/f_{cy}) for foamed concrete, whereas this factor was about 1.25 for regular concrete. This may be attributed to localized crushing. They studied foamed concrete with a dry density from 1400–1800 kg/m^3 with a water–cement ratio of 0.4. Generally, the behaviour of cellular material is expressed as a function of its relative density. Gibson and Ashby (Gibson and Ashby, 1999) showed that compressive strength of cellular solids can be expressed as a function of relative density with an exponent of 3/2.

2.7.2 Modulus of Elasticity

In general, the static modulus of elasticity of cement-based material is a function of its density and compressive strength. Since cellular concrete is lighter and has a lower compressive strength than regular concrete, its modulus of elasticity is much lower compared to regular concrete. Figure 2.9 shows the variation of

modulus of elasticity with dry density (Valore, 1954). This study indicated a parabolic relationship between the modulus of elasticity and relative density of foamed concrete, which also holds true for non-cement-based cellular solids (Gibson and Ashby, 1999). Wee *et al.* (2006) found, from both experimental and numerical results, that the inclusion of air bubbles in foamed concrete had a greater effect on the compressive strength than on the modulus of elasticity.

It is reported (ACI 523.1R, 1996) that the equation mentioned in ACI 318 (2005) to evaluate the modulus of elasticity is applicable to cellular concrete of density ranging from 370–1800 kg/m^3. In a study (Fouad, 2006) on the modulus of elasticity of foamed concrete with cast density varied from 1280–1872 kg/m^3, the following correlation was suggested:

$$E_c = W_d^{1.5}\, 37.04 \sqrt{f'_c} \quad (\text{N/m}^2) \qquad \text{Equation 2.9}$$

Where, W_d = air-dry density, which can be estimated by deducting 80 kg/m^3 from cast density (kg/m^3); f'_c = 28-day compressive strength (MPa)

2.7.3 Poisson's Ratio

A study (Valore, 1954) on foamed concrete showed that for cement–silica (ground fine silica used as weak pozzolan) cementitious foam Poisson's ratio is about 0.16. On the other hand, for foamed specimens with cement-fly ash mix constituents, Poisson's ratio was from 0.15 to 0.25. In both cases no significant variation in Poisson's ratio was observed over a range of dry densities. Zollo and

Hays (1998) reported that for fibre reinforced cellular concrete, with 0.5% (polypropylene) fibre content, the Poisson's ratio was from 0.3 to 0.4. It is already known to researchers that Poisson's ratio for non-cement-based cellular solids is independent of relative density of the material. It only depends on the cellular geometry (Gibson and Ashby, 1999). Figure 2.10 shows this independence of Poisson's ratio to the relative density in cellular solids based on polymers and metals.

2.7.4 Tensile Strength

The tensile strength of foamed concrete follows a similar relationship to compressive strength as with regular concrete. Tests (Valore, 1954) showed that the splitting tensile strength of cement-silica autoclaved concrete is 11–12% of cube compressive strength. Babu *et al.* (2005) found that the ratio between split tensile strength and cylinder compressive strength was about 11% for specimens without any aggregates. These ratios are very similar to that of regular concrete is about 10% of compressive strength (Raphael, 1984).

2.7.5 Flexural Strength

Being a low-density material, the flexural strength of cement-based foam is generally lower than that of normal weight concrete. Jones and McCarthy (2005) studied the performance of foamed concrete with a density between 1400–1600 kg/m3 using coarse sand as fine aggregates for structural applications. Their study

indicated a load-deflection (four-point bending) behaviour similar to that of normal weight concrete with a compressive strength of 25 MPa. However, the deflection at failure was up to 2.5 times higher than that of a normal weight concrete beam. As expected, unreinforced foamed concrete do not show any post-peak response after reaching peak load.

Research on autoclaved foamed concrete indicates that the ratio of flexural to cube compressive strength is 0.2–0.35 for cement-silica foamed concrete, whereas this value is reported to be 0.1–0.45 for cement-fly ash foamed concrete (valore, 1954). The overall ratio from 0.2–0.33 is generally accepted to be valid for this material.

2.8 Fibre-reinforced Cement-based Foam

The brittle performance of unreinforced cement-based foam is well known. Various investigations have been carried out in order to improve this behaviour. Since foamed concrete has a higher shrinkage strain, lower tensile strength and modulus of elasticity, consideration was given to the use of microfibres in an attempt to offset this performance. Because of their rigidity, steel and glass fibre have the tendency to behave poorly when interacting with thin cell walls. Instead, the more flexible polypropylene fibre has been used widely. Jones and McCarthy (2005) reported an increase in the compressive strength, flexural strength and modulus of elasticity with the use of polypropylene fibres in foamed concrete with cast densities ranging 1400-1800 kg/m^3. Since the addition of microfibre

significantly reduces workability of the mix, they recommended an optimum fibre dosage of 0.5% by volume.

A study on foamed concrete (cast density 750-1500 kg/m^3) performed by Kearsley and Mostert (2003) reported that there is no noticeable enhancement in the compressive strength, modulus of rupture and the modulus of elasticity upon addition of microfibres even at a dosage of 0.5% by volume. However, the effect of fibres in terms of the residual strength was evident as shown in Figure 2.11.

Papayianni and Milud (2005) studied the performance of fibre-reinforced foamed concrete (oven-dry density 400-550 kg/m^3) exposed to ambient conditions of 20°C with a relative humidity of 67%. They added polypropylene fibres at a dosage of 1.3 kg/m^3 (0.15% by volume) to foamed concrete that contained only cement and a mix with 30% cement replacement with high calcium fly ash. An improvement in terms of crack reduction was observed.

2.9 Evaluation of Flexural Toughness of Cement-based Composites

Flexural toughness is a measure of energy absorbed by the material under quasi-static or impact loading of a beam specimen. A characterization of this property is very important in terms of material selection for a specific demand. An unreinforced matrix fails in a brittle manner when subjected to flexure with the onset of cracking, while a fibre-reinforced material continues to resist load due to the presence of ductile fibres which assist in maintaining structural integrity.

Moreover, a properly reinforced fibre undergoes a pullout process, which leads to a significant improvement in the energy absorption (Banthia and Trottier, 1995).

The two most widely used methods of evaluating flexural toughness are ASTM C1609 (2007) and JSCE G-552 (1999). Both methods are criticized for their inability to distinguish between pre-peak and post-peak responses (Banthia and Trottier, 1995). In the ASTM standard, flexural toughness is defined as the area under the load vs. the deflection curve up to a deflection of span/150 and hence is a measure of energy dissipated. Whereas, the toughness factor evaluated using JSCE method is ameasure of strength and therefore is normalized for specimen dimensions. Figure 2.12 shows how differently the toughness is calculated using the ASTM and JSCE methods.

The JSCE G-552 flexural toughness factor (FTF) and residual strength can be calculated as follows:

$$FTF = \frac{Area\ OABC \times L}{\left(\frac{L}{150}\right) \times bh^2} \qquad \text{Equation 2.10}$$

$$Re_2 = \frac{FTF}{MOR}\ 100\ (\%) \qquad \text{Equation 2.11}$$

The ASTM C1609 toughness parameters can be calculated as follows:

$$Toughness = Area\ OABC \qquad \text{Equation 2.13}$$

$$Residual\ strength = \frac{Toughness \times 150}{first\ peak\ strength \times bh^2}\ 100\ (\%) \qquad \text{Equation 2.14}$$

2.10 Response under Impact Loading

Impact loading may occur during the service life of civil engineering structures from a variety of sources, including vehicle collision, aircraft landing, falling and swinging object from construction operation, flying objects from explosion, floating objects, extreme water wave action, earthquake, extreme wind action, etc. Material subjected to high strain rates are seen generally to behave differently from that under quasi-static loading. In Table 2.1 the magnitude of stress rate and strain rate from typical loading cases are listed.

2.10.1 Impact Testing Methods

A widely used test method to evaluate material response under a high strain rate is the Split Hopkinson Pressure Bar. This apparatus was first introduced by Kolsky (1949). The Split Hopkinson Pressure Bar is capable of testing material at strain rates between 100 – 10000 s^{-1}. The specimen is sandwiched between two pressure bars called an input and output bar. The input bar is loaded by a single traveling pulse through a separate bar called the striker bar. The pulse signals are monitored with the help of attached transducers and simultaneous data acquisition can be done for stress history, strain history and strain-rate history. The recorded data is then analyzed by a suitable integration technique to obtain the stress-strain response. The apparatus is highly versatile and capable of achieving different loading configurations including compression, tension and torsion. This test method is criticized for its high frictional effect between specimen and the input

pressure bar. The stress-strain data generated from stress history and strain history may suffer from the lag between the two histories.

The drop-weight impact technique (ASTM STP 563, 1973) is one of the simplest test methods. In this method, to study the dynamic response of a drop-hammer is lifted to a certain elevation and then released on top of the specimen. An un-instrumented version of the system only evaluates the number of drops required to reach a certain level of response from the specimen. This is a very gross estimation of energy absorption. No loading history can be obtained from such a system. The instrumented version of this system, however, is capable of recording load history, acceleration history and displacement history. This allows the evaluation of fracture toughness, energy dissipation, ultimate strength and strain at various levels of strain-rate. The instrumentation attached to such a system is sophisticated enough to record data during a very short impact event. The drop weight impact system is generally used for compression and flexural loading configurations. A rather different type of instrumented drop weight impact system is the Charpy impact system. In this method the hammer is allowed to swing from a certain angular position instead of dropping freely from a certain height.

2.10.2 Inertial Correction

The load data recorded in an impact system includes a load component due to rigid body motion of the specimen according to d'Alembert's principle. This load component is called the inertial load. Since inertial loading does not contribute to

the material response, it has to be deducted from the total load. Quasi-brittle materials including cementitious material fail due to impact loading while in acceleration. Cotterell (1962) was the first to consider inertial load correction for metal specimen experiments. Gopalaratnam and Shah (1984) used a rubber pad to reduce the inertial effect. But use of rubber causes a reduction in the loading rate by absorbing a considerable amount of energy.

Banthia *et al.* (1989) suggested a more rational approach of inertial correction for flexural loading configurations. By attaching an accelerometer at intermediate points along the test specimen, the acceleration distribution can be obtained to calculate distributed inertial load. Using the principle of virtual work, the generalized inertial load can be obtained. The actual bending load is then calculated by subtracting inertial load from the total recorded load. The researchers developed the following equations to evaluate inertial load:

For linear case,

$$P_i(t) = \rho A \ddot{u}_0(t) \left\{ \frac{l}{3} + \frac{8}{3} \frac{h^3}{l^2} \right\} \qquad \text{Equation 2.15}$$

For sinusoidal case,

$$P_i(t) = \rho A \ddot{u}_0(t) \left\{ \frac{l}{2} + \frac{2\pi^2}{3} \frac{h^3}{l^2} \right\} \qquad \text{Equation 2.16}$$

Where,

$P_i(t)$ = inertial load at time t
$\ddot{u}_0(t)$ = acceleration at time t
ρ = Density of the material
A = cross sectional area
l = span of the specimen
h = overhang of the specimen

While plain and fibre reinforced concrete without conventional reinforcement may have a linear geometry in flexure, longitudinally reinforced concrete is considered as sinusoidally deformed when subjected to bending.

2.10.3 Rate Sensitivity

Concrete as building material is sensitive to the rate of loading. The standard test method to evaluate compressive response, ASTM C469 specifies the stress rate as 241±34 kPa/s. It is important to assess rate sensitivity of a material subjected to dynamic loading. Generally, it is accepted that the higher the loading rate, the higher the strength of the material. However, it is reported that within the usual quasi-static testing range the loading rate effect on concrete is not significant (Jones and Richart, 1936). Researchers have also developed an empirical model to predict the material response under high loading (stress or strain) rate. Nadeau *et al.* (1982) obtained the effect of stress-rate on the material strength by the following relationship:

$$\ln \sigma_f = \frac{1}{N+1} \ln B\dot{\sigma} + \frac{1}{N+1} \ln\left(\sigma_i{}^{N-2} - \sigma_f{}^{N-2}\right) \qquad \text{Equation 2.17}$$

Where,

σ_f = stress at final condition

σ_i= stress at initial condition

B, N = constant

$\dot{\sigma}$ = stress rate

A plot of log strength versus log stress rate yields a line with a slope of 1/(N+1). The parameter *N* is dependent on material strength and stress-rate.

The CEB-FIP Model Code (1993) suggests that the dynamic increase factor (DIF) in tension under impact strain-rate may be estimated as follows:

$$\left.\begin{array}{ll} DIF = \left(\frac{\dot{\epsilon}}{\dot{\varepsilon}_s}\right)^{1.016\delta} & for\ \dot{\varepsilon} \leq 30s^{-1} \\ DIF = \beta\left(\frac{\dot{\epsilon}}{\dot{\varepsilon}_s}\right)^{\frac{1}{3}} & for\ \dot{\varepsilon} > 30s^{-1} \end{array}\right\} \quad \text{Equation 2.18}$$

Where,

$\dot{\epsilon}$= strain rate ranging from 3x10^{-6} to 300 s^{-1}; $\dot{\varepsilon}_s$= quasi-static strain-rate = 3x10^{-6} s^{-1}

$$\log\beta = 7.11\delta - 2.33$$

$$\delta = \frac{1}{\left(10+6\frac{f'_c}{f'_{co}}\right)} \quad \text{Equation 2.19}$$

f'_c = compressive strength, f'_{co}= 10 MPa

A review of CEB-FIP formulation by Malvar and Ross (1998) showed that the CEB model underestimates rate sensitivity when the strain-rate is lower than 30 s^{-1}. They proposed a modified form as follows:

$$\left.\begin{array}{ll} DIF = \left(\frac{\dot{\epsilon}}{\dot{\varepsilon}_s}\right)^{1.016\delta} & for\ \dot{\varepsilon} \leq 1s^{-1} \\ DIF = \beta\left(\frac{\dot{\epsilon}}{\dot{\varepsilon}_s}\right)^{\frac{1}{3}} & for\ \dot{\varepsilon} > 1s^{-1} \end{array}\right\} \quad \text{Equation 2.20}$$

Where,

$\dot{\epsilon}$= strain rate ranging from 10^{-6} to 160 s^{-1}; $\dot{\varepsilon}_s$= quasi-static strain rate = 10^{-6} s^{-1}

$$\log\beta = 6\delta - 2$$

$$\delta = \frac{1}{\left(1+8\frac{f'_c}{f'_{co}}\right)}$$ Equation 2.21

2.10.4 Strain-rate Sensitivity of Cement-based Composites

Research data reviewed by Bischoff and Perry (1991) indicates that plain concrete shows a definite logarithmic increase in compressive strength when rapidly loaded compared to quasi-static loading. For impact loading with a strain rate of 10 s^{-1} up to an 85% increase in compressive strength was reported. It was also concluded that an increase in the elastic modulus is associated with an increase in the strain rate. Bindiganavile (2003) reported that plain concrete in flexure is more sensitive to stress-rate than its fibre-reinforced counterpart. However, no influence of fibre type on rate sensitivity was observed, when considering steel and polypropylene fibres.

Works on polymeric foam by Tyler and Ashy (1986) showed that polyurethane foams show no strain rate sensitivity up to a strain-rate of 10^2 s^{-1}. However, in the presence of a pore fluid, they obtained noticeable rate sensitivity. Research by Ouellet *et al.* (2006) on expanded polystyrene revealed the fact that the strain-rate effect decreases with a decrease in the composite density decreases (Figure 2.13).

2.11 Sulphate Resistance

2.11.1 Mechanism of Sulphate Attack

Generally, the presence of aggressive chemicals in the surrounding environment causes the concrete to expand and eventually crack in a process called sulphate attack. Permeability of concrete increases due to the presence of this crack, which aids in transportation of deleterious fluid into the concrete. Sulphate attack can result in a progressive reduction in concrete strength and mass loss due to the reduction in cohesiveness (Mehta and Monteiro, 1993).

Expansion in the concrete can occur either because of ettringite formation or gypsum formation. If a sufficient amount of gypsum is present, then the following reaction takes place during the early stage of the cement hydration process:

$$C_3A + 3C\bar{S}H_2 + 26H = C_6A\bar{S}_3H_{32}$$ (ettringite)

Ettringite is a stable product in the presence of sulphate ions only. Since only a limited amount of gypsum is added there are not many sulphate ions left for the remaining C_3A. Ettringite eventually transforms into monosulphate by further reaction with C_3A as follows:

$$2C_3A + C_6A\bar{S}_3H_{32} + 4H = 3C_4A\bar{S}H_{12}$$ (monosulphate)

In the presence of sulphate ions, monosulphates again transform into ettringite. This process is highly expansive in nature causing deleterious effect to the concrete.

$C_4A\bar{S}H_{12} + 2C\bar{S}H_2 + 16H = C_6A\bar{S}_3H_{32}$ (ettringite)

The other expansive product that is responsible for distress in concrete during sulphate attack is gypsum, a chemical product formed by cation exchange. Both the C-H and C-S-H present in the hydrated cement paste may be converted to gypsum ($CaSO_4.2H_2O$) by sulphate attack (Mehta and Monteiro, 1993):

$Na_2SO_4 + Ca(OH)_2 + 2H_2O = CaSO_4.2H_2O + 2NaOH$
$MgSO_4 + Ca(OH)_2 + 2H_2O = CaSO_4.2H_2O + Mg(OH)_2$ (↓)
$3MgSO_4 + 3CaO.2SiO_2.3H_2O + 8H_2O = 3(CaSO_4.2H_2O) + 3Mg(OH)_2$ (↓) + $2SiO_2.H_2O$

The formation of $Mg(OH)_2$ reduces the pH of the environment causing instability of hydrated products, which require a higher pH level. That is why the presence of Mg^+ in sulphate solution is most damaging.

Another type of sulphate attack was discovered (Mehta and Monteiro, 1993) where in the sources of sulphate are internal. Sources of sulphate could be either gypsum-contaminated aggregate or an unusually high sulphate content of the cement. An indirect source of sulphate could be the phenomenon called “delayed ettringite formation” (DEF). It has been reported that steam-cured concrete is susceptible to DEF. Ettringite is not stable above 65°C; it disintegrates to form monosulfate when the steam-curing temperature is higher than 65°C. The sulphate ions released by the disintegration of ettringite are adsorbed by C-S-H. Later, when the sulphate ions are desorbed, the reformation of ettringite causes expansion and cracking.

2.11.2 Control of Sulphate Attack

Transportation of the sulphate ions can be controlled by reducing the permeability of the concrete, which is the best way of protection. Adequate thickness, high cement content, pozzolanic admixtures, low water–cement ratio, proper compaction and curing of fresh concrete are all important factors that contribute to low permeability (Wild *et al.*, 1997). A protective surface coating was also reported to be effective in reducing sulphate attack (Mirza and Al-Noury, 1986). The use of sulphate resistant cement (containing less than 5% of C_3A) might help control moderate levels of sulphate attack. When the attack level is severe the use of Portland cement blended with pozzolans might be beneficial.

2.11.3 Sulphate Resistance of Cellular Cementitious Systems

A study (Mirza and Al-Noury, 1986) of sulphate attack on autoclaved aerated (0.6% aluminum powder) concrete showed significant reduction in compressive strength. It was reported that specimens lost 40% of their compressive strength upon exposure to a 5% $MgSO_4$ solution at 28 days. After 90 days of exposure, the specimens lost about 60% of their compressive strength. Further investigation on the effect of surface treatment to control sulphate attack indicates a 20–40% improvement against sulphate attack. This improved performance can be attributed to reduced permeability due to surface coating.

Jones and McCarthy (2004) studied sulphate resistance of high density foamed concrete with cast densities of 1000–1400 kg/m^3. They observed indicated that foamed concrete has a good resistance to sulphate attack at least up to 12 months. Moreover, the length expansion of the lower density (1000 kg/m^3) foamed concrete due to sulphate attack was slightly greater than the higher (1400 kg/m^3) density category. This difference may be attributed to larger pores and more interconnected microstructures of the low density foamed concrete, enabling ingress of greater quantities of aggressive fluid. They also concluded that the dominant chemical reaction took place between magnesium sulphate, C-S-H and C-H resulting in the formation of gypsum, which was evident from the X-ray diffraction analysis.

Table 2.1: Stress and strain rates from various type of impact load (Reinhardt, 1982)

Loading type	Stress rate (MPa/ms)	Strain rate (s^{-1})
Collision with vessel	10^{-4} to 10^{-3}	10^{-5}
Collision with vehicle	10^{-3} to 10^{-2}	10^{-4}
Gas explosion	10^{-3} to 10^{-2}	10^{-4}
Crashing aircraft	10^{-1} to 10^{0}	10^{-2}
Earthquake	5×10^{-1} to 10^{2}	10^{-2} to 3×10^{0}
Pile driving	10^{0} to 3×10^{1}	3×10^{-2} to 10^{0}

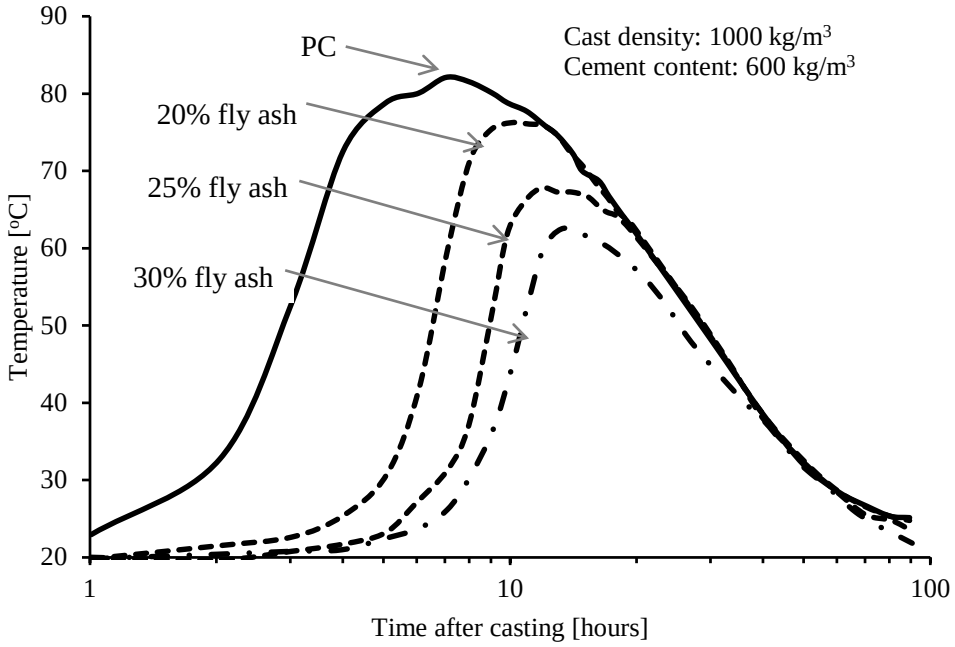

Figure 2.1: Influence of fly ash on the temperature development in foamed concrete (Jones and McCarthy, 2005)

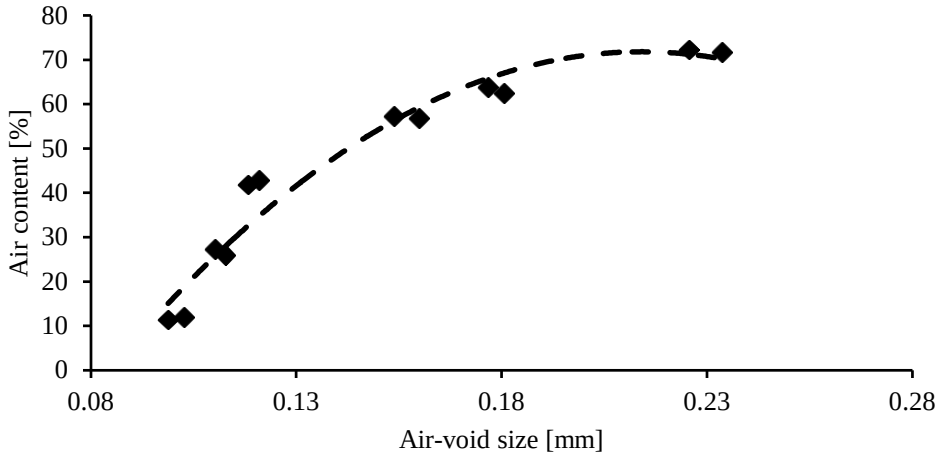

Figure 2.2: Effect of air content on size of air void in foamed concrete (Babu *et al.*, 2005)

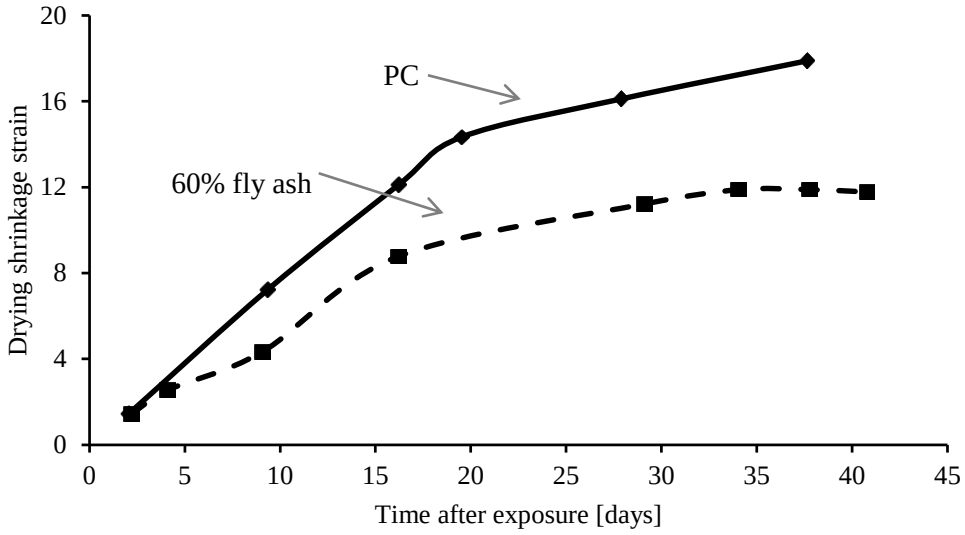

Figure 2.3: Shrinkage deformation of foamed concrete mixture (Papayianni and Milud, 2005)

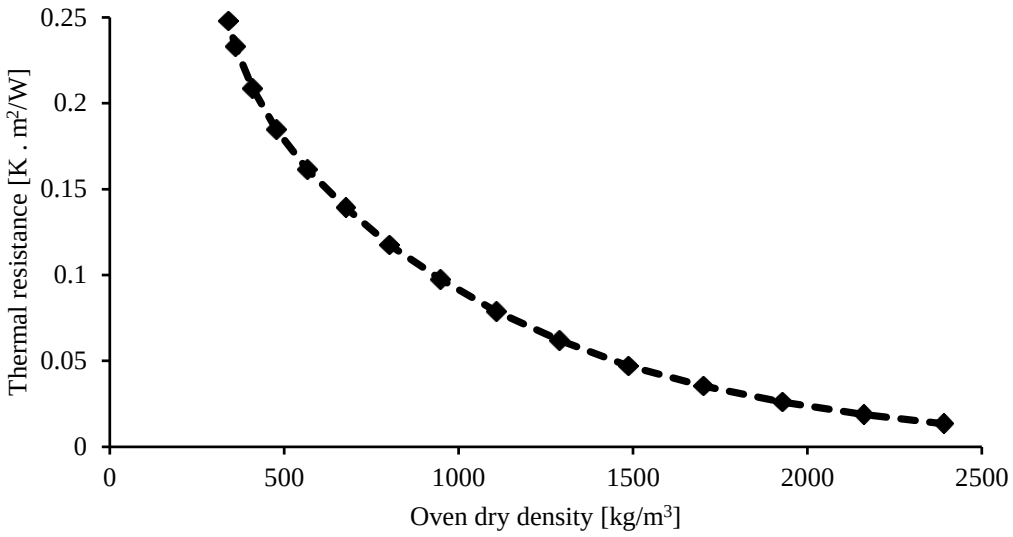

Figure 2.4: Relationship between thermal resistance and oven-dry density (Steiger and Hurd, 1978)

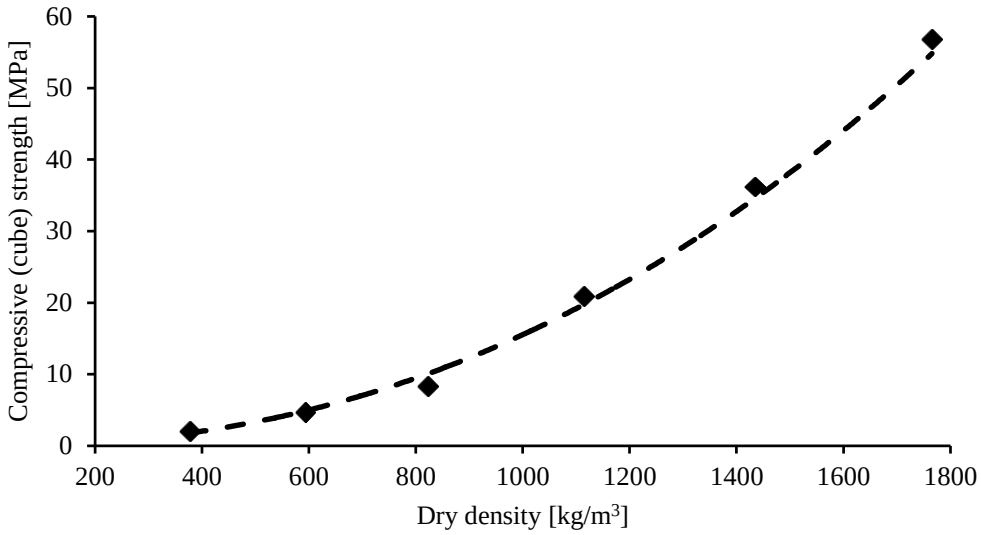

Figure 2.5: Effect of dry density on cube compressive strength (Wee *et al.*, 2006)

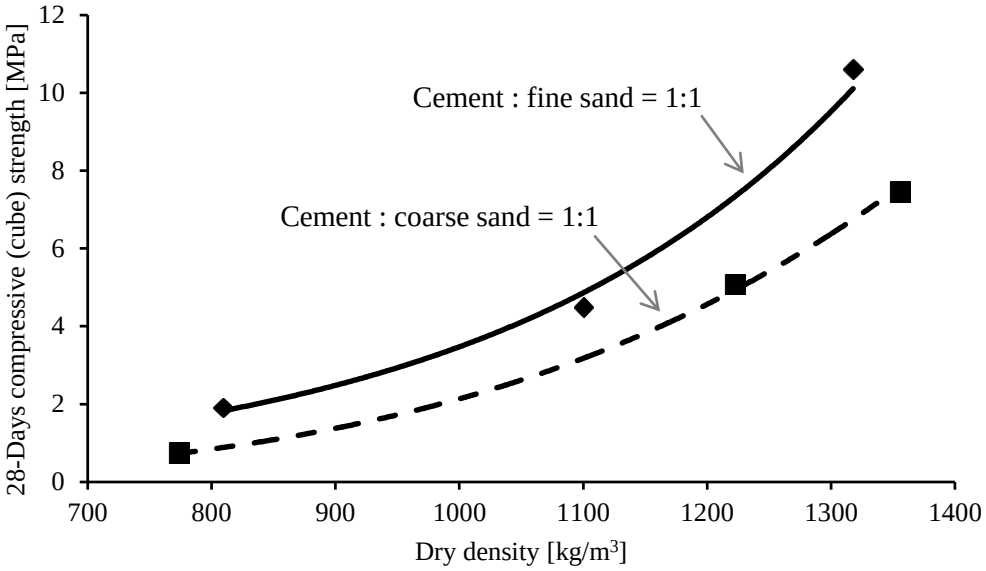

Figure 2.6: Effect of sand fineness of compressive strength
(Nambiar and Ramamurthy, 2006)

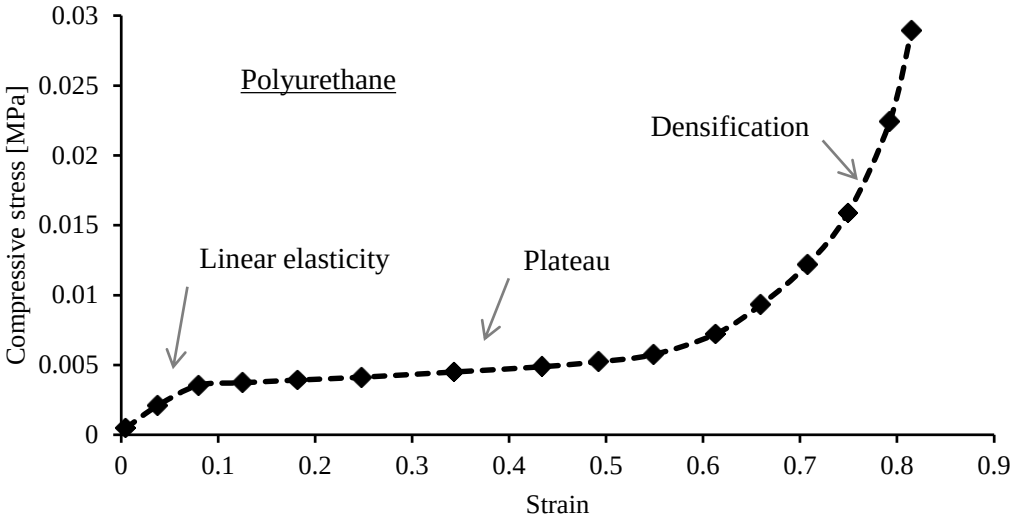

Figure 2.7: Typical stress-strain response of cellular solids under compression
(Gibson and Ashby, 1999)

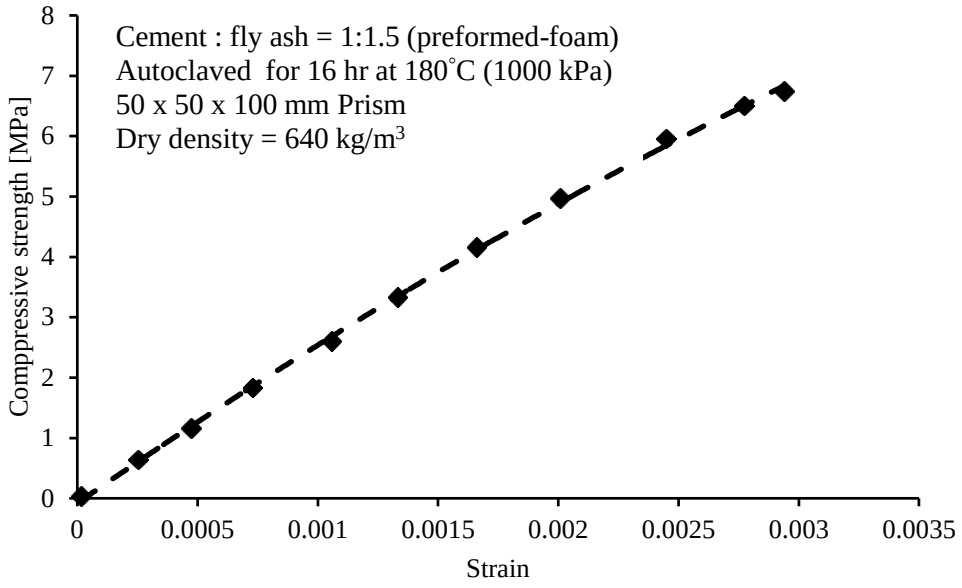

Figure 2.8: Stress-strain response of autoclaved foamed concrete (Valore, 1954)

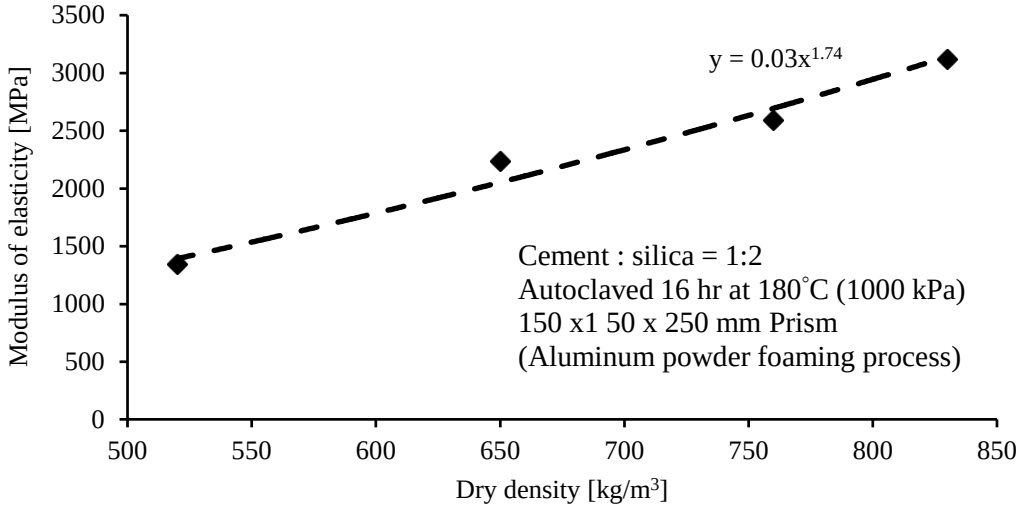

Figure 2.9: Relationship between modulus of elasticity and dry density (Valore, 1954)

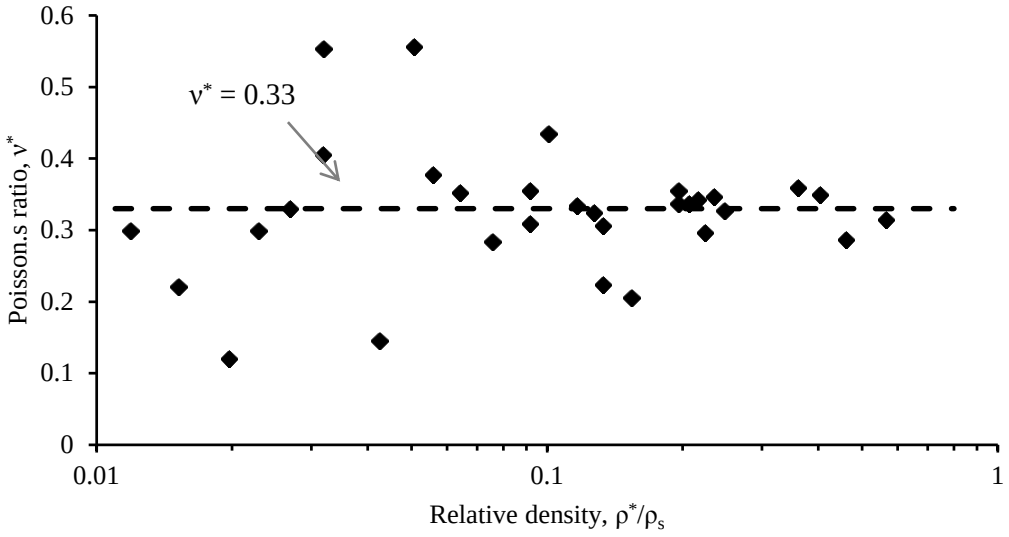

Figure 2.10: Poisson's ratio of cellular solids is independent of relative density (Gibson and Ashby, 1999)

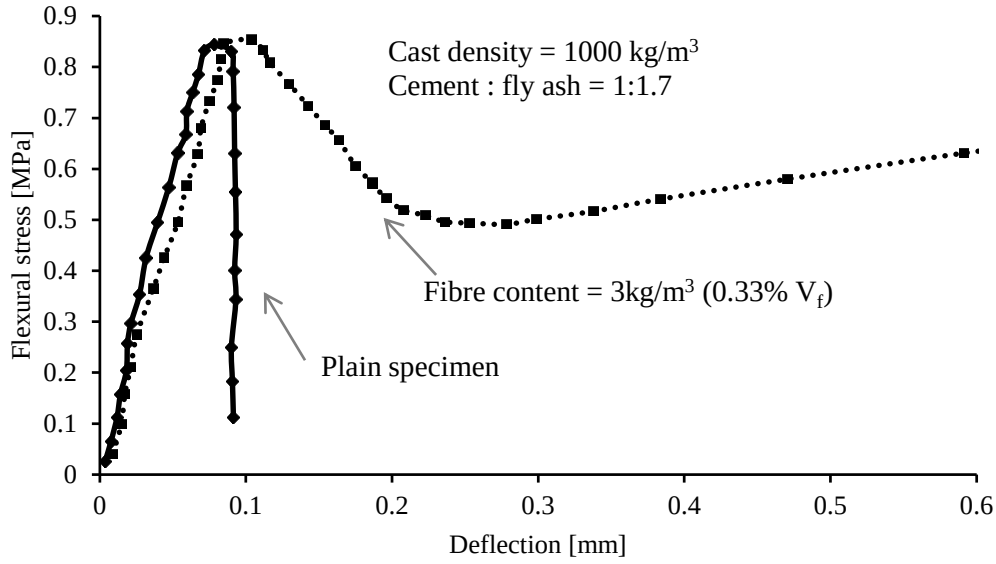

Figure 2.11: Effect of fibre reinforcement on flexural behaviour of foamed concrete (Kearsley and Mostert, 2003)

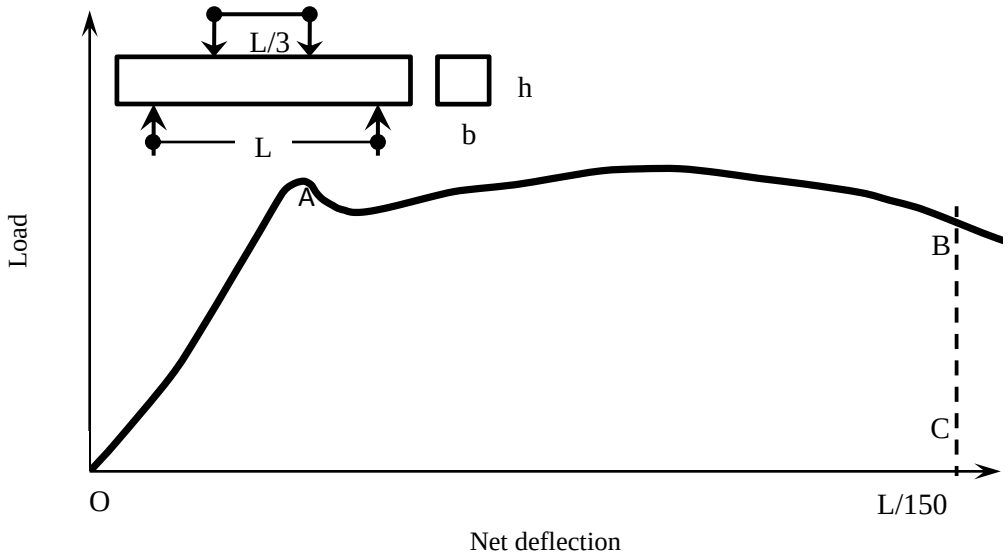

Figure 2.12: Evaluation of toughness parameter

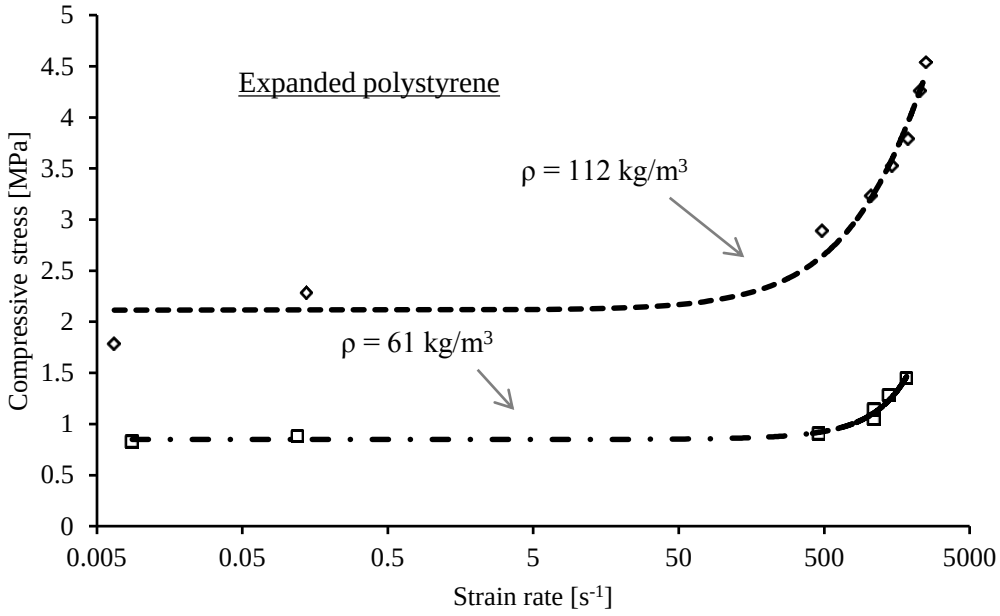

Figure 2.13: Strain rate sensitivity of expanded polystyrene under compression (Ouellet *et al.*, 2006)

Chapter 3

EXPERIMENTAL DETAILS

3.1 General

The mechanical characterization and sulphate resistance of cement-based foams were studied by conducting the experimental program described here. As was described in Chapter 2, the cast density is the principal controlling factor of the mechanical response of cellular cementitious material (Fouad, 2006). A range of cast densities was chosen for this test program based on the most commonly manufactured cement-based foams in the industry. A locally manufactured foaming agent was utilized to prepare the test specimens. The experiments were carried out on six types of mixes for direct compression and flexure. The test devices were chosen carefully, keeping in mind that a low strength material like cement-based foam requires the testing device to be sensitive enough to capture noise free test data at a low loading range.

3.2 Materials and Mixes

3.2.1 Materials

The principal ingredients of cementitious foam are cement, water and stable foam. A proper choice of material depends on the chosen cast density and strength requirement, which is dependent on the intended field of application. Usually, cementitious foam does not contain any fine aggregates, but for a cast density

higher than 1200 kg/m^3 it requires the use of fine aggregates. Coarse aggregates are used very rarely in the production of cement-based foams: If the intended use of certain high density foamed material demands specifically high strength then light weight aggregate may be required.

3.2.2 Portland Cement

The primary binding material of cementitious foam is Portland cement. Generally, Type HE Portland cement is used for the production of cement-based foams. Other types of Portland cement can be used depending on application requirements. For cement-based foams to be used in areas where the structure is susceptible to sulphate attack, special sulphate-resistant cement Type MS or Type HS can be used. Again, cement content in the foamed material may vary depending on the application. The usual range of cement content is 300–500 kg/m^3 (Beningfield *et al.*, 2005). For semi-structural use higher cement content may be required (Jones and McCarthy, 2005). Specimens for this study were cast in an industrial facility in Calgary and then transported to the Civil Engineering materials Laboratory at the University of Alberta after 3 months of curing in an ambient condition. The curing time was deliberately long in order to allow transport of specimens safely to the author's laboratory. The choice of high early strength cement (Type HE) was also in keeping with the need for faster strength gain.

3.2.3 Fly Ash

The utilization of cement blended with fly ash is a very common practice. Cementitious foam composite with cement partially replaced by fly ash reduces autogenous shrinkage (Lee *et al.*, 2003). The use of fly ash may affect the early-strength development, but considering the long-term benefits (i.e. strength), up to 75% of cement can be replaced (Nambiar and Ramamurthy, 2007). The cement-based foams prepared for this study were proportioned with 20% cement replacement. Class C (ASTM C618, 2008) fly ash was utilized in this study.

3.2.4 Foaming agent

The behaviour of cement-based foams is also dependent on the type of foaming agent used. Based on the cellular structure formed by the foaming agent, two types of commercially manufactured foaming agents are available as described in Section 2.2.3. The foaming agent used for this program was of a synthetic type that produces a predominantly closed-cell internal structure. A 3% (by volume) diluted foaming solution was used. Table 3.1 shows the generalized chemical composition of the foaming agent used for this study.

3.2.5 Microfibre

Most industry made foamed cementitious materials are fibre-reinforced. The most common fibre types used in foamed cement composites include glass and polymeric fibre. Unlike with conventional concrete, steel fibres are not

recommended due to their incompatibility with the soft low density cementitious foams. The microfibre reinforced specimens were prepared for this study by using discrete polypropylene fibre. The typical dosage level is 1–4 kg/m^3 of composite volume (Fouad, 2006). Foamed cement composites with fibre content higher than 0.5% (by volume fraction) has been observed to perform poorly (Jones and McCarthy, 2005). In this study the fibre content was 0.2% by volume fraction, V_f (ratio of volume of fibre to that of foamed cement composite). Table 3.2 shows the properties of the polypropylene microfibre used in this program.

3.2.6 Water–binder Ratio

Proper selection of the water–binder ratio is critical to foamed cementitious material. A ratio less than 0.35 can be a source of instability to the foam bubbles (Jones and McCarthy, 2005). The typical value of water–cementitious material ratio is 0.4–0.8. Again, the commercially available foaming agent requires a specified value of water–binder ratio for optimum performance. A ratio of 0.53 was used during the preparation of the specimens in this study.

3.2.7 Density Selection

Cement-based foams can be manufactured with cast density ranging from 400–1600 kg/m^3. For this test program, three cast densities namely 475 kg/m^3, 750 kg/m^3 and 1200 kg/m^3, were selected reflecting the typical manufacturing practice

in Canada. Both plain and microfibre reinforced specimens for all 3 above-mentioned densities were investigated for their mechanical response.

3.2.8 Mix Proportioning

The constituents used in the preparation of cement-based foams for this study are illustrated in Figure 3.1. As mentioned in the Section 2.3, no standardized mix design method is available. Unlike the mix design criteria for regular concrete, the cast density is an important mix design parameter for cement-based foams. Since the chosen density for this investigation is not greater than 1200 kg/m^3, no fine aggregates were required and thus the proportioning of mix ingredients was much simpler. As discussed earlier, cement-based foam is prepared by mixing an appropriate amount of pre-formed foam to a base mix of cementitious material and water slurry (when no fine aggregates are required). Thus, a mix design method involves proportioning a slurry mix and calculating the amount of foam to be added to the slurry. The mix proportion for the specimen used in this study is provided in Table 3.3 and 3.4. Basically, a common slurry mix composition was employed across all densities; naturally the only variation is in the amount of required foam volume. The density of the foam may differ depending on the foam generator. The density of the pre-formed foam was checked before adding it to the base mix. Microfibre-reinforced specimens were prepared by adding the polypropylene fibre at a dosage level of 1.8 kg/m^3 of foamed composite, which is equivalent to 0.2% by volume fraction. This is the most commonly used fibre-volume fraction.

3.2.9 Specimen Preparation

The specimens were prepared in a casting facility in Calgary. Steps involved in the production of foamed cementitious material in a laboratory were the generation of foam, preparation of binder-water slurry and mixing the foam into the slurry. A special foam generator (Figure 3.2) was employed to generate stable foam. The generator was operated by a 100 psi (0.7MPa) pressurized air source. The generator draws a 3% diluted foaming solution, mixes it rigorously in a mixing chamber and then forces it to pass through a nozzle by air pressure. The aerated foaming solution comes out of the nozzle as stable foam (Figure 3.3). Before addition to the slurry, the foam so generated was checked by measuring its density. It is to be noted that the size of the foam bubble was not measured in this study. However, a measure of void sizes was obtained from Figure 5.9 and 5.10 in Chapter 5. The cement-water slurry was prepared by mixing cement and fly ash to the water gradually (Figure 3.4). A rotary type hand mixer was utilized. The slurry was then checked for flow values with the aid of the Marsh cone flow testing device, which measures flow characteristics as the time required for 350 mL of slurry to pass through the Marsh cone. To achieve a cast density of 475 kg/m^3, 750 kg/m^3 and 1200 kg/m^3, the Marsh cone flow was found to be 45 s, 90 s and 120 s, respectively. The slurry was then placed into a rotary type drum mixer (Figure 3.5) and subsequently a measured amount of fibre was dispersed in the slurry. While keeping the mixer machine rotating, foam was added a little bit at a time to ensure proper mixing. At the same time, foamed composites were checked intermittently for cast density. Foam mixing was continued until the target cast

density was reached. Machine rotation continued until all visible foams were mixed. Mixing time was carefully controlled so as to avoid loss of internal bubble structure due to excessive rotation by checking the cast density frequently.

All test specimens for each cast density were prepared from the same batch of material. Specimens for the flexural test were sawn into a prismatic shape with dimensions of 100 x 100 x 350 mm from 1000 mm long beam (150 x 150 mm cross section) specimens. Table 3.5 summarizes the dimensions of the specimens employed in this test program. Compression test specimens were prepared from specimens tested under quasi-static flexure. Cylinders of 50 mm diameter and 100 mm height were cored from the broken halves of flexural specimens (Figure 3.6). Specimens were cored in accordance with ASTM C42 (2004). ASTM C42 requires a length to diameter (L/D) ratio of at least 1.75 for cored cylinders and an appropriate correction factor has to be applied when calculating compressive strength if the L/D ratio is ≤ 1.75. Since in this study the cored cylinders have an L/D ratio equal to 2, no correction factor was needed. The ends of the cored cylinders were sawn to get a flat and perpendicular surface to the longitudinal axis. Specimens were then sulphur capped to ensure the requirement of ASTM C617 (2009).

In order to investigate the performance of cementitious foams exposed to sulphate attack, eleven series of prismatic specimens from each mix were prepared. The dimensions of the prism were selected to be 50 x 50 x 200 mm. These prisms

were sawn from a bigger beam specimen of dimensions 150 x 150 x 1000 mm. Two sets of prisms were tested under flexure after each specified period of immersion in a sulphate and water bath, respectively. The tested (flexure) specimens were further sawn into cube specimens of 50 x 50 mm from the intact portion of the broken halves. These cubes were then tested under compression.

3.3 Test Setup for Mechanical Characterization

In order to get the mechanical response of the cement-based foams, two general test methods were chosen — to generate quasi-static and impact loading. Two loading configurations were also selected under quasi-static loading – compression and flexure. The experimental setups were prepared in accordance with relevant available test standards or techniques cited in the literature.

3.3.1 Quasi-static Test

3.3.1.1 Compression Test

Compression tests were conducted as per ASTM C469 (2002). As mentioned earlier, cored cylinders were used for evaluation. These cylinders were tested in two separate machines. The lowest density cylinder resists such a small amount of load that it requires a low capacity test machine. Use of a regular concrete crusher was not feasible since such machines are not calibrated for such a small loading range. Therefore, a screw-type displacement-control machine with a sensitive load cell with a loading capacity of 12 kN was selected for cylinders of 475 kg/m^3 cast

density. The load cell and stroke of the testing device were properly calibrated before conducting tests. Calibration charts are presented in the Appendix at the end of the thesis. The cylinders of cast densities 750 and 1200 kg/m^3 were tested on a servo-hydraulic machine with a loading capacity of 1000 kN. A special yoke system was prepared for this program which allows attachment of a transverse displacement measuring device. Altogether the yoke system was equipped with five Linear Variable Displacement Transducers (LVDT). In all cases, three LVDTs were placed 120° about the longitudinal axis to capture axial displacements together with two other LVDTs attached in a transverse direction to capture radial displacements. The test arrangements are shown in Figure 3.7. A displacement-control test configuration was set for all cases. In order to obtain the load and displacement history, a continuous-record data acquisition system was utilized. The sampling rate was set to 5Hz. The displacement rate was set to 1.25 mm/min, conforming to the displacement rate recommended by the test standard. Four cored specimens from each mix were tested.

3.3.1.2 Flexure Test

Flexure tests on cementitious foams were conducted using a four-point bending configuration. The tests were carried out in accordance with ASTM C1609 (2007). The testing machine employed for the flexure tests was a screw-driven machine (Figure 3.8), as described in the previous section, that was suitable for applying loads for all types of specimens. Specimen dimensions were 100 x 100 x 350 mm with an effective span of 300 mm. Specimens were notched with a depth

of 12.5 mm and width of 2 mm for the purpose of fracture analysis to be conducted at a future date (not within the scope of the current study). A yoke was fabricated in accordance with JSCE G-552 (1999). As shown in Figure 3.9, the yoke was installed around the specimens to attach LVDTs, one on either side. This yoke ensured that the displacement measured was that of the neutral axis and eliminated any errors due to support settlement. Use of two LDVTs on either side facilitates in minimizing errors resulting from twist in the specimen during test. Tests were performed using the displacement control method. The displacement rate was set to 0.10 mm/min, conforming to the requirements of ASTM C1609. The load and displacement histories were recorded with the aid of electronic data acquisition system at a sampling rate of 5 Hz.

3.3.2 Impact Test

No standardized test method is available for impact testing. As described in Chapter 2, the two most widely used methods are the Split Hopkinson Pressure Bar system and the instrumented drop-weight system. In this study, a drop-weight impact testing machine was used to conduct tests on cementitious foams, to study behaviour under high strain rates. This instrumented impact testing device allows for the capture of the full response history necessary to analyze material response. The drop-weight hammer of 62 kg has a maximum height capacity of 2.3 m and thus is capable of producing a maximum of 1.0 KJ impact energy (after accounting for friction in the guard rail) when the blade is released onto the mid-span of the flexural specimen. The support anvil is adjustable for

span length ranging from 200 to 600 mm. For this test prismatic specimens of 100 x 100 x 350 mm with effective span of 300 mm. A notch of 12.5 mm depth and 2 mm width was placed at the mid span of the specimen to study fracture behaviour (which is not within the scope of the present study).

Specimens were tested for two loading rates by selecting two separate drop heights — 250 mm and 500 mm. For the 250 mm drop height, the associated impact energy is 152 J with blade velocity of 2.20 m/s. Similarly a drop height of 500mm is capable of producing 304 J impact energy with blade velocity of 3.13 m/s. These numbers do not consider friction. In order to capture a very short duration event like impact (several milliseconds), high-frequency data acquisition system was required. As part of the data-acquisition system load cell, an accelerometer and high-speed cameras were utilized. A bridge load was attached to the striking end of the blade to capture the pulse between hammer and specimen upon contact with the specimen. An accelerometer was attached under the specimen adjacent to the notch to record the mid-span acceleration during impact. A PVC block was attached to the specimen by using epoxy, which served as a holder for the accelerometer. A five-channel data-acquisition system was used to record test data. The data acquisition rate for the load cell and accelerometer was selected as 100,000 Hz, which is sufficient enough to get the full history without losing any critical data points. Also, two high-speed cameras were placed at an obtuse angle to facilitate 3D imaging. The captured images were analyzed later using image correlation technology to obtain the displacement

history. The image resolution was at least 192 x 256 pixel, which is adequate for analysis. At this resolution, the cameras were capable of capturing images at a rate of 10,000 frames per second. This instrumented system was equipped with an infrared sensor, which served as a triggering device. The sensor was placed 2 mm above the top surface of the specimen. As soon as the striking edge of the blade crossed the sensor's optical path the devices were triggered immediately. The trigger caused the electrical signal to drop from 4.5 volts to 0 upon a break in the infrared path. The use of the sensor helped synchronize all the raw data within the same time frame. Figures 3.10–3.12 show the detailed experimental setup. Three specimens were tested from each mix for each loading rate.

3.4 Test Setup for Evaluating Sulphate Resistance

The effect of an adverse sulphate environment on cement-based foams was evaluated through their mechanical performance in flexure and compression. It was recognized that standard testing techniques such as ASTM C452 (ASTM, 2006) or ASTM C1012 (ASTM, 2009), which are used to assess the sulphate resistance of conventional cement-based composites, would not reflect the distress in low-strength cement-based materials such as foams. For one, the length change measurement is hard to make with the compressive strength being so low. For another, the source of sulphate attack is by far through external ingress and not through internal generation as envisaged by ASTM C452 (ASTM, 2006). Therefore, it was decided that while the testing conditions would be simulated as per ASTM C1012 (ASTM, 2004), the interpretation of the effect of sulphate

exposure should be determined differently from that adopted by this standard. Accordingly, a sodium sulphate bath was prepared in which the specimens were immersed and later extracted to be tested in flexure. In order to facilitate the flexural tests, the cross-section of the prism specimens was chosen to be larger than that specified in ASTM C1012 (ASTM, 2004). Figure 3.13 shows specimens immersed in the sulphate bath.

3.4.1 Immersion in Sulphate Solution and Water Bath

In order to capture changes to the cement-based foams due to submersion in a liquid, a companion series was examined after immersion in water. For each cast density and fibre content, 15 prisms were immersed in a bath of sulphate solution and 15 more in a water bath. The sulphate solution was made with Na_2SO4 with a concentration of 50g/L in accordance with ASTM C1012 (ASTM, 2004). The temperature of the sulphate bath was about 23^oC and the pH value was measured to be 6.5 which is within the range specified by the ASTM C1012 (ASTM, 2004). Three prisms were left unexposed to either water or sulphates, to form a reference data set. For each set, the prisms were submerged in the water or sulphate bath for up to 90 days. Three prisms were taken out for subsequent mechanical tests at 7, 15, 30, 60, and 90 days of immersion. A visual examination was made of all prisms before immersing them into the bath. This was repeated at each stage of exposure prior to the mechanical tests to record the onset of what evolved into map cracking.

3.4.2 Compression and Flexural Tests

Compression tests on cube specimens prepared from specimens tested under flexure were conducted using a compression test machine with a capacity of 3000 kN (Figure 3.14). Three specimens were tested from each mix after each stage of immersion in the sulphate solution and water. A fresh series of cubes (not exposed to sulphate or water) was also tested to serve as a control group. The tests were carried out as per ASTM C109 (ASTM, 2008). This was done in order to examine the variation in compressive strength with exposure to sulphates and relate that to the flexural response.

The specimens extracted from both the sulphate solution and the water bath were tested subsequently under four-point bending using the exact same test facility as described in section 3.3. A typical experimental setup is shown in Figure 3.15. Experimental details for this quasi-static flexural test were the same as described earlier. The data was collected till the mid-span deflection reached a value of 150^{th} of the clear span (or 1 mm in this case).

3.4.3 Scanning Electron Microscopy

At every stage of testing (i.e. corresponding to the six time steps of immersion into sulphate or water bath), a random sample from each mix was examined under the Scanning Electron Microscope (SEM) to observe changes, if any, in the microstructure. Scanning electron microscopy is usually performed in a high

vacuum, as molecules in the air interfere with the electron beam. Specimens were exposed to room temperature until they were sufficiently dry for the Sputter, a machine used to apply gold coating, to work properly. A layer of gold was then deposited evenly onto the specimen surface with a thickness of 10–20 nm (Figure 3.16). This gold coating essentially acts as a reflective surface for the electron beam. Finally, specimens were placed under the microscope and high-resolution images were taken at a desired location with 100X, 1000X and 10000X magnifications.

3.4.4 X-Ray Diffraction

Finely powdered dust from an adjacent portion of the viewed specimen was scanned using the X-Ray Diffraction (XRD) technique to identify the chief crystalline products as evidence of any change in the internal composition. The scanning processes were conducted using copper radiation. The target hydration products were Portlandite (P), Gypsum (G), Ettringite (E) and Calcite (C). Figure 3.17 shows powdered specimens for X-Ray diffraction.

Table 3.1: Composition of synthetic foaming agent

Ingredient	Weight (%)
Fatty Alcohol	1-10
Alcohol	6.5-35
Fatty Acid	10-65

Table 3.2: Properties of polypropylene fibre

Length	20 mm
Denier	3
Specific gravity	0.91
Ultimate strength	550 MPa
Elastic modulus	3.5 GPa

Table 3.3: Slurry mix proportions of foamed concrete

Cast density (kg/m^3)	Cement (kg/m^3)	Fly ash (kg/m^3)	Water (kg/m^3)	Fibre content (kg/m^3)	Foaming agent	Foam volume (%)
1200 -plain	900	230	600	0.0	CF-1	31.4
1200 -fibre	900	230	600	1.8	CF-1	31.4
750 -plain	900	230	600	0.0	CF-1	57.8
750 -fibre	900	230	600	1.8	CF-1	57.8
475 -plain	900	230	600	0.0	CF-1	74.0
475 -fibre	900	230	600	1.8	CF-1	74.0

Water-to-binder ratio = 0.53; Foam density = 33 kg/m^3

Table 3.4: Cement content in foamed composite

Cast density (kg/m^3)	Expansion ratio	Cement content (kg/m^3 of slurry)	Cement content (kg/m^3 of composite)
1200	1.43	900	630
750	2.3	900	390
475	3.6	900	250

Table 3.5: Test specimens

Test	Preparation	Method	Dimension (mm)
Compression	Cored cylinder	ASTM C469	50 x 100
Compression	Sawn cube	ASTM C42	50 x 50
4 Point bending	Sawn prism	ASTM C1609	100 x 100 x 350
4 Point bending	Sawn prism	ASTM C1609	50 x 50 x 200
3 Point bending	Sawn prism	Drop-weight impact	100 x 100 x 350

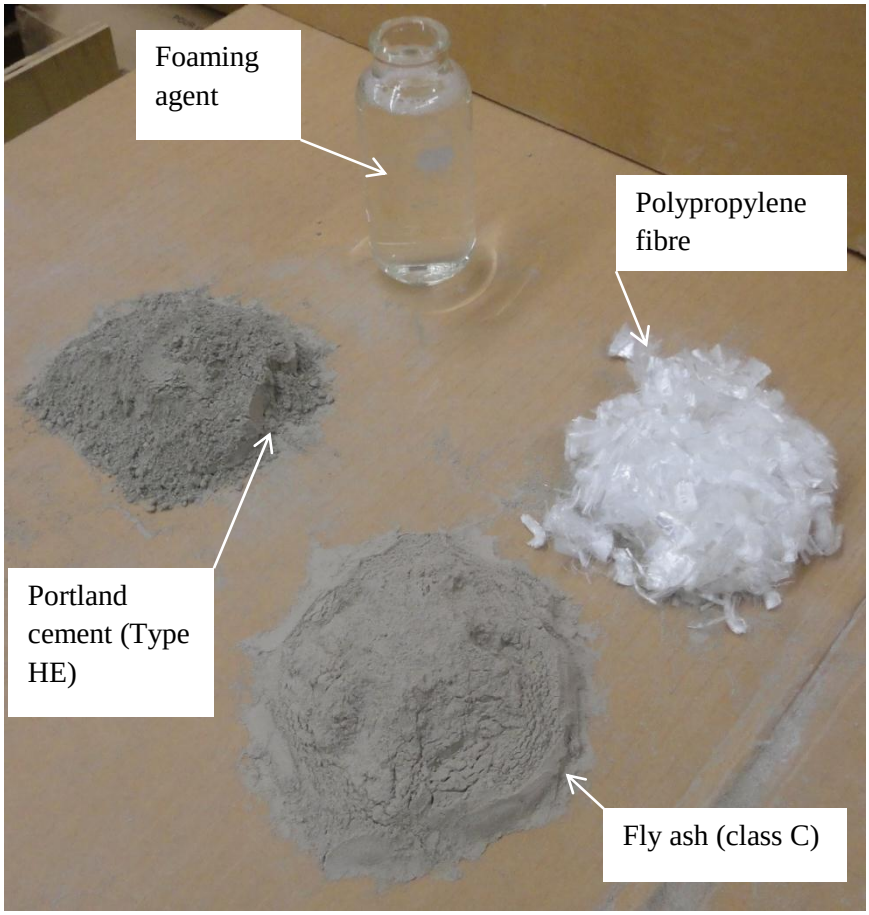

Figure 3.1: Mix constituents of cement-based foams

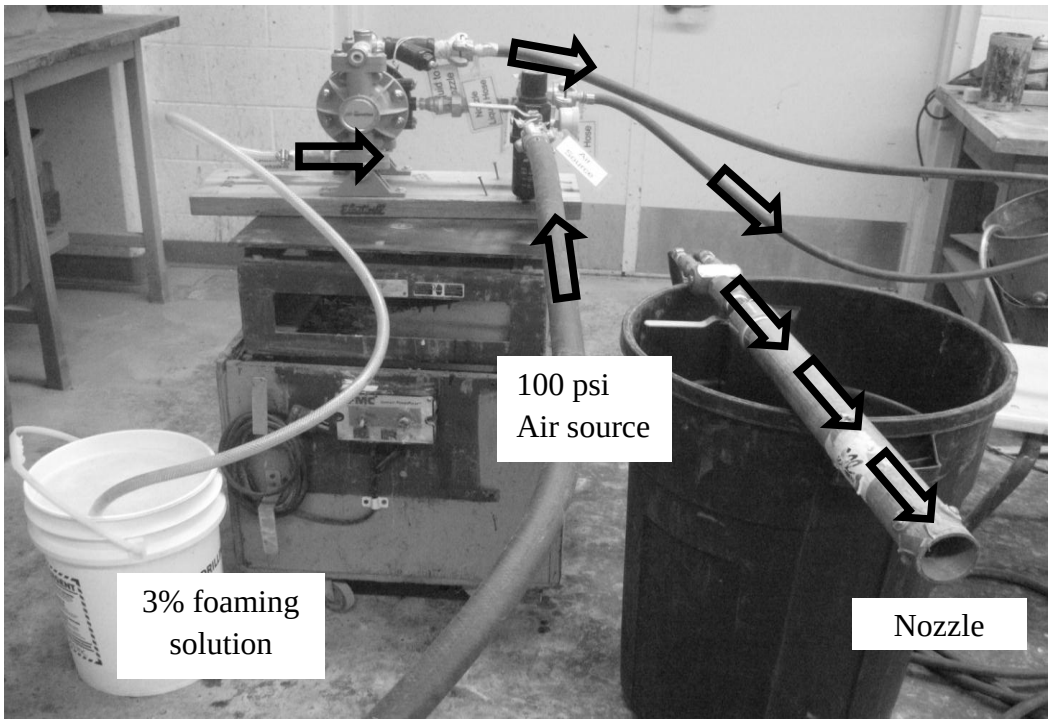

Figure 3.2: Foam generator used to prepare specimens for this program

Figure 3.3: Stable foams coming out through the nozzle

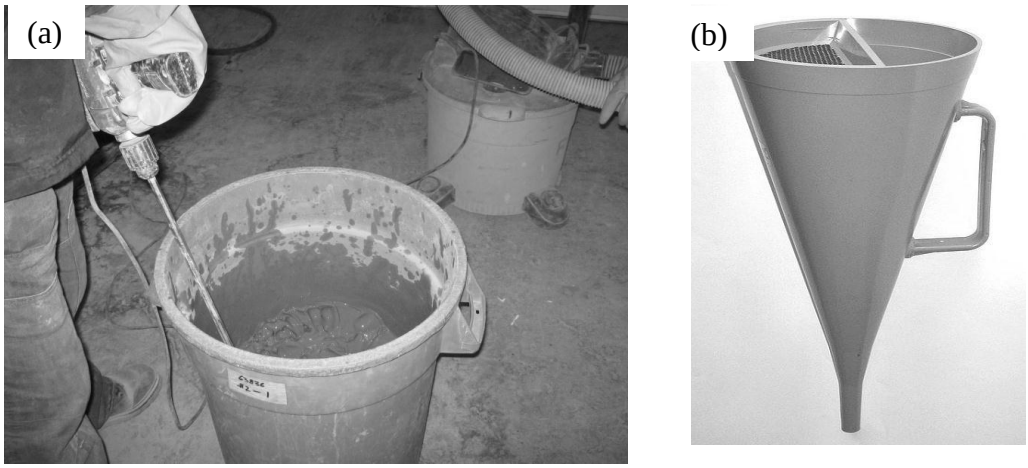

Figure 3.4: Preparation of slurry (a); Marsh Flow Cone (b)

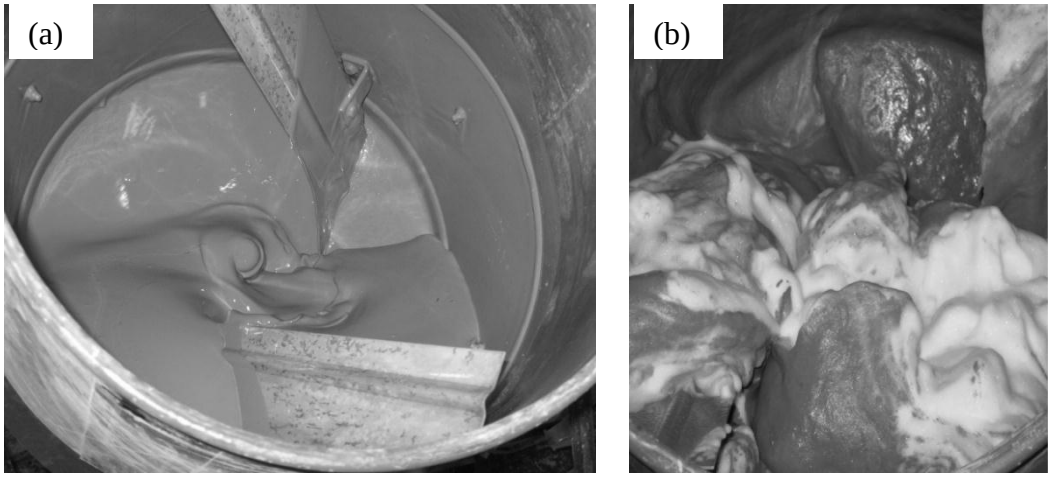

Figure 3.5: Slurry in the drum mixer before addition of foam (a); Foam is added to the slurry (b)

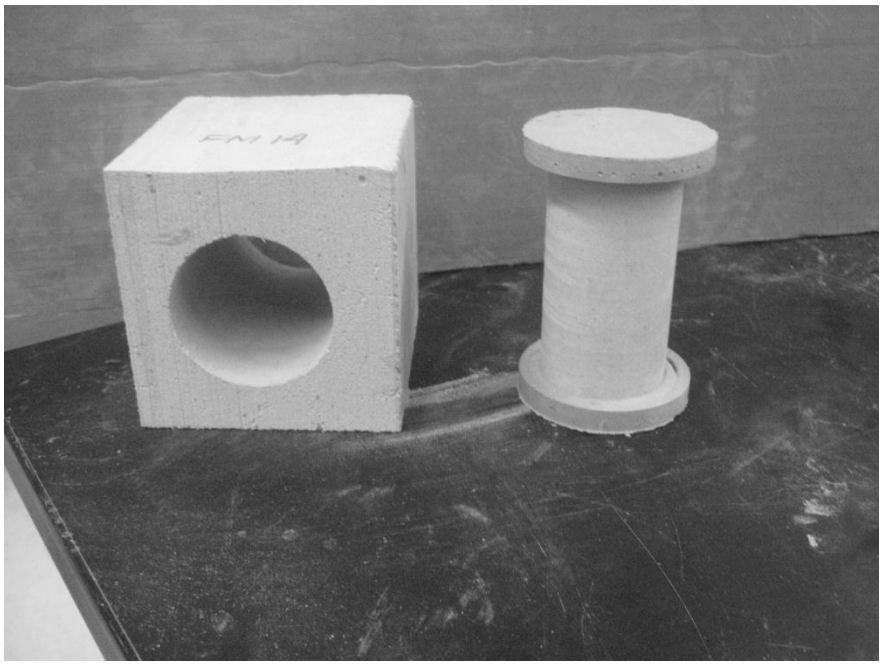

Figure 3.6: Cored cylindrical specimen for compression test

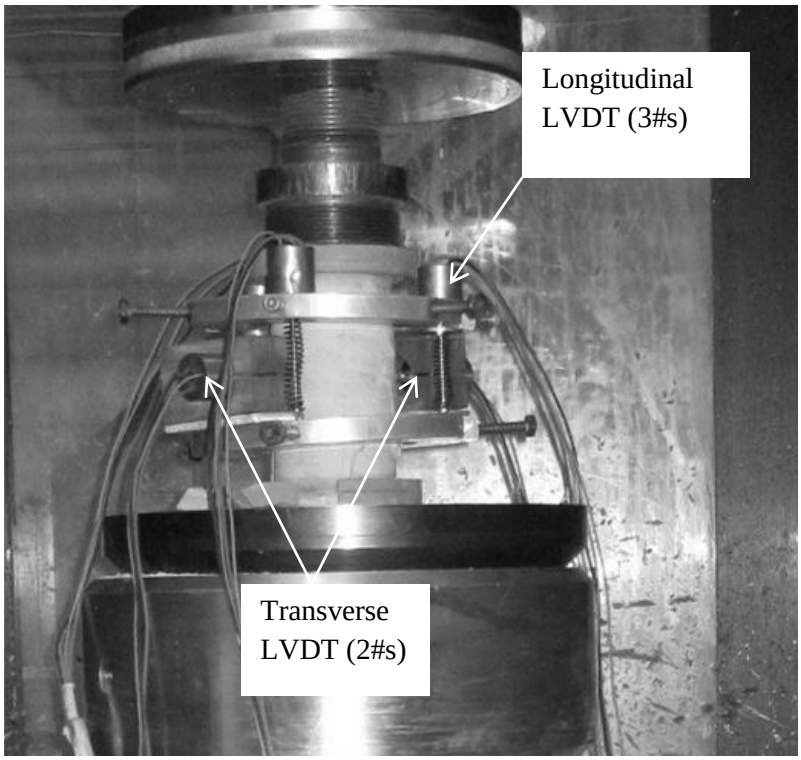

Figure 3.7: Quasi-static compression test setup

Figure 3.8: Screw-type test machine used for compression and quasi-static flexure test

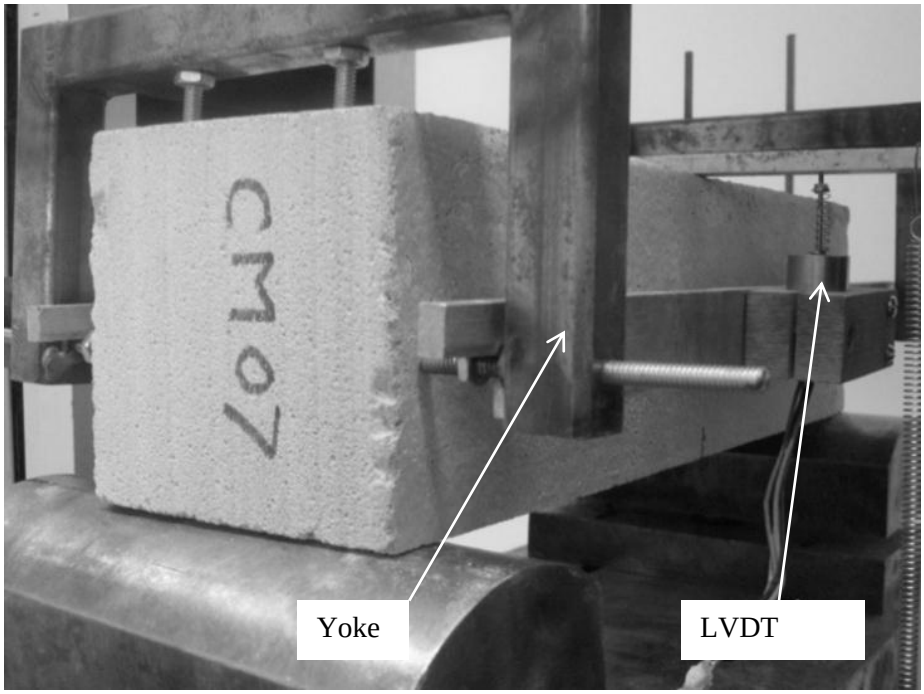

Figure 3.9: Quasi-static flexural test setup

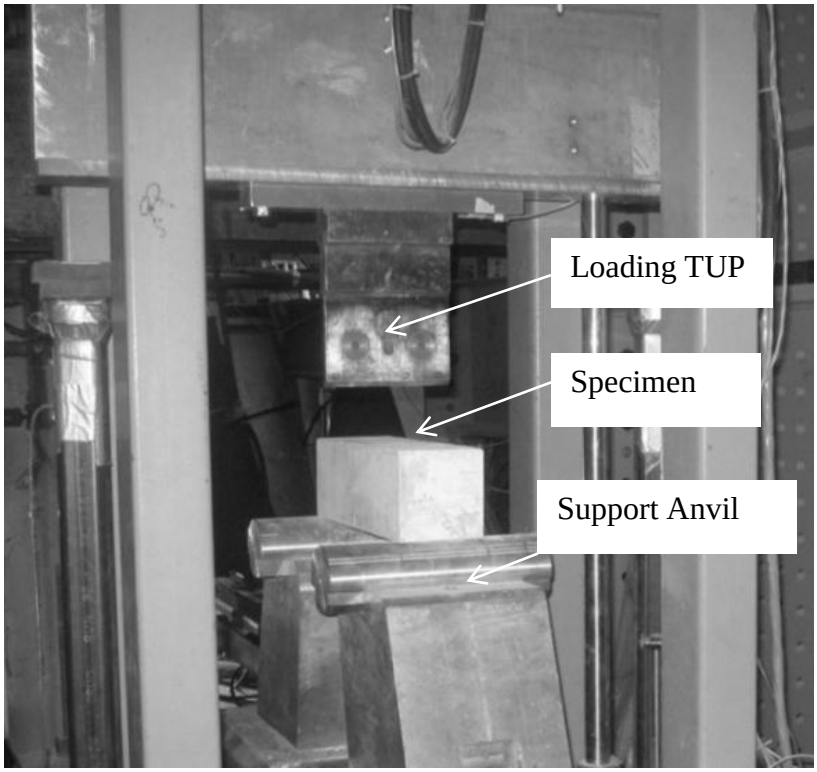

Figure 3.10: Drop-weight impact test machine

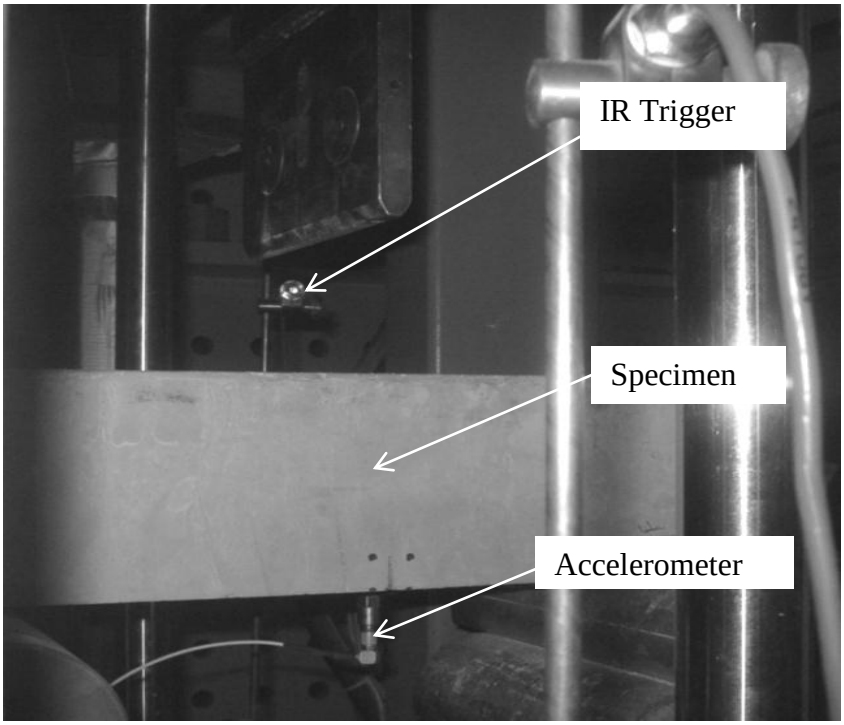

Figure 3.11: Instrumentation for drop-weight impact machine

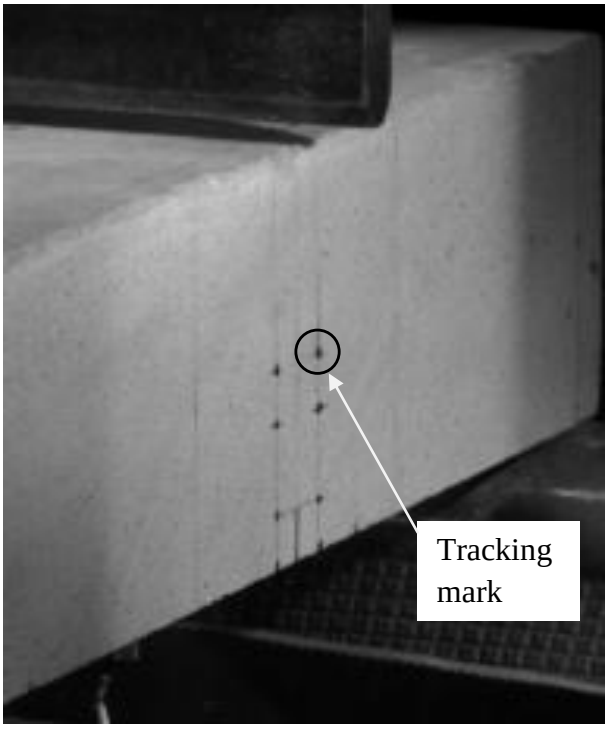

Figure 3.12: Drop-weight impact specimen showing tracking mark later used to analyze image

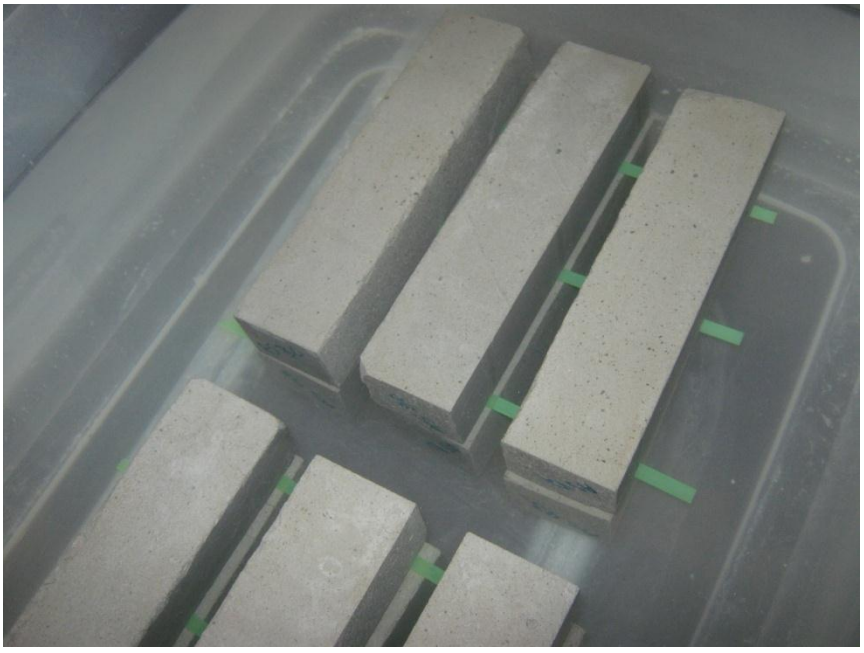

Figure 3.13: Specimens immersed in sodium sulphate bath

Figure 3.14: Compression test on cube specimens

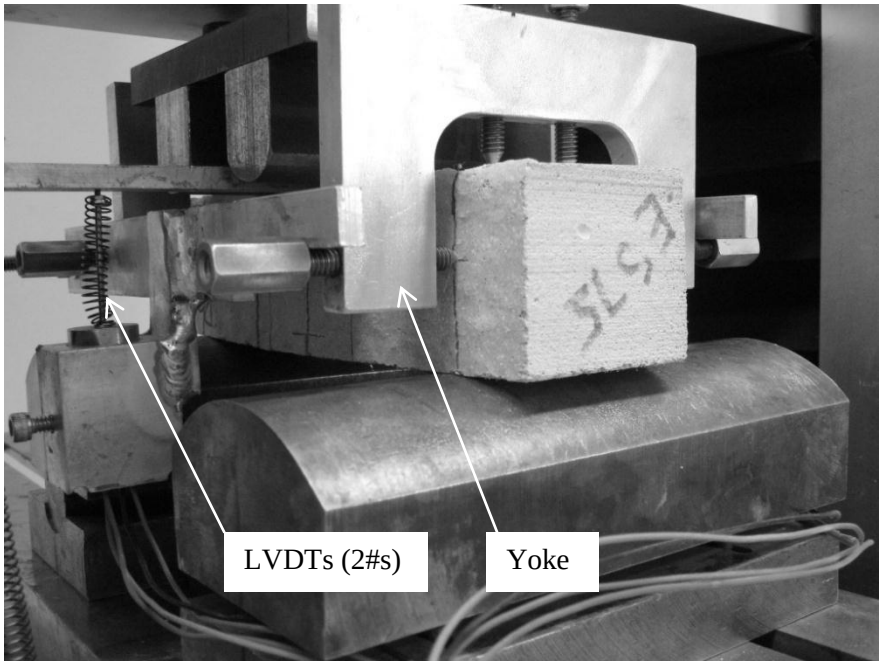

Figure 3.15: Quasi-static flexural test on prisms extracted from sulphate or water bath

Figure 3.16: Specimens coated with gold for Scanning Electron Microscopy

Figure 3.17: Powdered specimens used in X-Ray Diffraction

Chapter 4

QUASI-STATIC AND DYNAMIC EVALUATION, PART 1: EXPERIMENTAL RESULTS

4.1 General

The results of mechanical tests conducted in this research program are presented in this chapter. Recall that specimens were cast at three densities from 475–1200 kg/m^3. As mentioned in the previous chapter, the test program included three tests: quasi-static compression of cylindrical specimens, quasi-static four-point bending and three-point flexure under impact on prismatic specimens. The raw test data were processed to get the response histories. In order to get stress-strain or load-displacement data, the processed response histories were combined to the same time stamp. For each test configuration, a minimum of three specimens were tested. These responses were then averaged by taking the ordinates from each specimen corresponding to a selected set of abscissa. The mechanical responses presented here are the representative average results. The statistical variations are reported in terms of the coefficient of variation.

4.2 Quasi-static Response

4.2.1 Compressive Response

The three plain and three fibre-reinforced mixes were tested under direct compression conforming to ASTM C469 (ASTM 2002). As mentioned in Chapter 3, Section 3.2.9, cored cylindrical specimens of 50 mm diameter and a height of

100 mm from cast densities of 1200, 750 and 475 kg/m^3 were tested. In order to capture the full response history, the tests were continued until a near-zero resistance from the specimens. The longitudinal displacement was evaluated by averaging data from three displacement-transducers attached vertically to the yoke system. On the other hand, the transverse displacement was evaluated by taking the algebraic sum of the deformation recorded by the two transverse displacement-transducers. The longitudinal strain was evaluated from the displacement using a gauge length of 50 mm. The transverse strain was determined from displacement by taking the average diameter of the specimen as the gauge length.

The observed fracture patterns were categorized using the schematic diagram shown in Figure 4.1 as per ASTM C39 (ASTM, 2009). Figure 4.2 shows the representative failure pattern for the lightest category of plain cement-based foams with cast density of 475 kg/m^3. The formation of a columnar vertical splitting crack was observed, which falls under the Type 3 fracture pattern as mentioned in ASTM C39 (ASTM, 2009). Cracking initiated at the top of the specimen and propagated to the bottom. The type of failure observed in specimens of higher (ρ > 475 kg/m^3) cast densities was different from that seen in the lightest mix. As can be seen from Figure 4.3, failure initiated at a location in the top third and cracked diagonally to the bottom. This fracture pattern is categorized as Type 4 in ASTM C39, which may be described as diagonal fracture with no cracking through the ends. The two halves of the diagonally-failed tested specimen shown

in Figure 4.3 were fairly typical of specimens with cast densities of 750 and 1200 kg/m^3. The shifting of the failure pattern from vertical cracking to diagonal fracture may be the result of increased resistance offered by heavier cementitious foams.

Figure 4.4 shows a representative failure pattern of the fibre-reinforced specimens subjected to compressive load. The failure pattern can be described as vertical splitting which falls under ASTM Type 3 fracture pattern. The efficiency of polypropylene fibre was observed in terms of post-peak behaviour in the lightest mix, whereas fibre reinforced specimens with 1200 and 750 kg/m^3 densities crushed almost at the time they reached peak resistance. The stress-strain response of plain and fibre-reinforced cement-based foams is presented in Figures 4.5 and 4.6 respectively. As expected, the peak strains were increased with the increase in cast density. It is noticeable that the peak strain in the specimen with cast density of 750 kg/m^3 decreased due to the presence of microfibres and this was unusual. The presence of fibre slightly improved the compressive strength of the heaviest mix (Figure 4.7), whereas in the case of the lighter specimens the compressive strength decreased, which was more pronounced in the mix with cast density of 475 kg/m^3, which may be attributed to the weaker cell wall resembling “broken egg-shell” in the fibre-reinforced foams.

4.2.2 Flexural Response

Quasi-static flexural tests were conducted on prismatic plain and fibre-reinforced specimens. The midspan deflection was evaluated by taking the average of the data recorded by two LVDTs. Load-deflection behaviour of plain specimens is presented in Figure 4.8. The peak flexural load was reached at a total midspan deflection ranging from 0.06–0.08 mm. Figure 4.9 shows representative tested specimens in the plain category. In most cases, the crack propagation initiated at the crack tip and advanced to the top causing the specimen to fail suddenly. In some cases the failure path did not follow the notch placed at the midspan. However, failure initiated from a location within the middle third of the effective span. The response of fibre-reinforced cementitious foams is shown in Figure 4.10. All flexural tests were continued up to a deflection of 150^{th} of the effective span, or 2 mm in this case. It is noticeable that the heavier ($\rho \geq 750$ kg/m^3) specimens showed a sudden drop in bending load resistance after reaching the peak. Mixes with a cast density of 1200 kg/m^3 showed a drop in load to 22% of the peak load. In the case of the mix with cast density of 750 kg/m^3, the peak load dropped to a level of 33% of peak load. On the other hand, the lightest mix showed no significant drop. In all mixes, the post-peak resistance appears to be constant until the end of the test. Figure 4.11 summarizes the flexural strength, which shows enhancements in the modulus of rupture due to the presence of microfibre. It is also noticeable that the lightest mix shows significant improvement in flexural strength compared to the other two mix categories. Figure 4.12 shows a representative picture of the tested specimens with polymeric

microfibres, which demonstrates the improved integrity of cement-based foams when microfibres are added to the mix. It is noticeable that the fibres are capable of bridging the crack as the two halves of the prism are still connected. Table 4.2 summarizes the flexural strength under quasi-static loading.

4.3 Impact Response

The raw test data from each drop-weight impact test was captured as acceleration history from the accelerometer, the history of the tup, the trigger data and a sequence of images for the duration of the event. The data was captured at a frequency of 100,000 Hz for both the load cell and the accelerometer. In order to get noise-free data, an appropriate loading scale was set during data acquisition. On the other hand, high-speed cameras were configured to capture images during impact event at a rate of 10,000 images per second. The use of a trigger timing point helped extract response history from a fairly large amount of raw data.

As discussed in Chapter 3, Section 3.2, the acceleration was recorded by a piezoelectric accelerometer attached underneath the test specimen. The data collected by the piezoelectric device was dependent on specimen orientation during impact event, therefore a correction factor was applied to get the vertical component of the acceleration. Besides this direct measurement, the acceleration data were also derived from two other sources namely the bridge load cell attached to the striking blade and the high speed images. The cameras record displacements and the acceleration was derived using Correlation Image

technology with the aid of a commercial software named TEMA (TEMA, 2009). Figures 4.13–4.18 show the acceleration histories for the plain cement-based foams. Note that the accelerometer data yields uniformly higher values than those from either the load cell or the image analysis. The acceleration history of fibre-reinforced specimens is shown in Figures 4.19–4.24. In most cases the data from the blade load cell and image analysis are in good agreement. The midspan acceleration as derived by the accelerometer is known to be higher than that seen by the load cell. However, the results from this study are somewhat in contradiction to the data by Chan and Bindiganavile (2010) who found that the image analysis correlates well with the acceleration as derived from the accelerometer. The difference between the data captured by accelerometer and camera may be attributed to the difference in the data acquisition rate. The use of low sampling rate may result in a failure to capture critical data points. Primarily, acceleration recorded by the accelerometer was used to derive load-deflection response from raw data. In very few cases the accelerometer was not able to capture data probably due to issues associated with the epoxy used to connect it with the specimen. In those cases the acceleration data were derived from the blade load cell. The midspan deflection of the prisms tested under impact was derived by integrating the vertical component of the acceleration. Figures 4.25-4.27 show the typical deflection histories derived from all three sources. If the deflection as derived from the accelerometer is compared with that from the other two sources, it is seen that the difference is generally increasing with time, which is more pronounced for mixes with cast density of 1200 kg/m^3.

The study of high strain-rate sensitivity requires test data from multiple drop heights. All six mixes as listed in Table 3.3 were tested using two drop heights — 250 and 500 mm. As mentioned in Chapter 2, the inertial load was deducted from the total load to get the effective bending load by using Equation 2.15 (Banthia *et al.*, 1989). Figures 4.28 and 4.29 show the load-deflection response of plain and fibre-reinforced specimens for a drop height of 250 mm, respectively. One sees that the fibre-reinforced specimens have higher peak loads than the plain specimens for the denser mixes (cast density $\geq$ 750 kg/m^3). The effect of fibre-reinforcement was not pronounced in the lightest mix. Usually, higher strength matrices offer better fibre pull-out resistance and stronger bond (Bindiganavile and Banthia, 2005), which might be the reason behind fibre inefficiency in the lightest mix. The response of cement-based foam to impact loading corresponding to a 500 mm drop height is shown in Figures 4.30 and 4.31. Almost all types of specimens showed considerable increase in peak load when subjected to higher impact loading. It is clear from the load-deflection response that post-peak behaviour was more pronounced in lower-density cementitious foams. In Tables 4.3 and 4.4 the flexural strength for impact loading is presented. It is clear that the lighter mixes do not show significant enhancement in load resistance with increase in impact energy. Figures 4.32–4.35 show the representative tested specimens after testing under impact. It was observed that failure initiated at the notch and propagated almost vertically to the top of the specimen. In all cases, about 8-10 mm length of fibre was observed at the failure section sticking out of the matrix, which may be attributed to fibre pull-out mechanism. The flexural

strength of cement-based foams is summarized in Figures 4.36 and 4.37. It is clear that the heaviest specimens resisted significantly a higher impact loads with an increase in the loading rate. A detailed discussion on stress and strain rate sensitivity of cement-based foams is presented in next chapter.

Table 4.1: Compressive strength of cement-based foams

Cast density (kg/m^3)	Compressive strength (MPa)	COV	Compressive strength (MPa)	COV
	Plain		Fibre-reinforced	
1200	16.6	13.3%	17.40	20.3%
750	4.1	23.4%	4.10	12.2%
475	1.6	0.6%	1.10	12.7%

Note: COV ≡ Coefficient of variation

Table 4.2: Flexural strength of cement-based foams under quasi-static load

Cast density (kg/m^3)	Flexural strength (MPa)	COV	Flexural strength (MPa)	COV
	Plain		Fibre-reinforced	
1200	0.57	14.0%	0.72	18.03%
750	0.53	10.0%	0.58	13.70%
475	0.10	10.0%	0.28	14.28%

Note: COV ≡ Coefficient of variation

Table 4.3: Flexural strength of plain cement-based foams under impact loading

Cast density (kg/m^3)	Flexural strength (MPa)	COV	Flexural strength (MPa)	COV
	Drop height 250 mm		Drop height 500 mm	
1200	10.25	5.7%	13.13	17.5%
750	4.43	5.8%	5.15	3.0%
475	1.47	3.0%	1.68	9.3%

Note: COV ≡ Coefficient of variation

Table 4.4: Flexural strength of fibre-reinforced cement-based foams under impact loading

Cast density (kg/m^3)	Flexural strength (MPa)	COV	Flexural strength (MPa)	COV
	Drop height 250 mm		Drop height 500 mm	
1200	11.38	1.9%	16.60	0.4%
750	5.34	7.4%	6.12	2.1%
475	1.53	5.1%	1.82	7.7%

Note: COV ≡ Coefficient of variation

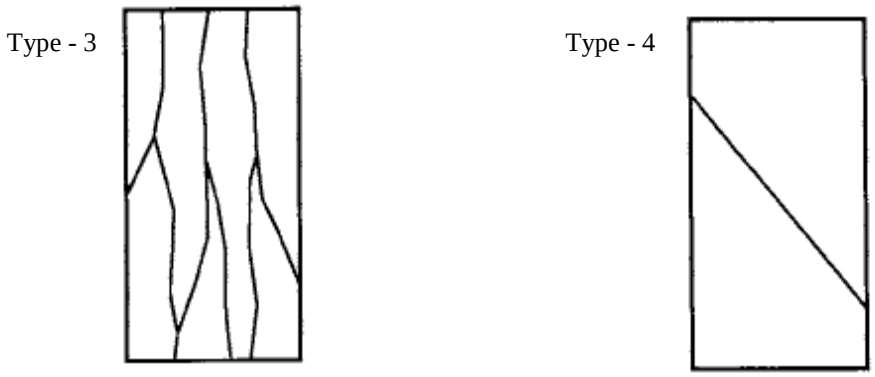

a) Columnar vertical cracking through both ends, no well-formed cones

b) Diagonal fracture with no cracking through ends

Figure 4.1: Schematic diagram of fracture pattern in cylinders under compression (ASTM C39, 2009)

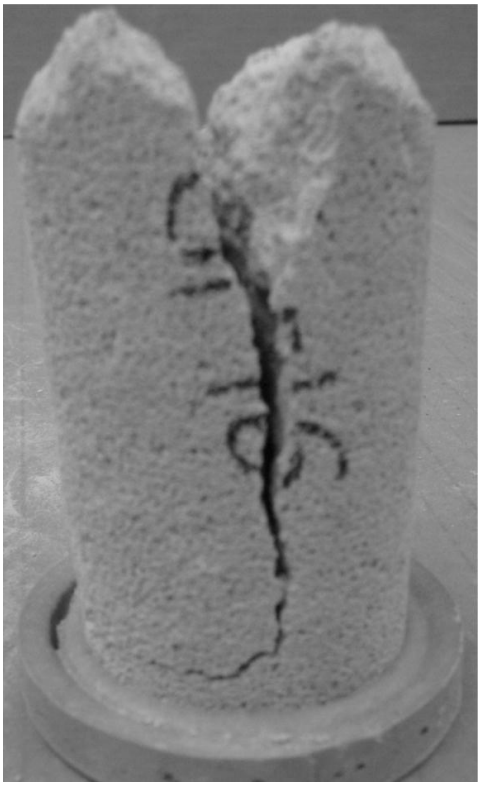

Figure 4.2: Compression test on **plain** cement-based foam cylinders (cast density 475 kg/m^3)

Figure 4.3: Compression test on **plain** cement-based foam cylinders (cast density 750 kg/m^3)

Figure 4.4: Compression test on **fibre-reinforced** cement-based foam cylinders (cast density 1200 kg/m^3)

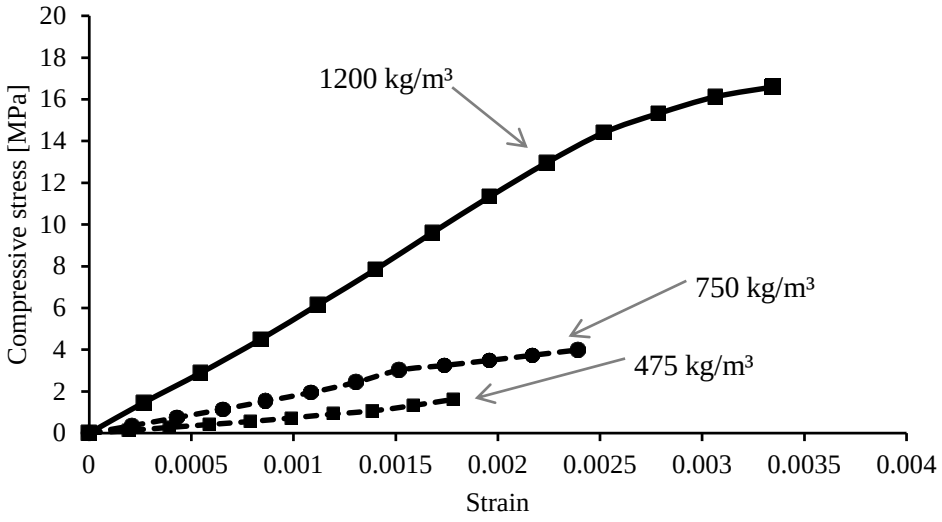

Figure 4.5: Stress-strain response of **plain** cement-based foams under compression

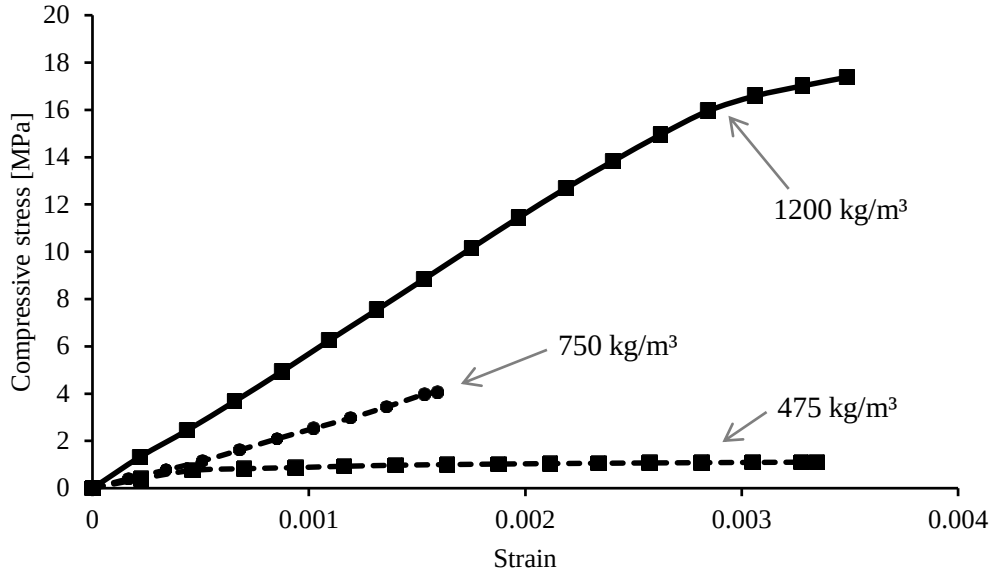

Figure 4.6: Stress-strain response of **fibre-reinforced** cement-based foams under compression

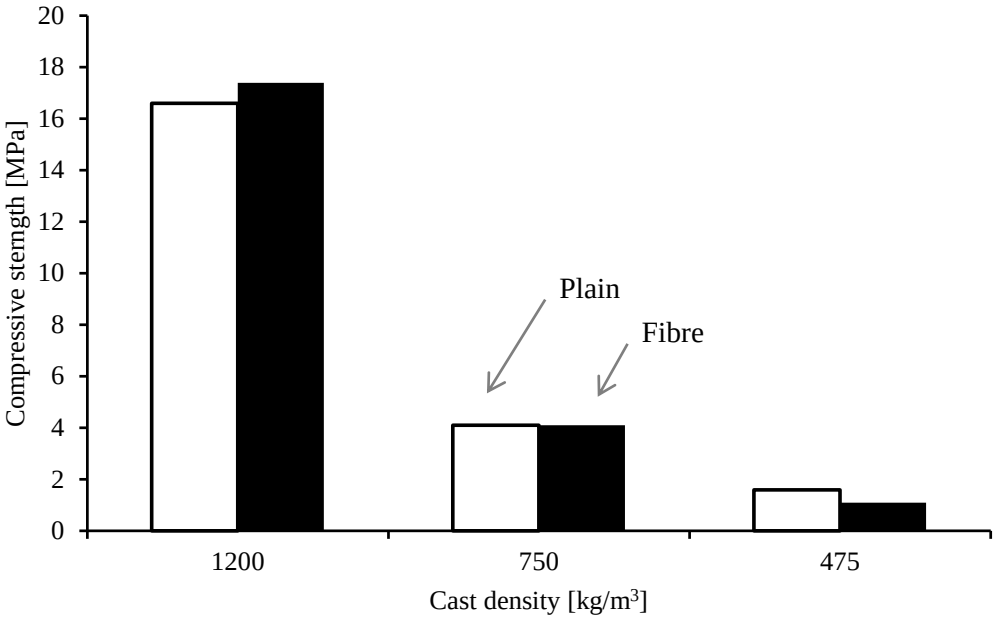

Figure 4.7: Compressive strength of cement-based foams (quasi-static)

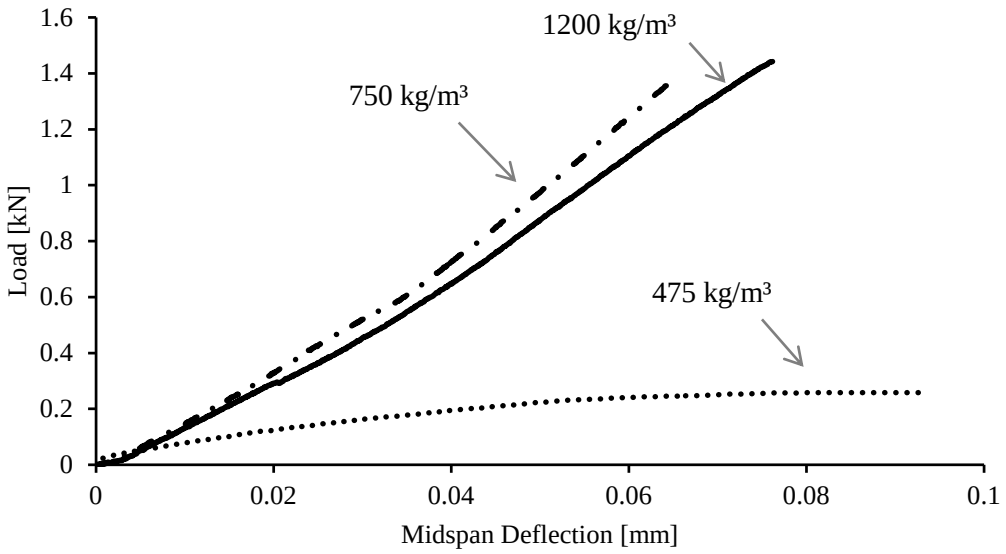

Figure 4.8: Response of **plain** cement-based foams under quasi-static flexure

Figure 4.9: Quasi-static flexure test on **plain** cement-based foam (cast density 750 kg/m^3)

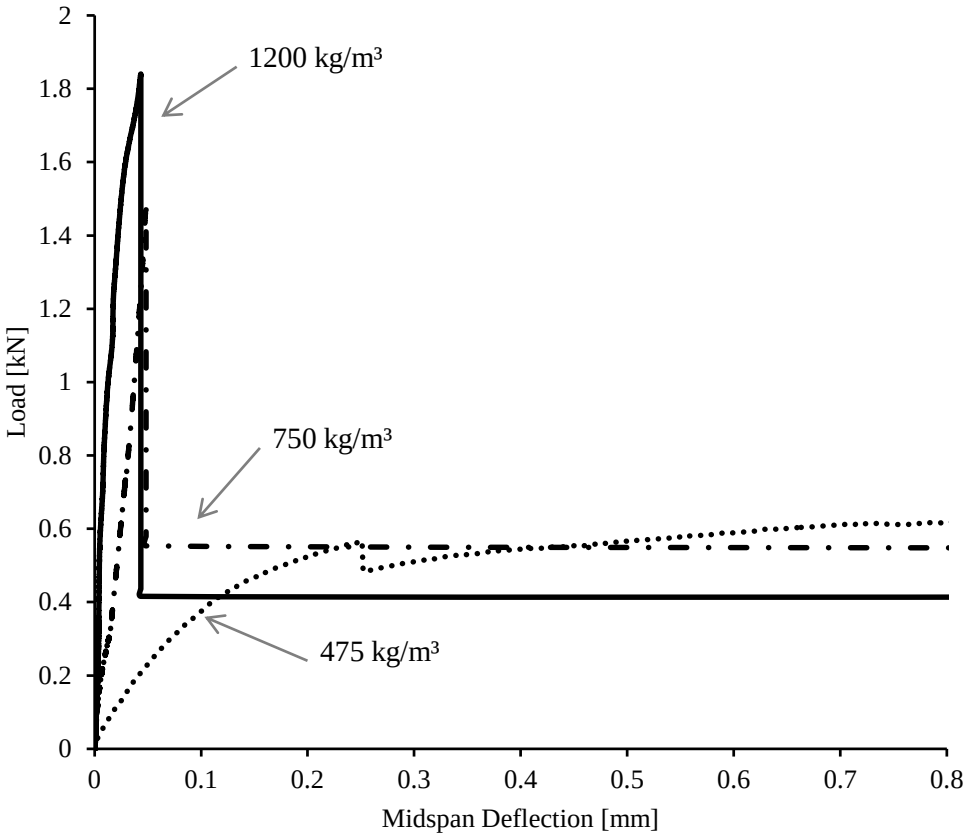

Figure 4.10: Response of **fibre-reinforced** cement-based foams under quasi-static flexure

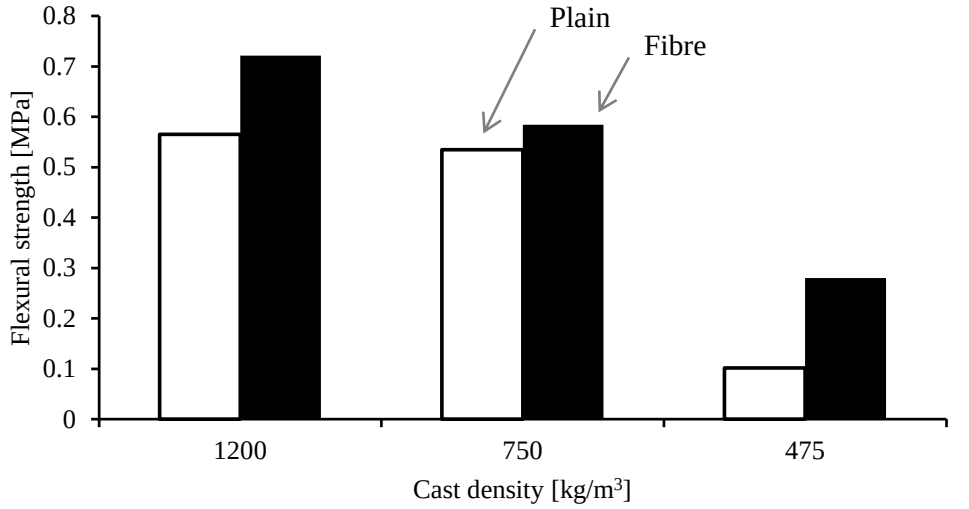

Figure 4.11: Flexural strength of plain and fibre-reinforced foams under quasi-static bending

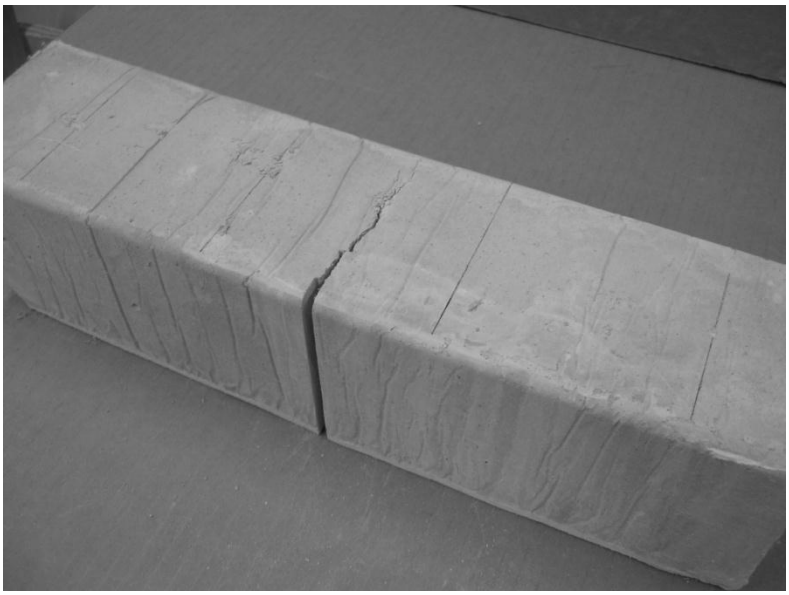

Figure 4.12: Quasi-static flexure test on **fibre-reinforced** cement-based foam (cast density 750 kg/m^3)

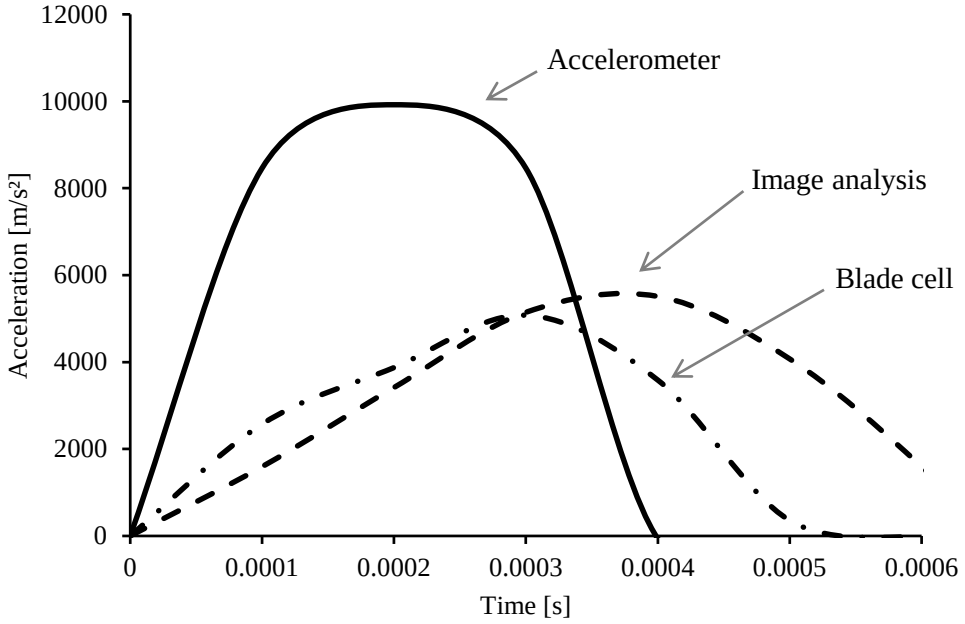

Figure 4.13: Acceleration history of **plain** cement-based foams under drop-weight impact loading with drop height 250 mm (1200 kg/m^3)

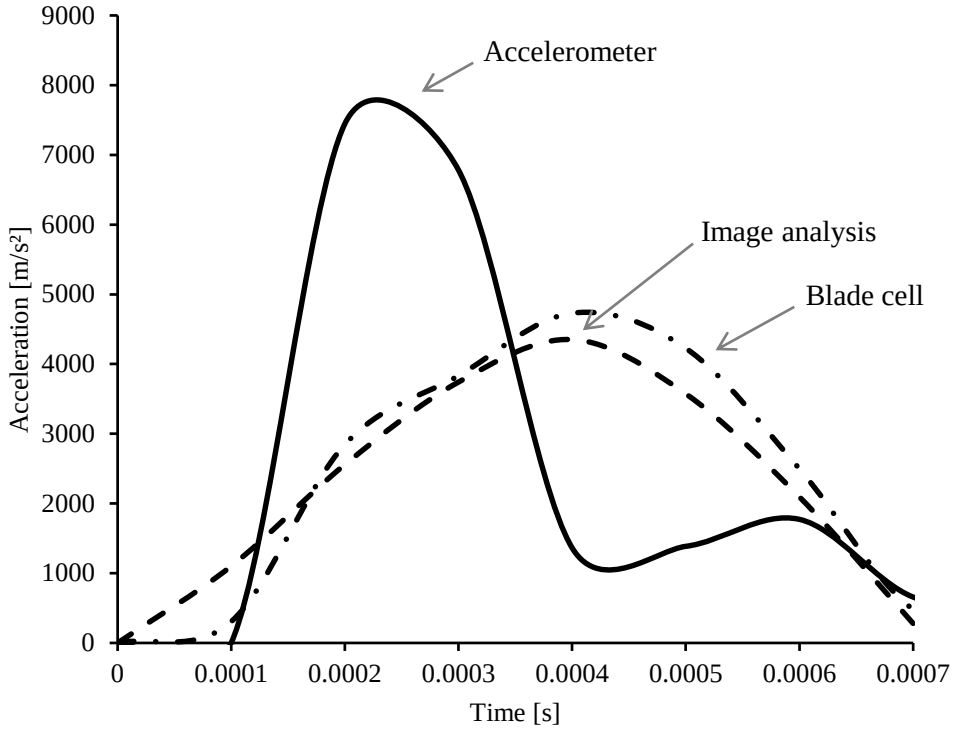

Figure 4.14: Acceleration history of **plain** cement-based foams under drop-weight impact loading with drop height 250 mm (750 kg/m^3)

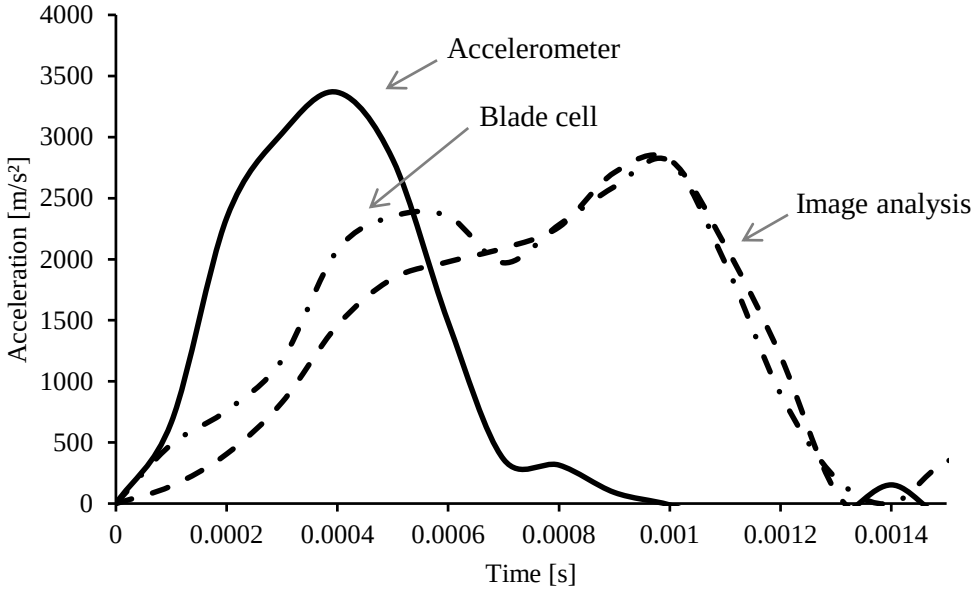

Figure 4.15: Acceleration history of **plain** cement-based foams under drop-weight impact loading with drop height 250 mm (475 kg/m^3)

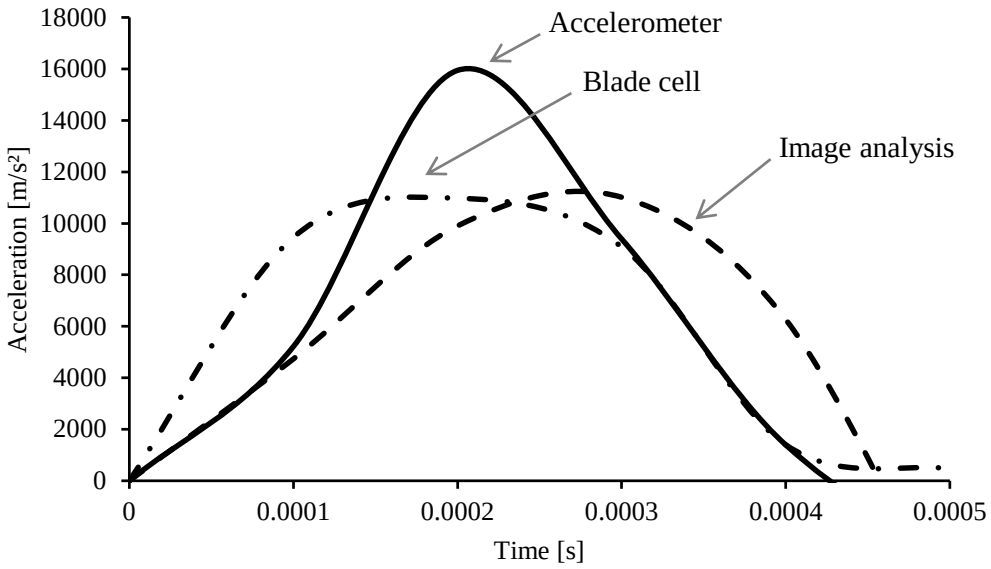

Figure 4.16: Acceleration history of **plain** cement-based foams under drop-weight impact loading with drop height 500 mm (1200 kg/m^3)

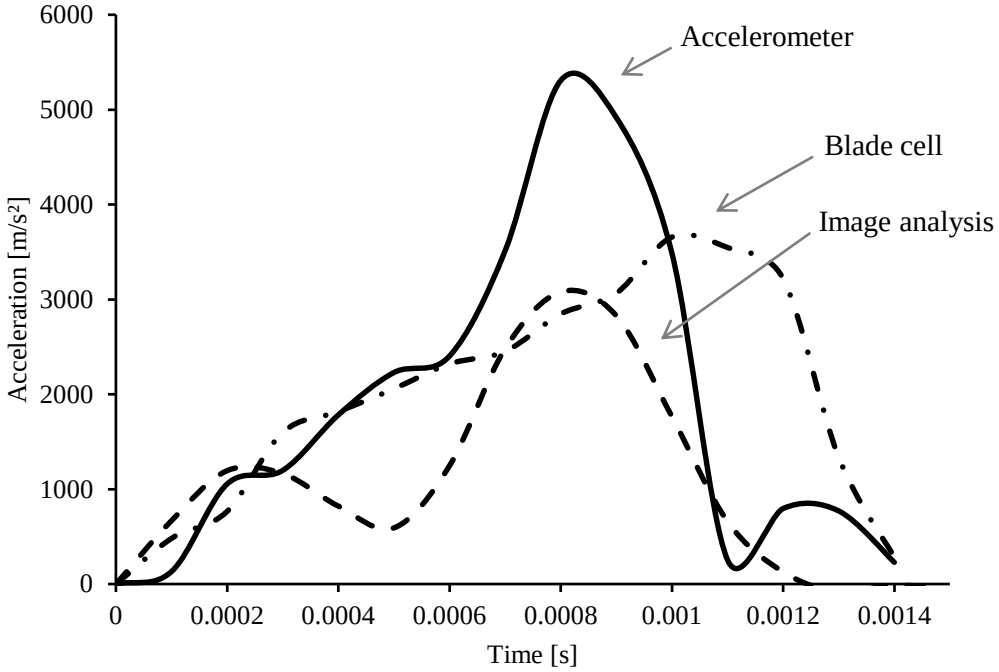

Figure 4.17: Acceleration history of **plain** cement-based foams under drop-weight impact loading with drop height 500 mm (750 kg/m^3)

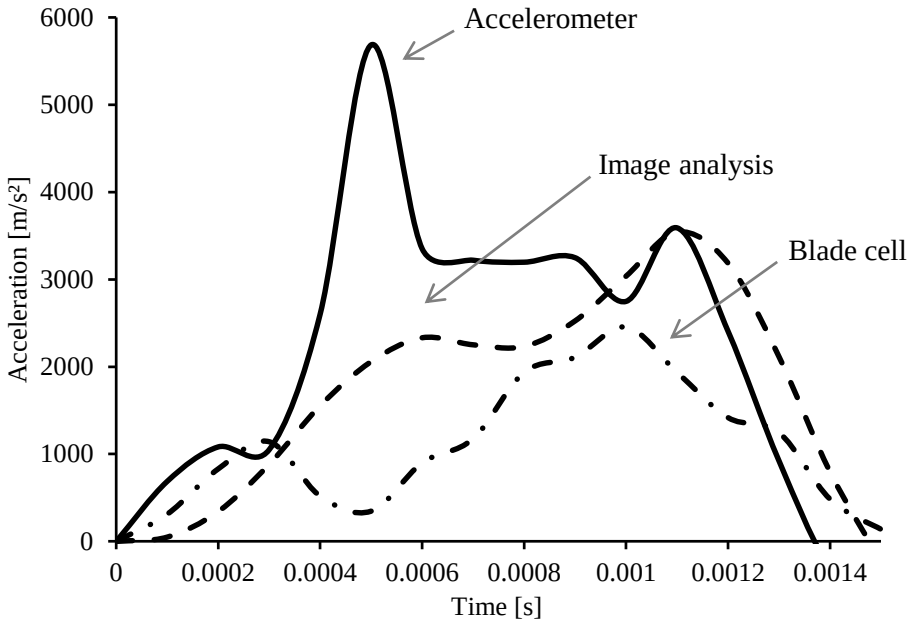

Figure 4.18: Acceleration history of **plain** cement-based foams under drop-weight impact loading with drop height 500 mm (475 kg/m^3)

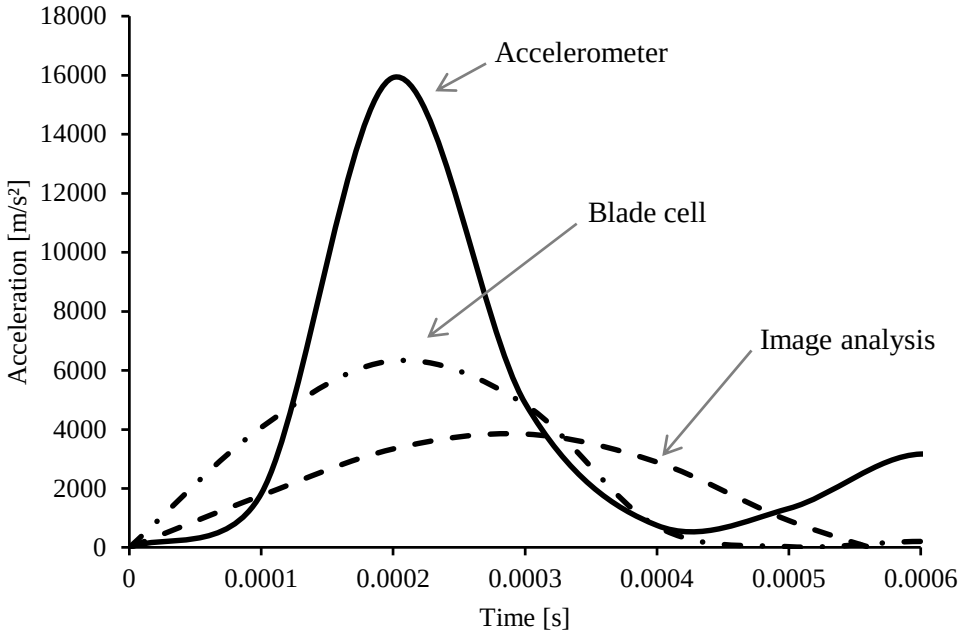

Figure 4.19: Acceleration history of **fibre-reinforced** cement-based foams under drop-weight impact loading with drop height 250 mm (1200 kg/m^3)

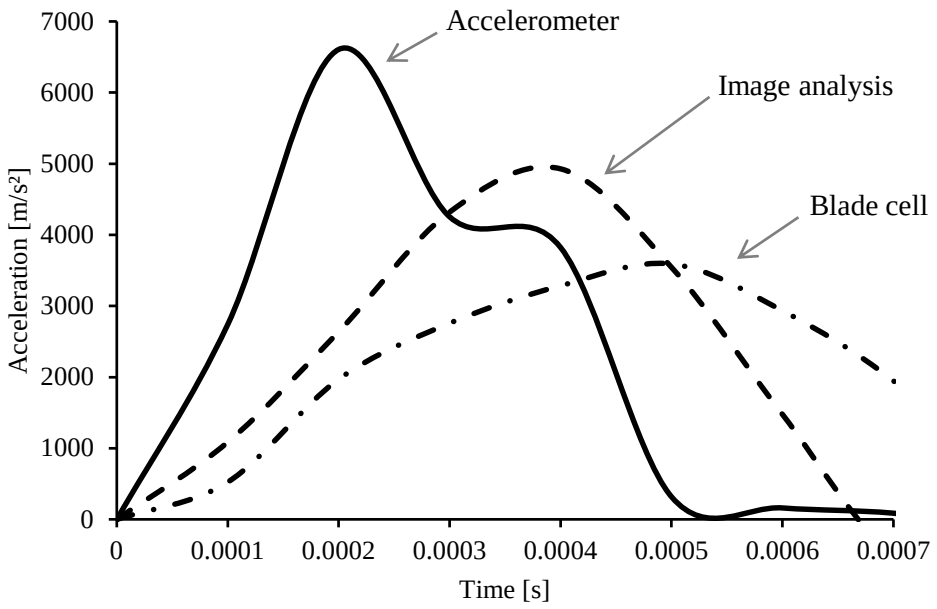

Figure 4.20: Acceleration history of **fibre-reinforced** cement-based foams under drop-weight impact loading with drop height 250 mm (750 kg/m^3)

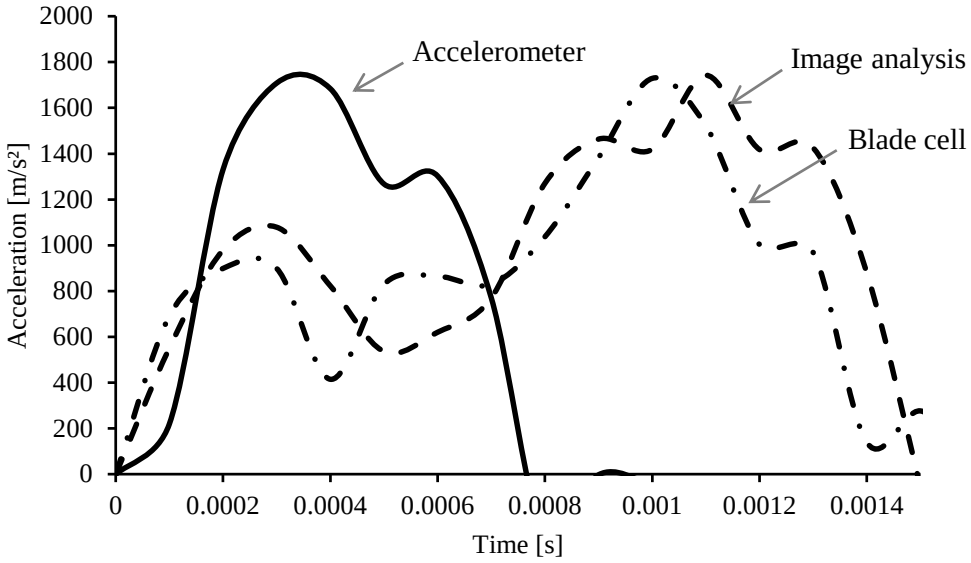

Figure 4.21: Acceleration history of **fibre-reinforced** cement-based foams under drop-weight impact loading with drop height 250 mm (475 kg/m^3)

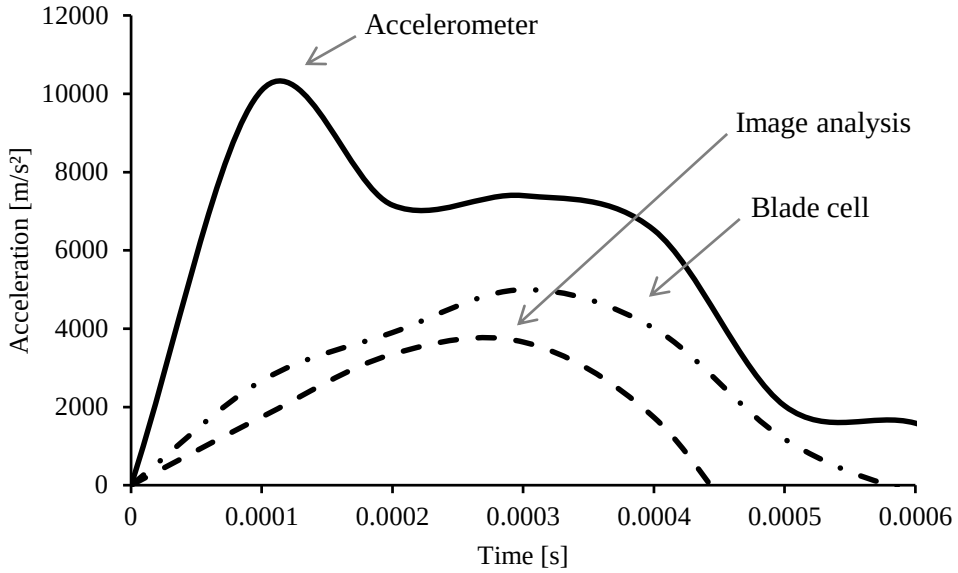

Figure 4.22: Acceleration history of **fibre-reinforced** cement-based foams under drop-weight impact loading with drop height 500 mm (1200 kg/m^3)

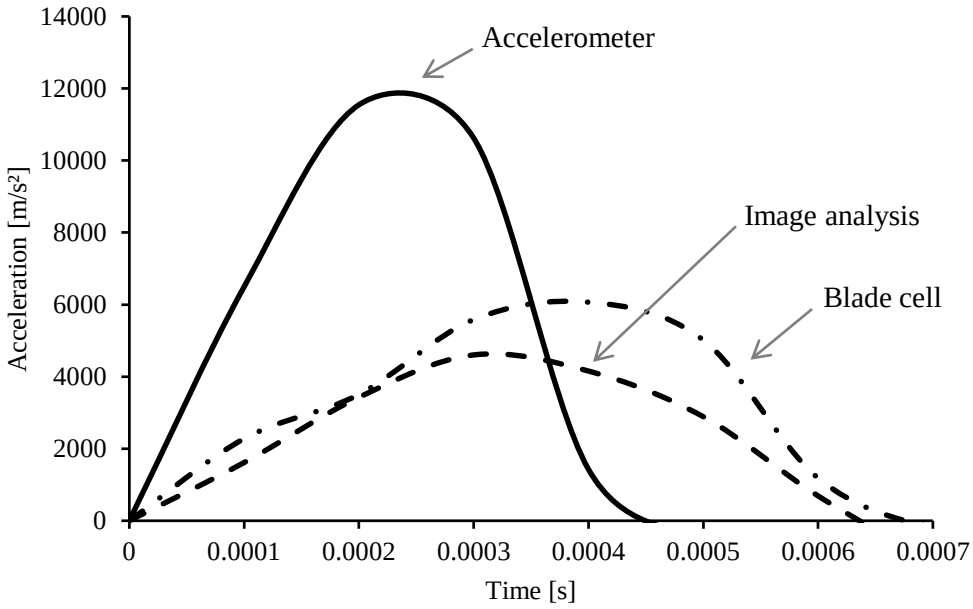

Figure 4.23: Acceleration history of **fibre-reinforced** cement-based foams under drop-weight impact loading with drop height 500 mm (750 kg/m^3)

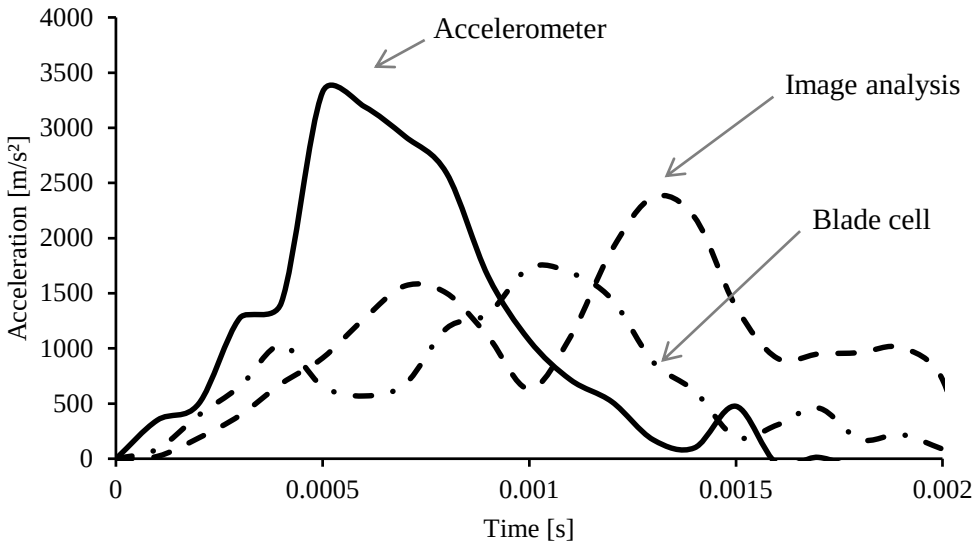

Figure 4.24: Acceleration history of **fibre-reinforced** cement-based foams under drop-weight impact loading with drop height 500 mm (475 kg/m^3)

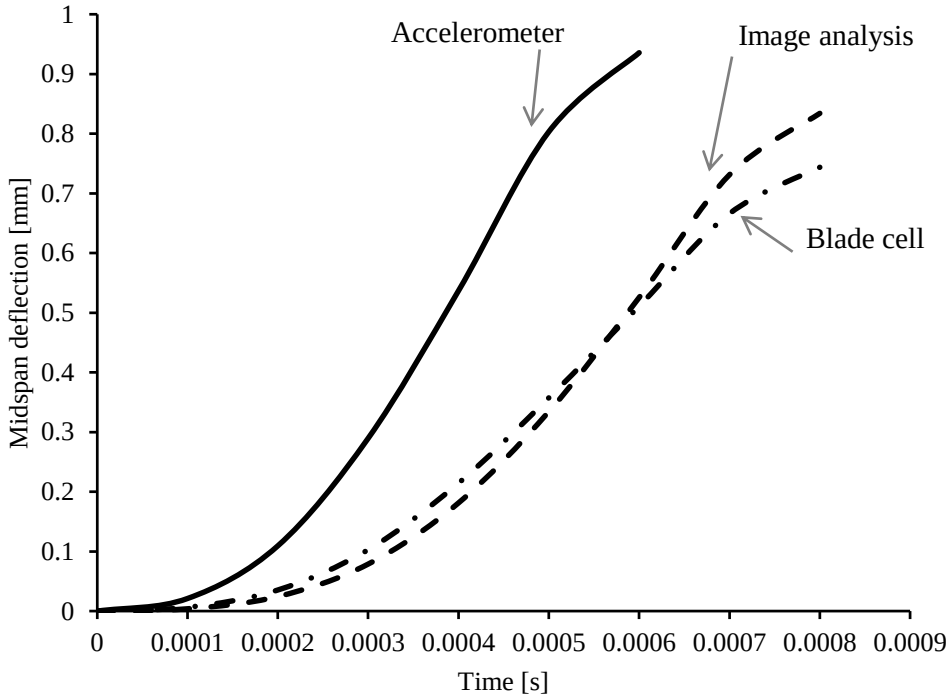

Figure 4.25: Deflection histories derived from three different sources (1200 kg/m^3, **plain**)

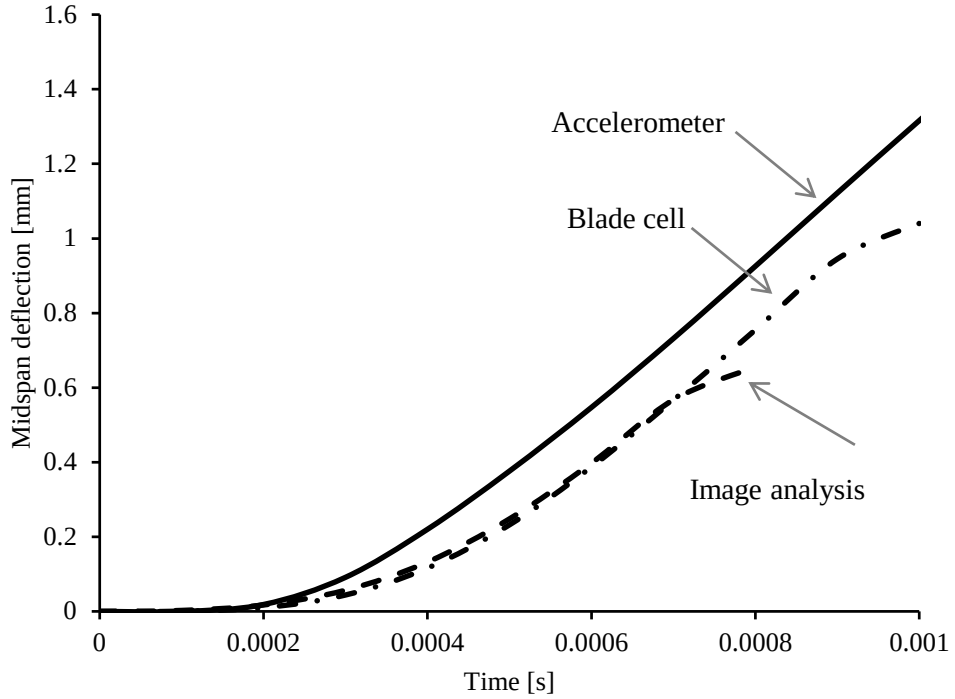

Figure 4.26: Deflection histories derived from three different sources (750 kg/m^3, **plain**)

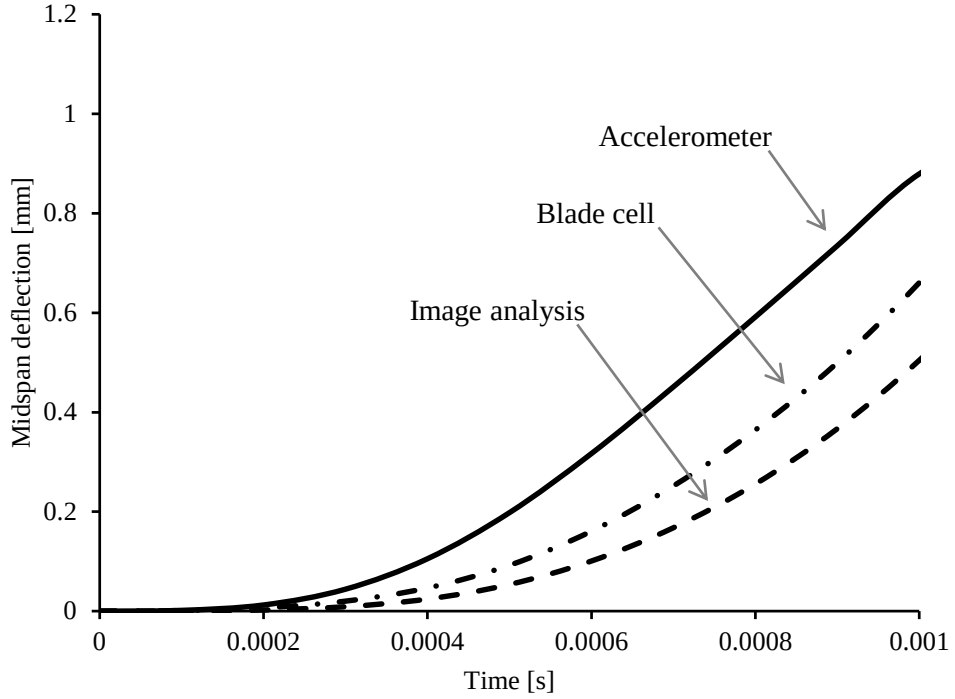

Figure 4.27: Deflection histories derived from three different sources (475 kg/m^3, **plain**)

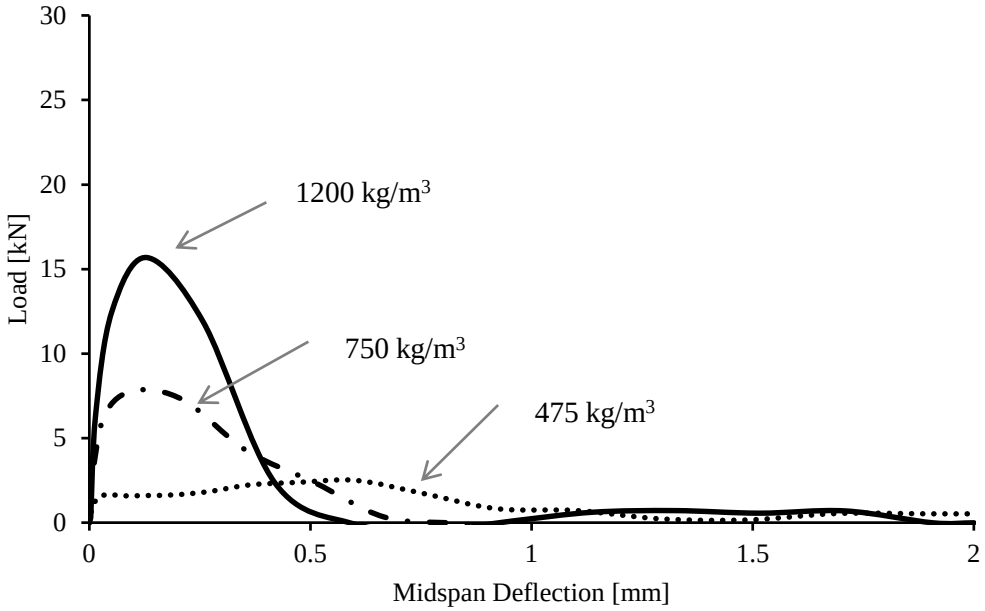

Figure 4.28: Response of **plain** cement-based foams under drop-weight impact bending with drop height 250 mm

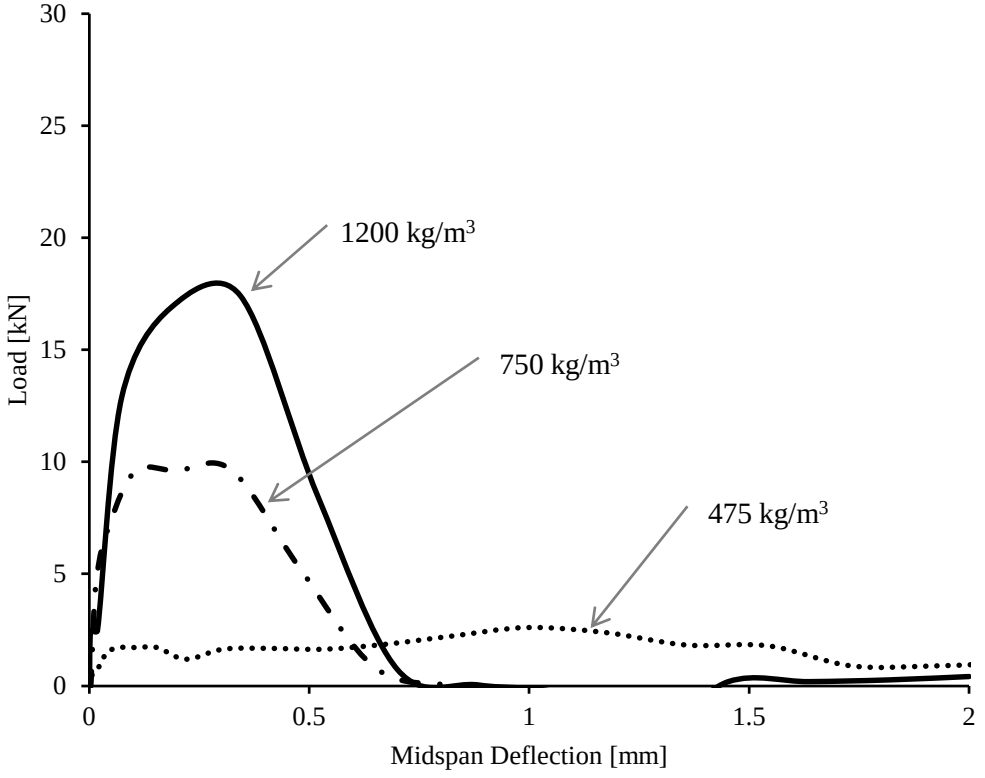

Figure 4.29: Response of **fibre-reinforced** cement-based foams under drop-weight impact bending with drop height 250 mm

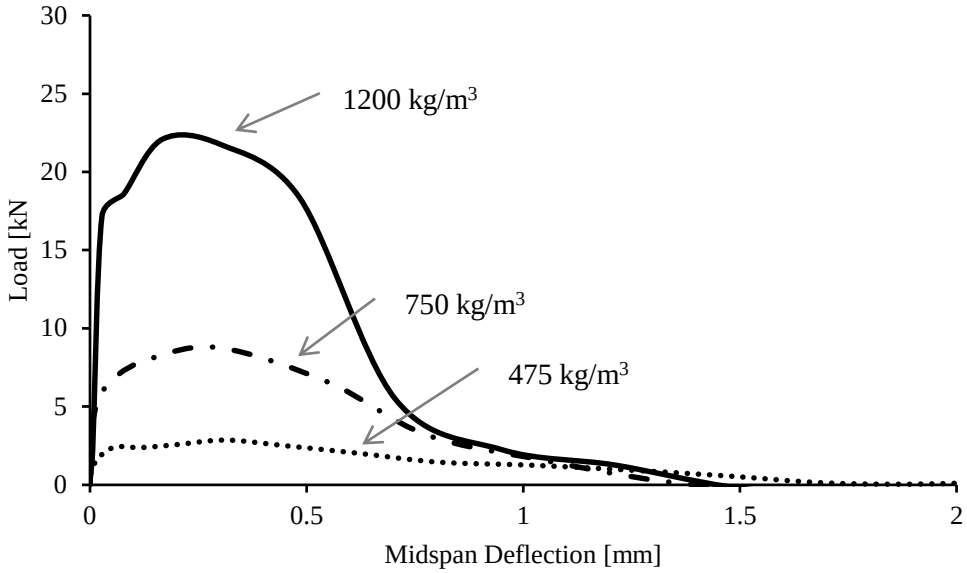

Figure 4.30: Response of **plain** cement-based foams under drop-weight impact bending with drop height 500 mm

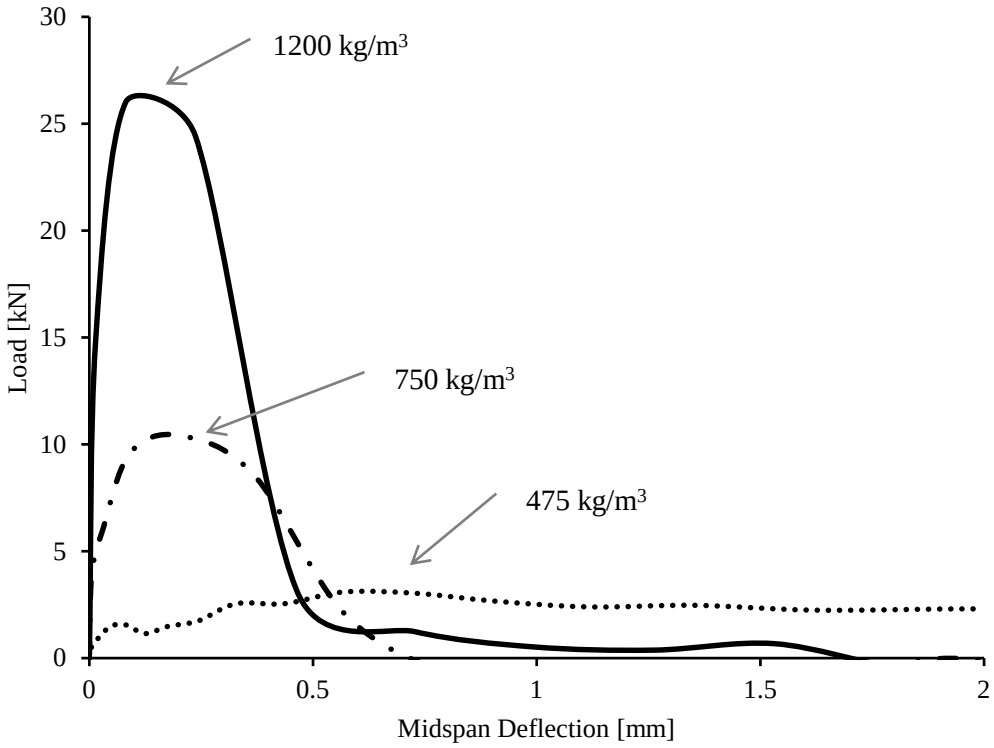

Figure 4.31: Response of **fibre-reinforced** cement-based foams under drop-weight impact bending with drop height 500 mm

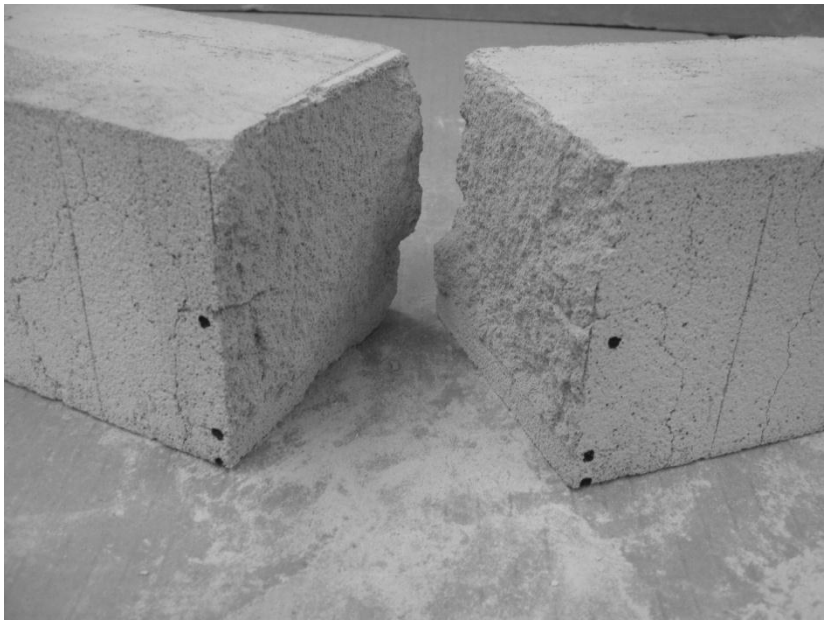

Figure 4.32: Impact test on **plain** cement-based foam for a drop height of 250 mm (cast density 475 kg/m^3)

Figure 4.33: Impact test on **plain** cement-based foam for a drop height of 500 mm (cast density 475 kg/m^3)

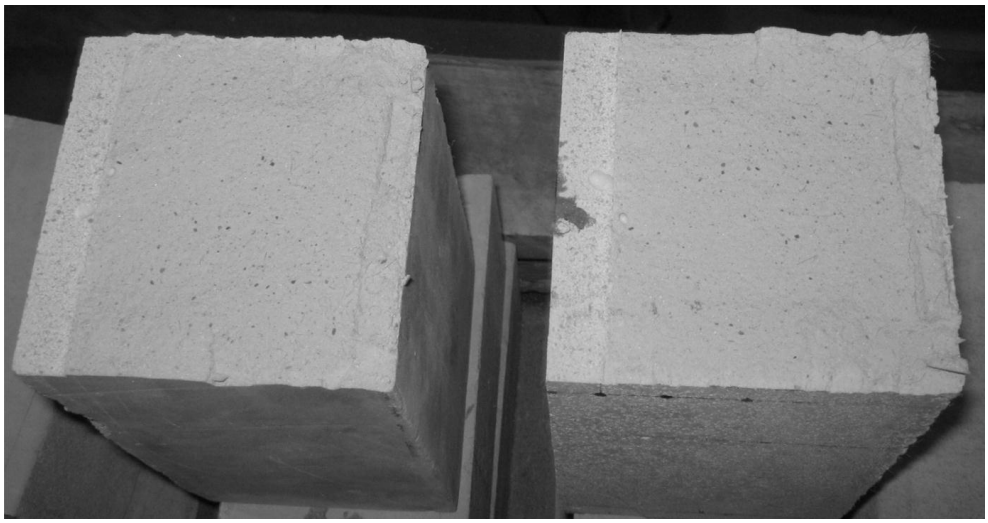

Figure 4.34: Impact test on **fibre-reinforced** cement-based foam for a drop height of 250 mm (cast density 1200 kg/m^3)

Figure 4.35: Impact test on **fibre-reinforced** cement-based foam for a drop height of 500 mm (cast density 1200 kg/m^3)

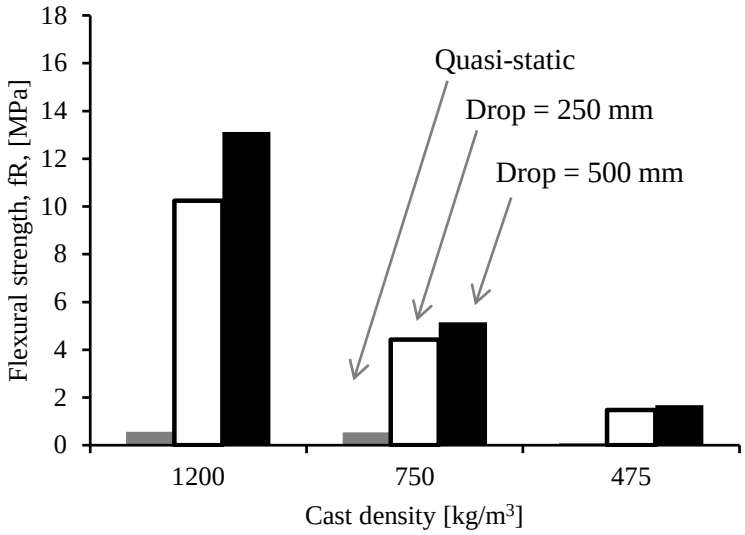

Figure 4.36: Flexural strength of **plain** cement-based foams under drop weight impact bending

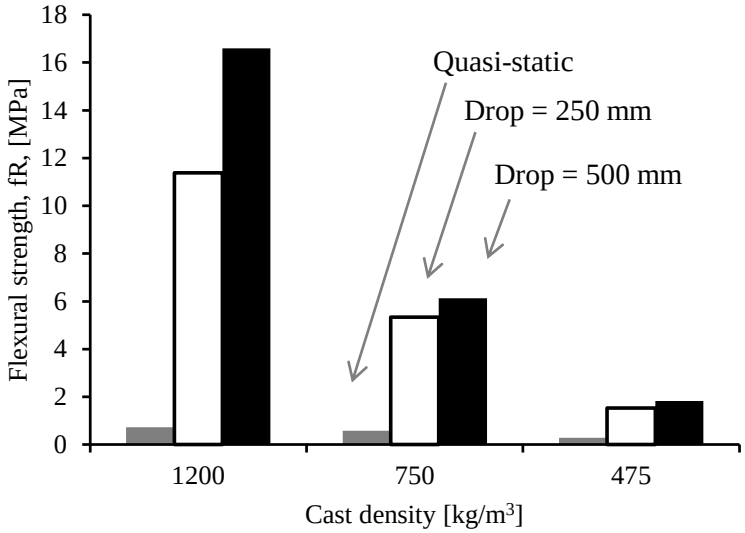

Figure 4.37: Flexural strength of **fibre-reinforced** cement-based foams under drop weight impact bending

Chapter 5

QUASI-STATIC AND DYNAMIC EVALUATION, PART 2: ANALYSIS AND DISCUSSION

5.1 General

The results of various test configurations including compression, quasi-static flexure and impact were discussed in the previous Chapter. The effects of cast density, microfibre reinforcement and loading rate on the mechanical response of cement-based foams are presented in this chapter. The data gathered from quasi-static tests under compression and flexure were analyzed to study the influence of fibre and cast density on various mechanical properties including the modulus of elasticity, Poisson's ratio, flexural strength and flexural toughness. Altogether three loading rates were generated in flexure — quasi-static loading as per ASTM C1609 (2007) and impact loading corresponding to drop heights of 250 mm and 500 mm. The flexural responses thus obtained were analyzed to establish stress and strain rate sensitivity of the cementitious foam. The test results were compared with available published data and other response prediction models.

A version of this chapter has been accepted for publication. Mamun & Bindiganavile 2010. International Journal of Protective Structures. 1(3): 409-424

5.2 Effect of Cast Density and Fibre Reinforcement

5.2.1 Compressive Strength

The stress-strain behaviour of cementitious foams under compression was discussed in Chapter 4. Note that none of the plain specimens showed any post-peak response. The cylinders failed upon reaching the peak compressive load. The stress-strain behaviour of brittle cellular solids is characterized first by a linear elastic behaviour followed by a plateau, which, in turn, is ultimately followed by a rapid rise due to densification (Gibson and Ashby, 1999). In the case of cement-based foams examined here, this densification was not observed. The properties of cellular solids are generally modelled as a function of their relative density, defined as the ratio of the density of the composite to that of the material in the cell wall. The density of the cell wall was taken as that of the cementitious paste and was found equal to 1900 kg/m^3. Gibson and Ashby (1999) examined various open-cell cellular solids to show that the crushing strength is a function of the relative density and scales according to the power of 1.5. The exponent is a measure of the sensitivity to cast density in cellular solids. A similar relationship was plotted in Figure 5.1 for the compressive strength. Note that the exponent is about 2.5 for plain cement-based foams with a modest increase in fibre reinforced foams. The strength of cement-based composites is strongly affected by their porosity (Fagerlund *et al.*, 1973; Older *et al.*, 1987). A porosity-based model was developed by Kearsley and Wainwright (2001) to relate compressive strength and porosity of cement-based foamed composite as $f_c' = k\,(1-p)^{3.6}$, where k is a constant, p is the porosity and the term $1-p$ in fact a measure of the relative

density. Thus the porosity based model for foamed composite shows a relationship between compressive strength and relative density with an exponent of 3.6.

Recall that the lightest of the fibre-reinforced specimens (cast density = 475 kg/m^3) show a slight post-peak resistance. As expected, the effect of microfibre reinforcement on the compressive strength of the composite is not significant. Figure 5.2 shows the effect of cast density on the compressive strength of cementitious foam based on results from the literature. One notes that the compressive strength of low density foams from this study is in agreement with recently published results (Nambiar *et al.,* 2006; Kearsley and Wainwright, 2002).

5.2.2 Static Modulus of Elasticity in Compression

The modulus of elasticity of cement-based foams was evaluated as per ASTM C469 (2002). Figure 5.3 shows the effect of relative density on the static modulus of elasticity. For brittle cellular solids, Gibson and Ashby (1999) showed that the modulus of elasticity scales according to the square of the relative density. Similarly, for a range of cast density between 600 –1500 kg/m^3, Kearsley and Mostert (2003) found a quadratic relationship. The plot shown in Figure 5.3 confirms such a parabolic relationship for plain specimens. However, the modulus of elasticity values as listed in Table 5.1 were somewhat lower than those observed by Kearsley and Mostert (2003), especially for the cast density of 1200

kg/m^3. On the other hand, data from earlier research (Valore *et al.* 1954) on autoclaved cellular concrete match with the results from this study.

Figure 5.4 shows the effect of cast density on the modulus of elasticity of fibre reinforced cementitious foams. An exponent of about 2.0 indicates once again the parabolic relationship with relative density. It is clear from Figure 5.4 that microfibres do not significantly affect the modulus of elasticity. This is in agreement with the previous finding that polymeric microfibres do not significantly affect either the compressive strength or the modulus of elasticity in cement-based foams (Kearsley and Mostert, 2003). However, a study by Jones and McCarthy (2005) showed enhanced performance in terms of the modulus of elasticity due to the presence of polypropylene microfibre in the foamed cement matrix.

5.2.3 Poisson's Ratio

Poisson's ratio was determined in accordance with ASTM C469 (2002) for all mixes and the influence of relative density is shown in Figure 5.5. A typical Poisson's ratio history is shown in Figure 5.6. As expected, this parameter remains largely unaffected by the relative density of the foamed composite. The independence with respect to the relative density may be attributed to the proportional increase in both lateral and longitudinal strains, with an increase in bending deformation of the cell wall, regardless of the relative density of the composite, so long as the cellular geometry remains constant (Gibson and Ashby,

1997). In this study a value of 0.22 was found for cement-based foams with slightly lower values for fibre-reinforced mixes. However, the existing database for brittle foams yields a Poisson's ratio of 0.33. Zollo and Hays (1998) reported a Poisson's ratio ranging from 0.3–0.4 fibre-reinforced cellular concrete with a fibre volume fraction of 0.5%.

5.2.4 Flexural Strength

The effect of cast density on flexural strength is shown in Figures 5.7–5.8. The flexural strength was calculated by using the effective cross-sectional dimensions after accounting for the notch introduced for fracture toughness analysis (not within the scope of this study). In plain composites, the flexural strength was found to vary with the square of the relative density.

The use of fibres significantly improved the modulus of rupture (MOR) for the lightest foam with moderate benefits at higher cast densities as observed in Figure 4.11. It is clear from Figure 5.8 that for fibre reinforced foams, the MOR is in linear proportion to the relative density under quasi-static loading. This has been noted before by Kearsley and Mostert (2003), who included a comparable amount of fibres at 0.16% volume fraction in a cast density range of 750–1500 kg/m^3. Figure 5.9 shows the scanning electron micrographs for all three mixes. The micrographs revealed the fact that the internal cellular structure of heavier mixes is predominantly closed-cell. It is also evident that the cellular structure in the lightest mix is partially closed-cell. The fibre dimension is comparable (Figure

5.10) to the cell wall in the lightest mix and this enables greater reinforcing ability witnessed at quasi-static loading. As depicted in Figures 4.29 and 4.31 in Chapter 4, the presence of fibres improved the modulus of rupture considerably in mixes with cast density of 1200 kg/m^3 at all impact loading rates. It was seen that the flexural strength of cement-based foams increases with an increase in the loading rate, which demonstrates the sensitivity of cement-based foams to higher loading rate. This sensitivity was more pronounced in fibre-reinforced specimens as the relationship between flexural strength and relative density varies from linear to quadratic with an increase in rate of loading.

5.2.5 Flexural Toughness

Flexural toughness factors (FTF) were evaluated using Equation 2.10 as per JSCE G-552 (1999). Figure 5.11 shows the effect of cast density on flexural toughness factors of plain cementitious foams. FTF for plain mixes varied linearly with relative density for all rates of loading. In Table 5.2 the FTF for plain mixes are summarized for all rates of loading. It is notable that the flexural toughness factors for heavier mixes ($\rho \geq 750$ kg/m^3) increased by about two times as the impact loading rates increased from 250 mm drop height to 500 mm drop height. This increase in FTF can be explained through the resistance offered by the relatively thicker cell walls in the heavier mixes, which lead to higher tensile loads as the cells rupture below the neutral axis and higher buckling loads in the cell above the neutral axis.

On the other hand, the flexural toughness factor for fibre-reinforced mixes was almost independent of relative density for quasi-static flexure (Figure 5.12), which shows that the effect of cast density of fibre reinforced mixes on toughness was not significant. This is likely due to the fact that in the post-crack phase only fibres are effective and not the rest of the foam. However, with an increase in the loading rate a linear relationship was introduced. This transformation of relationship implies the loading rate sensitivity of cement-based foams in terms of post-peak energy absorption is largely due to the strain rate sensitivity of the fibre pullout process (Bindiganavile and Banthia, 2005).

5.3 Rate Sensitivity

The dynamic increase factors were calculated by taking ratios of flexural strength as obtained from impact tests to that obtained from the quasi-static test. The effect of strain-rate on the DIF for flexural strength is shown for plain foams in Figure 5.13 and for fibre-reinforced foams in Figure 5.14. As expected, in plain mixes, the quasi-static flexural strength was the lowest in the lightest mix. Upon adding fibres, the relative improvement in the flexural strength was the highest in the lightest mix. That is, as a percentage of the original flexural strength of the plain counterpart, the fibres were most efficient with the lightest mix. This holds generally true for low modulus microfibres (such as were used in this study) in low strength cement-based matrices. Since by definition the DIF is a normalized value with respect to the quasi-static case, the improvement under high strain rates

(which induce brittle behaviour) was not as high in the case of the fibre reinforced foam at 475 kg/m^3.

Existing literature reveals that in concrete, a lower strength results in a higher DIF at the same strain-rate (Malvar and Ross, 1998; Cowell, 1966). However, for brittle cellular solids, the strength is largely independent of the strain-rate up to 10^4/s (Lacy, 1965; Rinde and Hoge, 1971). On the other hand, the data shown in Figure 10 clearly indicates that low density cement-based foams were strain-rate sensitive at 1/s. Tyler and Ashby (1986) highlighted the significance of liquids within the cells on rate sensitivity of the cellular solids, so that water filled polymeric foams were distinctly rate-sensitive at 10/s. It is therefore likely that the presence of pore fluid within the cell walls in cement-based foams imparts a strain rate sensitivity, as suggested by Rossi (1991). However, the dynamic impact factor from Figure 5.14 dropped with a decrease in the cast density which was contradictory to the results of Li and Muthyala (2008) on cement-based foams containing hollow rubber cells. Nevertheless, adapting Equation 2.20 to the three cast densities shows that the rate sensitivity of low-density foams ($\leq$750 kg/m^3) is overestimated by the CEB-FIP formulation. A recent study on hydraulic lime mortar (Rachel and Bindiganavile, 2010), which has a compressive strength comparable to low-density cementitious foams, showed a very similar mismatch between the dynamic response and the DIF predicted by Equation 2.20. Clearly, to assess shock absorption in controlled low-strength or lightweight cement-based composites such as cement-based foams, modified expressions are needed to

describe the strain-rate sensitivity. This was attempted through stress-rate sensitivity descriptors as explained below.

To describe stress rate sensitivity, the formulation as shown in Equation 2.17, proposed by Nadeau *et al.* (1982), was employed. The *N* value thus evaluated describes the slope of the corresponding segment of the plot. A lower *N* value denotes higher stress rate sensitivity. Figure 5.15 shows the stress-rate sensitivity of plain cement-based foams. This study showed that cementitious foam is stress-rate sensitive. It is clear that lighter mixes showed higher stress rate sensitivity. If the mixes were categorized as per the definition of low-density cement based foams and designated as a low-density controlled low-strength material (LD-CLSM) (ACI 523.1R, 2006), then mixes with density below 800 kg/m^3 can be regarded as LD-CLSM (in this case of 475 kg/m^3 and 750 kg/m^3). The stress-rate sensitivity of plain cement-based foams, which fall under LD-CLSM decreased with an increase in cast density.

The stress-rate sensitivity of fibre-reinforced cementitious foams is shown in Figure 5.16. It is evident that the lightest specimens are most sensitive when subjected to a higher stress rate. Again, within the boundary of LD-CLSM, it can be concluded that stress-rate sensitivity decreased as the cast density increased. In general, it was observed that stress-rate sensitivity of flexural strength increased for all mixes due to the presence of polymeric microfibre.

Table 5.1: Static Modulus of Elasticity of cement-based foams

Cast density (kg/m^3)	Modulus of Elasticity (MPa)	COV	Modulus of Elasticity (MPa)	COV
	Plain		Fibre reinforced	
1200	5563	10.7%	5668	10.2%
750	1812	3.6%	2398	2.5%
475	750	7.9%	1198	31.0%

Note: COV ≡ Coefficient of variation

Table 5.2: Flexural toughness factor of plain cement-based foams under impact loading

Cast density (kg/m^3)	Flexural Toughness Factor (kPa)	COV	Flexural Toughness Factor (kPa)	COV	Flexural Toughness Factor (kPa)	COV
	Quasi-static		Drop height =250 mm		Drop height =500 mm	
1200	10	10.3%	903	2.9%	1901	16.6%
750	8	4.2%	587	1.5%	1208	7.6%
475	4	7.1%	439	8.5%	678	2.8%

Note: COV ≡ Coefficient of variation

Table 5.3: Flexural toughness factor of fibre-reinforced cement-based foams under impact loading

Cast density (kg/m^3)	Flexural Toughness Factor (kPa)	COV	Flexural Toughness Factor (kPa)	COV	Flexural Toughness Factor (kPa)	COV
	Quasi-static		Drop height =250 mm		Drop height =500 mm	
1200	267	1.9%	1571	11.3%	2076	9.4%
750	222	5.5%	913	2.4%	1437	19.1%
475	243	1.6%	699	1.6%	934	3.7%

Note: COV ≡ Coefficient of variation

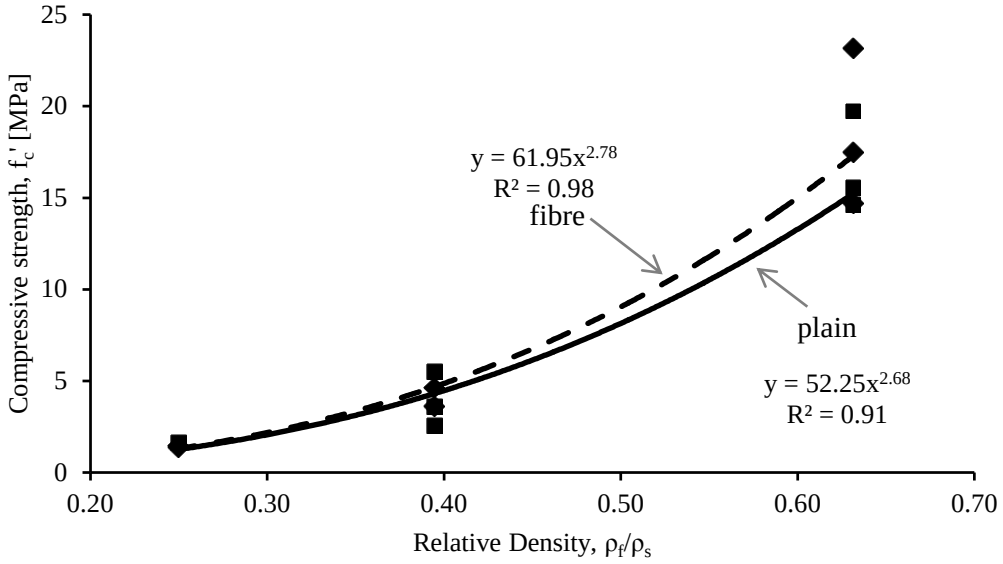

Figure 5.1: Effect of relative density on compressive strength of cement-based foams

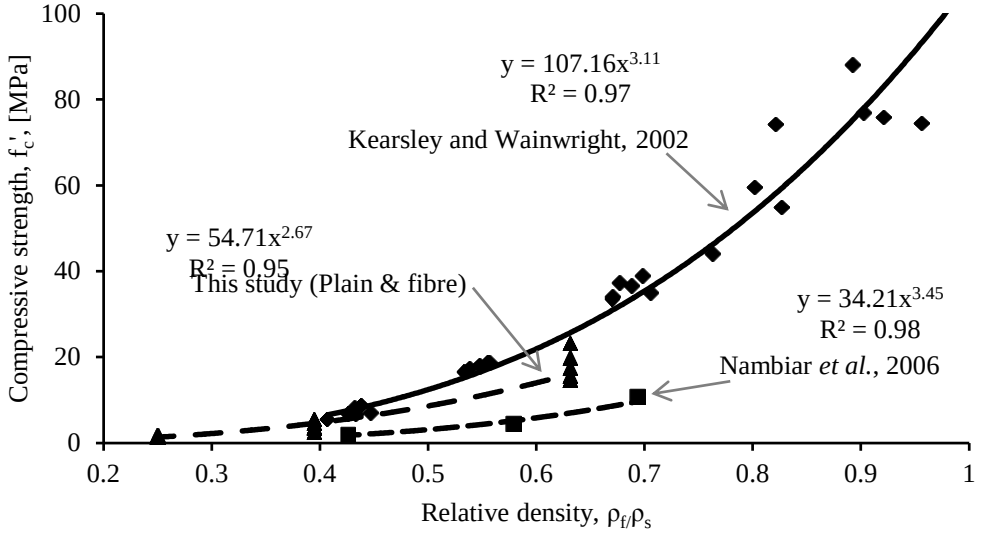

Figure 5.2: Effect of relative density on compressive strength cement-based foams (comparison with published literature)

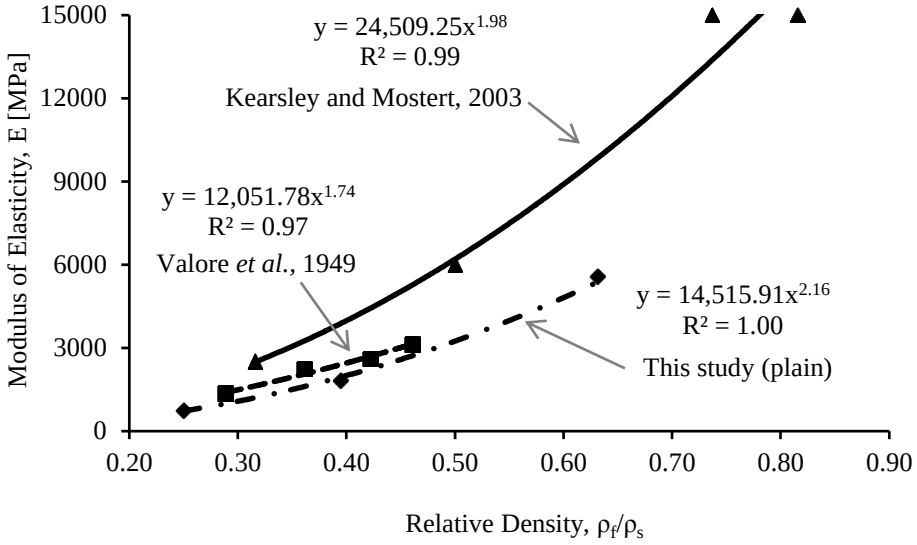

Figure 5.3: Effect of relative density on modulus of elasticity of **plain** cement-based foams

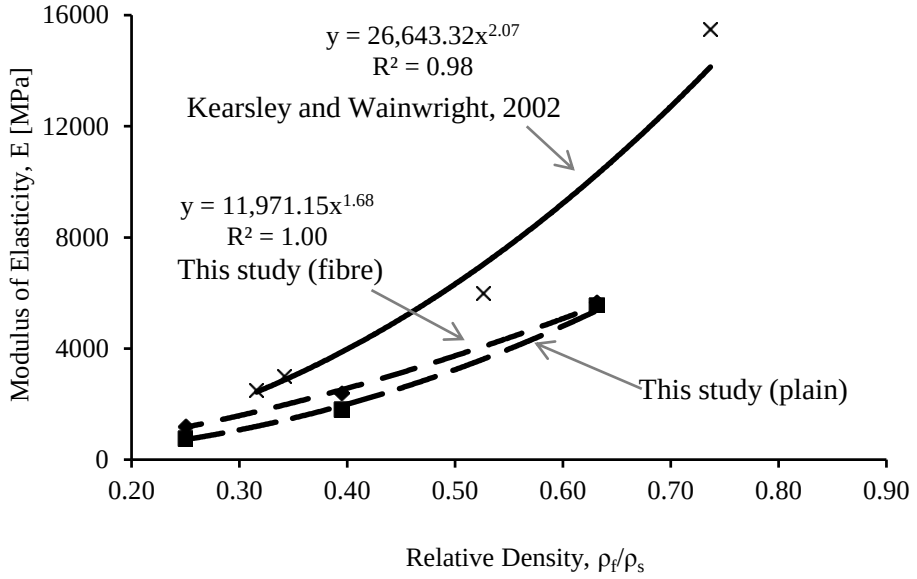

Figure 5.4: Effect of relative density on modulus of elasticity of **fibre-reinforced** cement-based foams

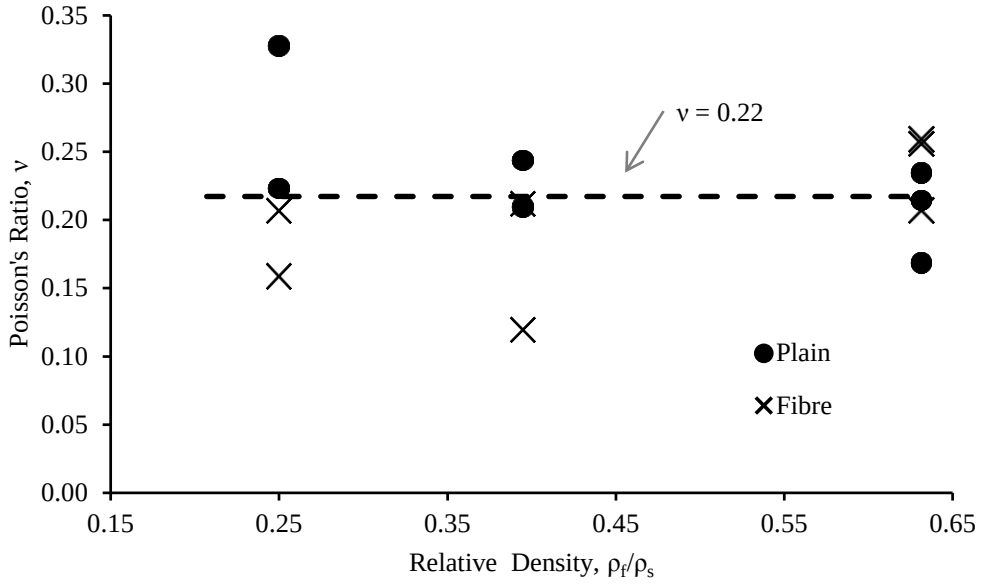

Figure 5.5: Poisson's ratio of cement-based foams for various cast density

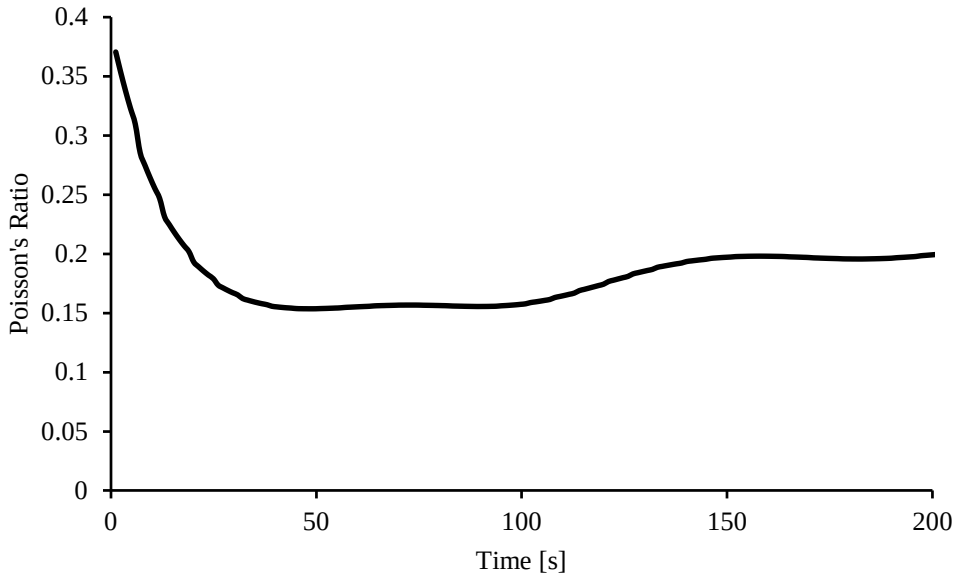

Figure 5.6: Typical Poisson's ratio history of cement-based foams under quasi-static loading

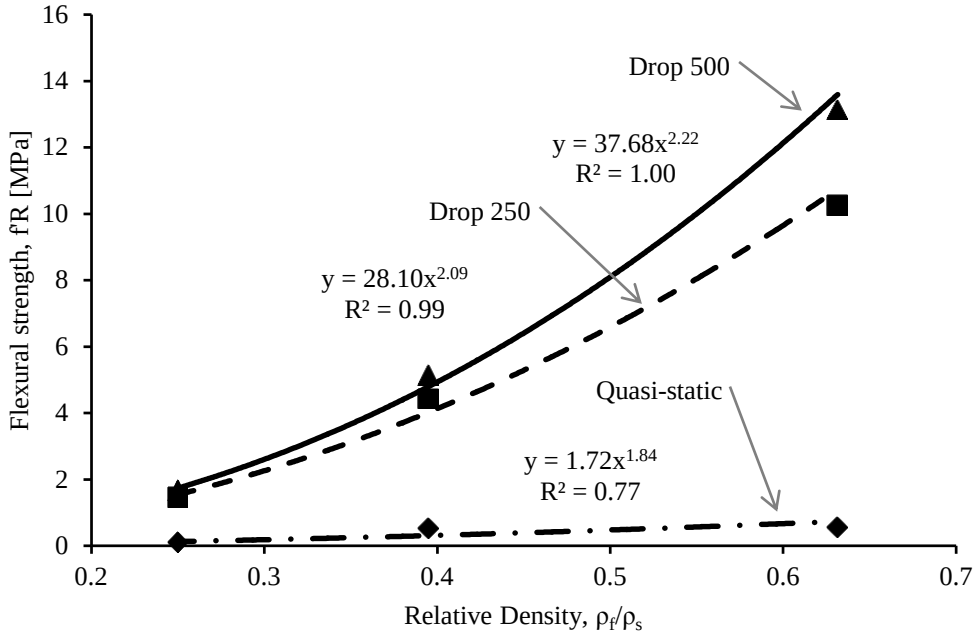

Figure 5.7: Flexural strength of **plain** cement-based foam expressed as a function of relative density

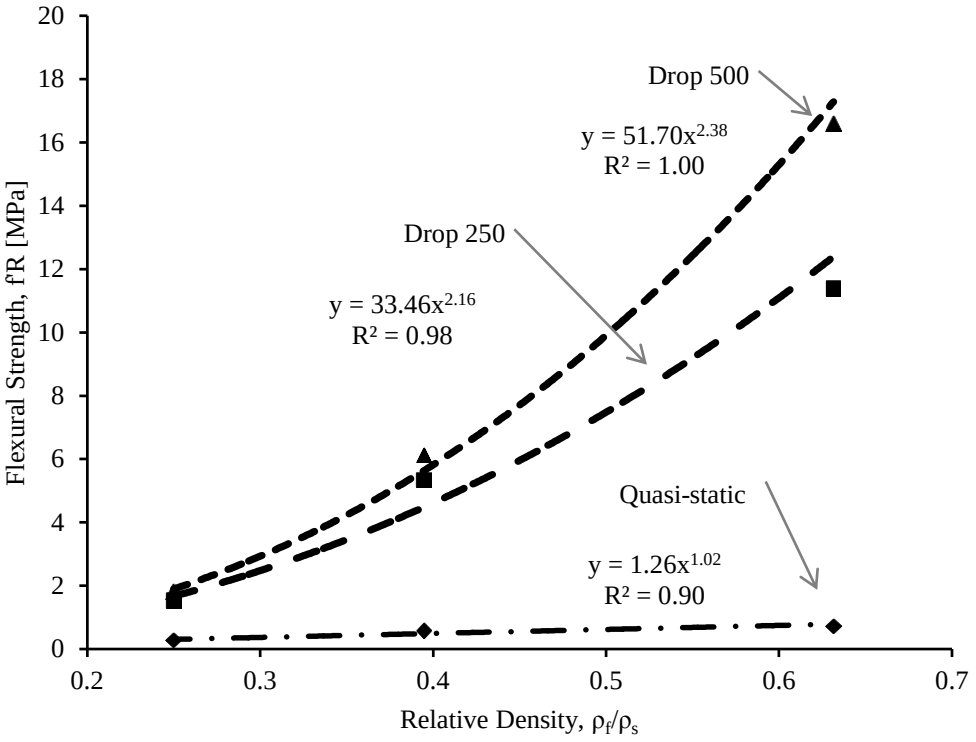

Figure 5.8: Flexural strength of **fibre-reinforced** cement-based foam expressed as a function of relative density

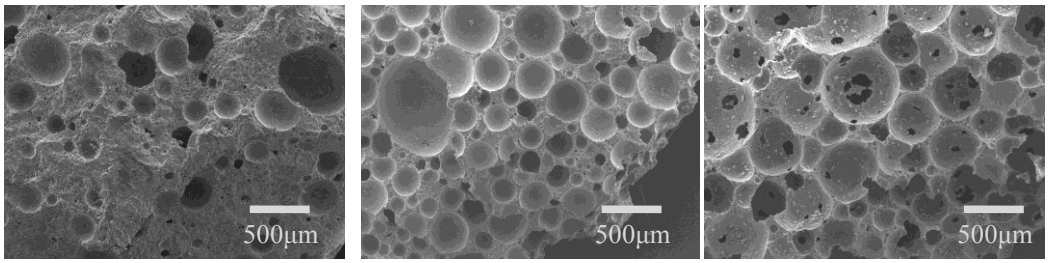

(a) (b) (c)

Figure 5.9: Scanning electron micrograph (100x) of **plain** cement-based foams generated for this study (a) 1200 kg/m^3; (b) 750 kg/m^3; (c) 475 kg/m^3

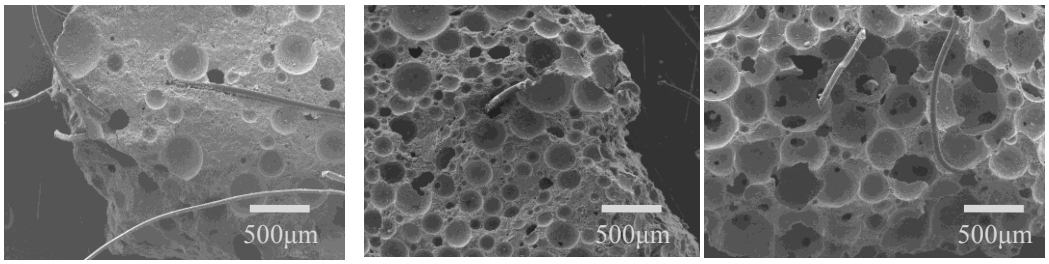

(a) (b) (c)

Figure 5.10: Scanning electron micrograph (100x) of **fibre-reinforced** cement-based foams generated for this study (a) 1200 kg/m^3; (b) 750 kg/m^3; (c) 475 kg/m^3

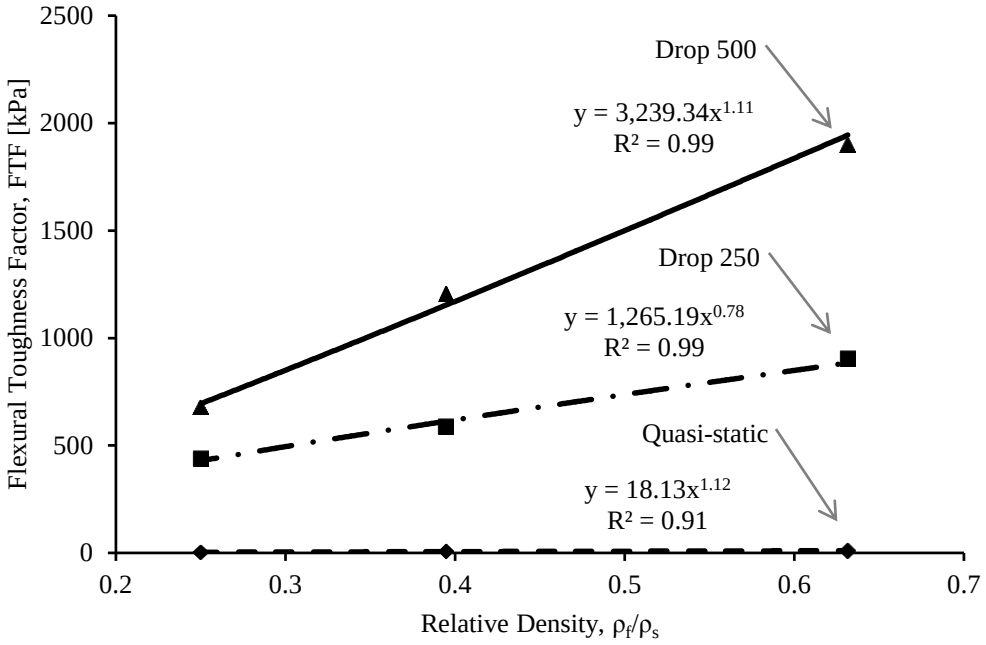

Figure 5.11: Effect of relative density on flexural toughness factor of **plain** cement-based foam

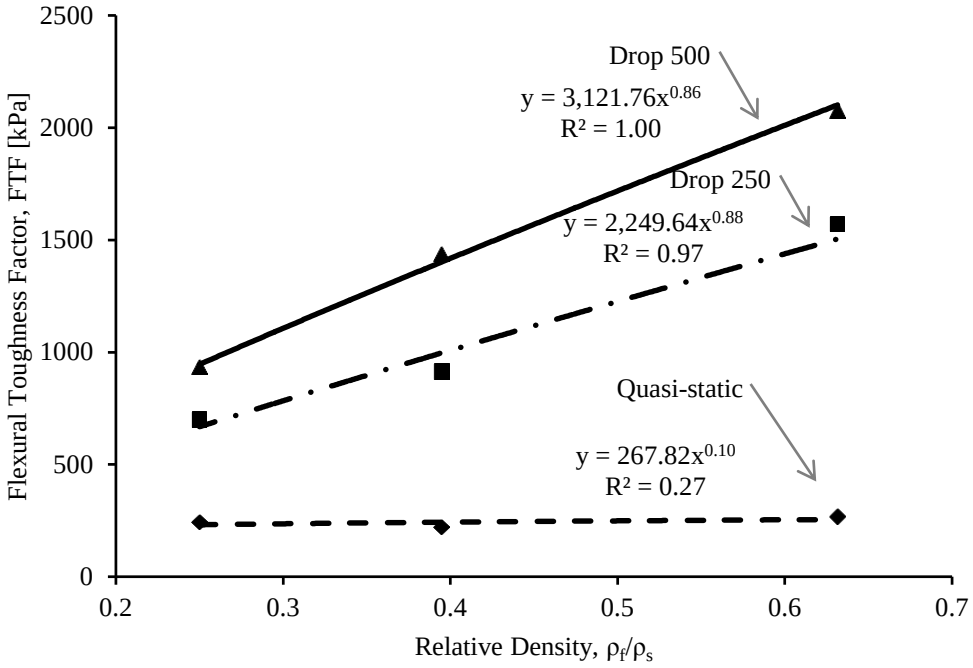

Figure 5.12: Effect of relative density on flexural toughness factor of **fibre-reinforced** cement-based foam

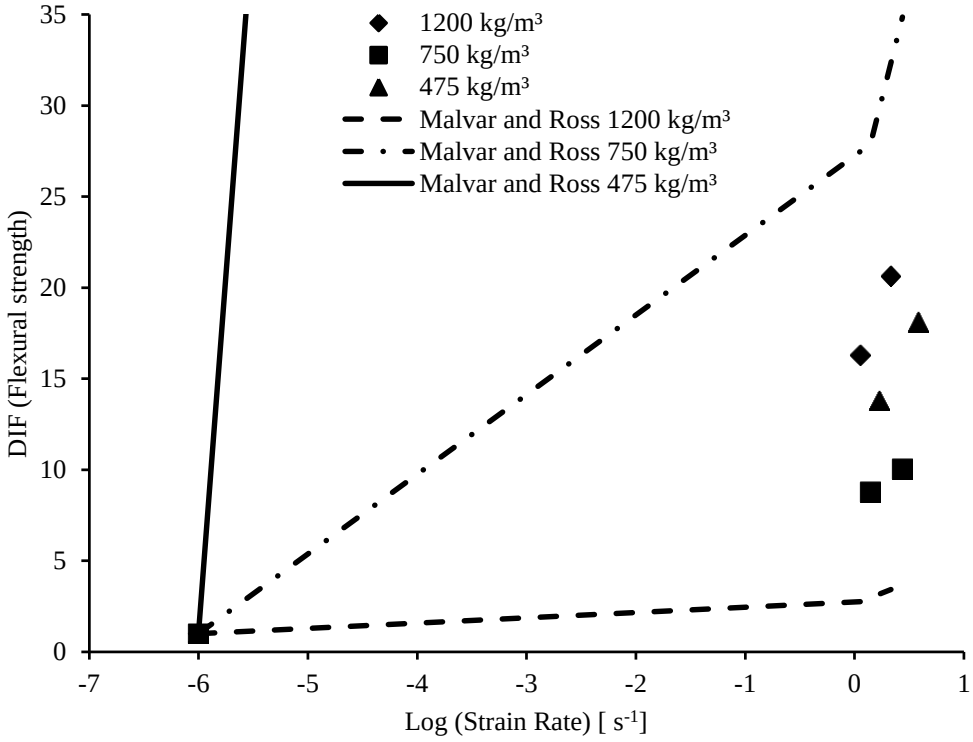

Figure 5.13: Strain-rate sensitivity of **plain** cement-based foam

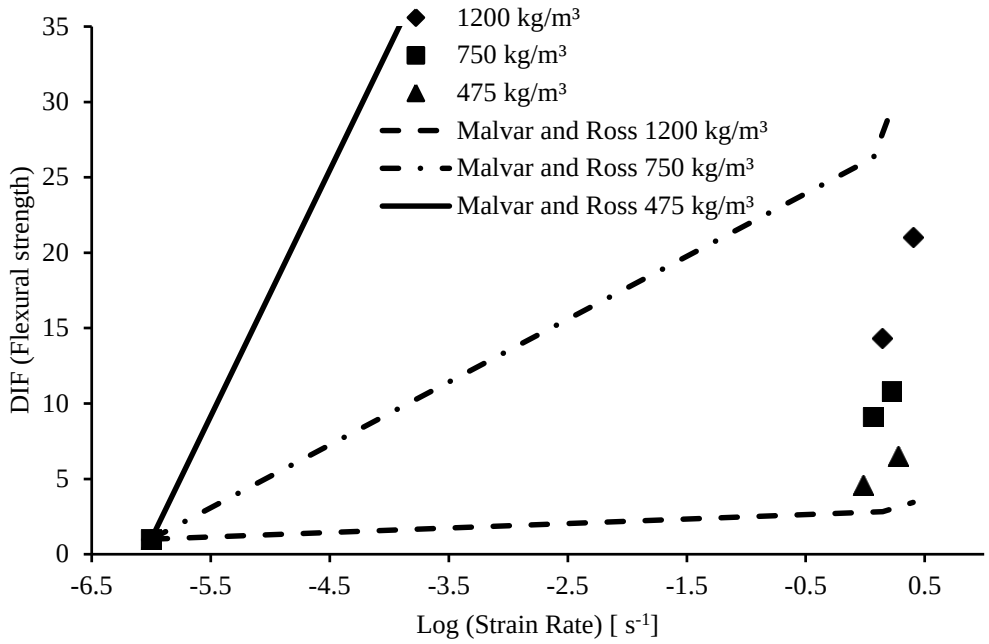

Figure 5.14: Strain-rate sensitivity of **fibre-reinforced** cement-based foam

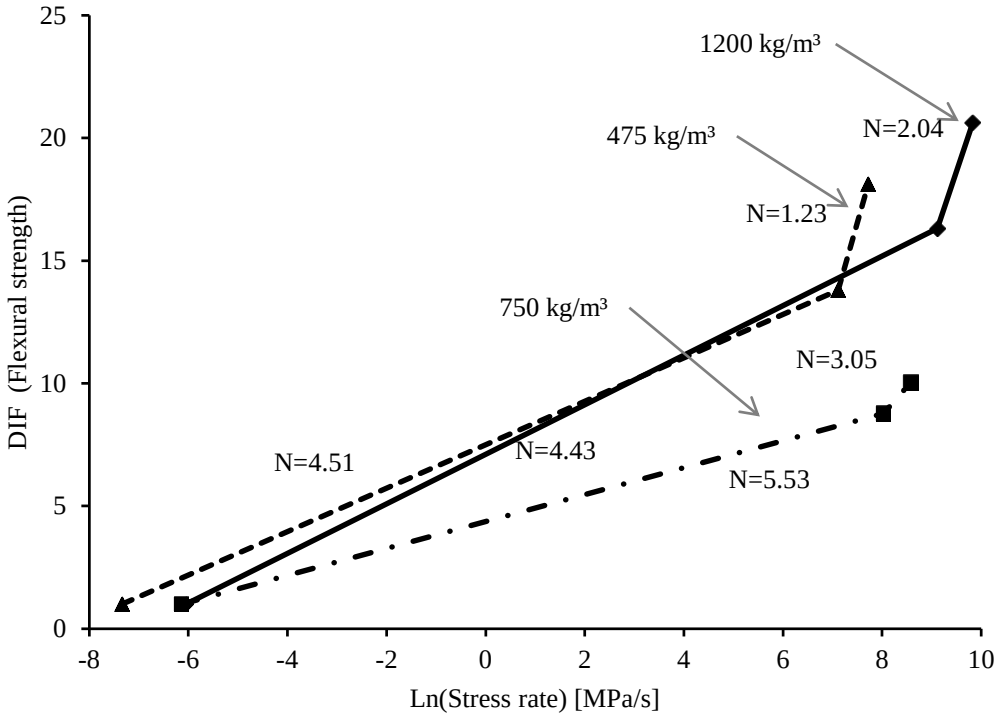

Figure 5.15: Stress-rate sensitivity of **plain** cement-based foam

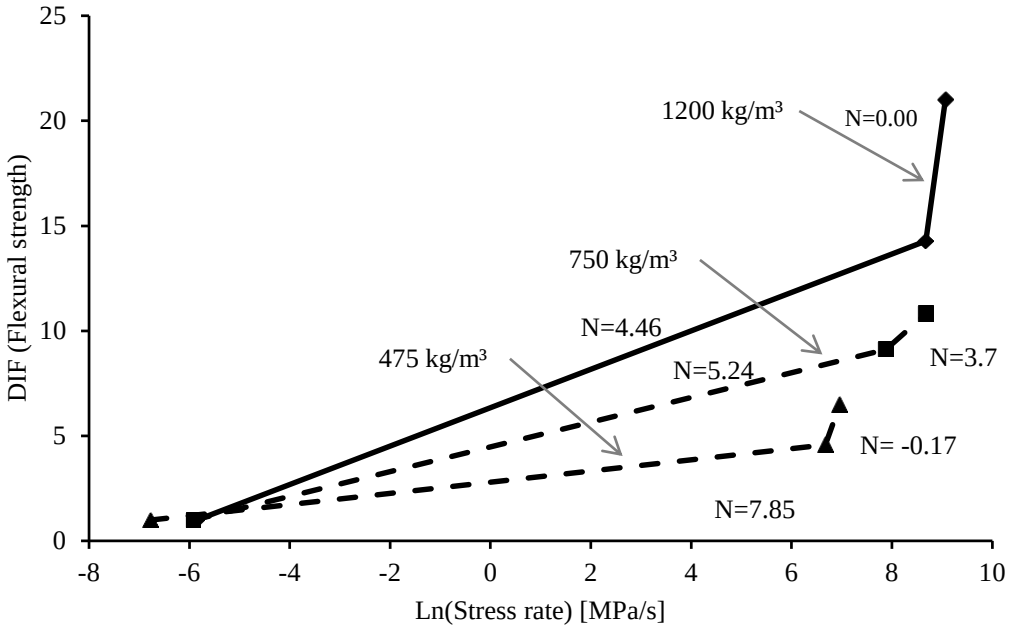

Figure 5.16: Stress-rate sensitivity of **fibre-reinforced** cement-based foam

Chapter 6

RESULTS AND DISCUSSION: SULPHATE RESISTANCE OF CEMENT-BASED FOAMS

6.1 General

The sulphate resistance of conventional cement-based composites is evaluated by means of measuring length change. However, dimensional changes alone are unlikely to be sensitive enough with controlled low-strength building materials such as low-density cementitious foams. Moreover, any change in the internal cellular structure is likely to have a crucial impact on cementitious foams for their continued use as thermal insulators. Accordingly, the present study included a detailed experimental investigation on the mechanical response of plain and fibre-reinforced cement-based foam composites after exposure to a sulphate-rich environment. The mixes described in Chapter 3, Section 3.2.9 were examined. The mechanical performance was evaluated as per ASTM C1609 (2007) and JSCE G-552 (1999) standards that assess post-crack residual strength, and the effects of sulphate exposure were verified through microscopic analyses.

As described in Chapter 3, Section 3.4.1, two separate sets of prisms were immersed in sulphate and water bath, respectively. These were extracted after specific durations of exposure and tested subsequently under compression and four-point flexure. The following Sections in this Chapter compare the

A version of this chapter has been submitted for publication. Mamun & Bindiganavile 2010. Journal of Construction and Building Materials.

mechanical response of cement-based foam exposed to sulphate solution and water. The results from mechanical tests on the samples extracted at different stages of exposure are listed in Tables 6.1 to 6.3. While all six durations of exposure are reported in these tables, the data for the 0, 30, and 90-day exposures are compared below as these were seen to represent critical stages in this study.

6.2 Compressive Response

The compressive strength of plain cement-based foams is shown in Figure 6.1(a) for sulphate exposure and in Figure 6.1(b) for water exposure. Table 6.1 summarizes the compressive strength of specimens extracted from both sulphate and water baths. Recall that the samples had been cast 1 year prior to being immersed in sulphate or water. There was no perceptible change in the compressive response with water immersion. However, when immersed in the sulphate solution, while the compressive strength of the densest foams (cast density = 1200 kg/m^3) decreased by 30%, the lighter specimens saw no significant change in their compressive strength. The reduction in compressive strength in densest foams may be attributed to the crack developed due to the extra formation of etrrigite for which very little space is available compared to the lighter specimens. Figure 6.2 shows the response in compression for the fibre-reinforced cement-based foams. For the unexposed samples it was seen that regardless of fibre content, the compressive strength bore a relation to the relative density of the foamed composite, which may be expressed as $f_c' \propto (\rho_f/\rho_s)^{\alpha}$, where $\alpha \approx 2.50$.

6.3 Flexural Response

The flexural response of plain cement-based foams is illustrated in Figures 6.3–6.5. Note that the modulus of rupture from all six stages of exposure is listed in Table 6.2. While the prisms that were immersed in a sulphate bath are described in part (a) of Figures 6.3–6.5, those that were immersed in water are described in part (b). With increasing duration of exposure, there was a steady deterioration in the pre-peak performance for the densest mix (Figure 6.3). While this was to be expected from sulphate exposure, it was equally true for prisms submerged in water, much like conventional mortar (Alexander, 1980). The lightest mix, on the other hand, had minimal variation in the pre-peak flexural response. Note that there was a slight improvement in the lighter mixes at 90 days of sulphate exposure, indicating a self-healing action. Self-healing action may be described as filling up the crack formed during the initial stage of sulphate exposure with ettringite crystals and thus bridging across the crack at a later stage. For the fibre-reinforced composites, the flexural response was evaluated till a mid-span deflection of 150^{th} of the clear span, as shown in Figures 6.6–6.8. Again, specimens under sulphate exposure are described in part (a) of Figures 6.6–6.10, while those immersed in water are described in part (b). Note that for fibre-reinforced cement-based foams, only the heaviest mix showed a consistent drop in performance with increasing exposure to sulphates. However, one can see that even for this dense mix (1200 kg/m^3) going from 30-day to 90-day immersion in water, the flexural performance showed a marked improvement. This improvement with increasing exposure time is evident for the mix cast at 750

kg/m^3, where the post-peak response was clearly better until 30 days of exposure. The lightest mix showed an improvement in both pre-peak and post-peak response till the 30th day inside the bath. In all cases, there was a drop in performance for prisms immersed beyond 30 days. The lightest mix showed the least variation upon immersion in water as seen from Figures 6.5(b) and 6.8(b).

It is seen from Figures 6.9 and 6.10 that the modulus of rupture of the unreinforced specimens of higher-density foams (cast densities equal to 1200 kg/m^3 and 750 kg/m^3) decreased with an increase in the duration of sulphate exposure. The same trend was witnessed for the fibre-reinforced mixes, although the presence of fibres led to a slightly higher flexural strength compared to the plain composites. On the other hand, the lightest mix (cast density = 475 kg/m^3) witnessed at first an increase in the modulus of rupture upon sulphate exposure before registering a drop beyond 30 days of exposure.

However, as with the higher densities, fibre reinforcement only slightly improved the modulus of rupture regardless of exposure time. The post-crack resistance was evaluated through flexural toughness factors (FTF) as per JSCE-G 552 (1999). When the post-crack response is taken into account, the self-healing effect of sulphate exposure is clearly seen as evident from the flexural toughness factors shown in Figures 6.11 and 6.12 and listed in Table 6.3. Note that only the heaviest mix (cast density = 1200 kg/m^3) showed a consistent drop in FTF with the duration of exposure, whereas even the mix with a cast density of 750 kg/m^3

registered an increase up to 30 days, similar to what was seen with the lightest mix. It is clear that with an increase in the exposure time, the sulphate resistance of higher density composites dropped, whereas the response at lower cast densities may even exceed that of the unexposed specimens. Thus, the difference across the densities became gradually less with an increase in the duration of exposure. The flexural strength of unexposed specimens obeyed the relation of $f_r \propto (\rho_f/\rho_s)^{1.66}$, which is very close to the theoretical exponent of 1.5 associated with brittle cellular solids (Gibson and Ashby, 1999). On the other hand, for those prisms that were exposed to a sulphate solution, the variation with relative density was very different from that of the unexposed specimens, such that the exponent was less than unity. This may be attributed to a gradual loss in the cellular solid structure upon sulphate exposure, which is discussed further in the following section. The exposure to sulphate attack is evident in the flexural response more clearly than in the compressive response.

6.4 Microstructure

In order to explain the perceived improvement in the flexural behaviour of the lighter foams upon sustained exposure to sulphates, samples chosen randomly after the mechanical tests were examined under a scanning electron microscope and the micrographs are shown in Figures 6.13–6.24. Once again, only three representative stages were considered, namely at 0, 30, and 90 days of exposure. The images captured in Figures 6.13 and 6.14 show the insides of a cell in the heaviest unreinforced mix, for sulphate exposure and water exposure, respectively. In the former, note that the cell transforms from being nearly empty

to increasingly filled with cementitious products over the course of 90 days of sulphate exposure. On the other hand, when immersed in water, the cells take on a lightly dusted appearance with minimal additional hydrated products, so that the contours of the spherical cell are still clearly evident. The cementitious products of exposure are illustrated under higher magnification in Figures 6.15 (sulphate exposure) and 6.16 (water exposure). Similarly, for mixes with a cast density of 750 kg/m^3, the individual cells were examined as shown in Figures 6.17 and 6.18, with a magnified image of the cementitious products shown in Figures 6.19 and 6.20. Again, a random cell from three stages of the lightest mix is shown in Figures 6.21 and 6.22, while the magnified images of the products inside are shown in Figures 6.23 and 6.24. Note that unlike the spherical cavity seen in Figure 6.21(a), the cellular structure became indistinguishable after exposure to sulphates due to the profusion of crystalline products completely filling up the air voids, Figure 6.21(c). The identity of these crystals was further confirmed through powder X-ray diffraction charts shown in Figures 6.25–6.30. The notations for the crystals identified are as follows: P = Portlandite (CH); G = Gypsum ($C\bar{S}H_2$); E = Ettringite ($C_6\bar{S}_3H_{32}$); C = Calcite ($CaCO_3$). Note that there initially was a relatively low intensity for ettringite as seen from the mixes unexposed to sulphates. On the other hand, with an increase in the exposure time one marks the appearance of distinct peaks that correspond to ettringite crystals (Figures 6.25, 6.27 and 6.29). With all three cast densities, immersion in water led to the formation of calcite, as evidenced from the X-ray diffraction charts in Figures 6.26, 6.28 and 6.30. Snap shots of the specimen taken at each stage are shown in

Figures 6.31-6.36. It must be highlighted that for the heavier mixes, i.e. cast densities of 1200 kg/m^3 and 750 kg/m^3, it was noted that the unreinforced prisms developed map cracking after a week of sulphate exposure. On the other hand, such a crack pattern was not evident in the lightest mix with a cast density of 475 kg/m^3 until 30 days of exposure (Figures 6.31 and 6.32). Clearly, the distress in the higher density mixes caused by sulphate attack was not witnessed by the low-density foams at the early stages of exposure. This implies that the lightest mix (cast density = 475 kg/m^3) had enough space available to accommodate the ettringite crystals and prevent any attendant cracking until this space was filled up. In contrast, the cellular space in the heavier mixes was not enough to accommodate the expansive formation of ettringite, which, therefore, caused the specimens to crack and achieve lower strength and toughness with continued exposure to the sulphates.

It is clear that in cement-based foams, sulphate exposure leads to the densification of the cellular microstructure due to the formation of ettringite. This in turn results in the closure of cracks which is further helped by the presence of fibres, as evident from the increase in FTF in the lighter fibre-reinforced mixes upon exposure to sulphates. To be sure, such self-healing will result in stronger and tougher cement-based foams especially at lower cast density. However, this very same densification is likely to increase the thermal conductivity of these lightweight composites upon sulphate attack and thus hinder their prevalent use as an insulating material. Research is in progress to address this concern (Batool, 2010).

Table 6.1: Compressive strength of cube specimens sawn from prisms tested under flexure

Mix	Compressive strength [MPa]					
	Sulphate Immersion (days)					
	0	7	15	30	60	90
1200	21.50	13.67	15.00	15.04	15.10	14.60
(PF)	(8 %)	(2 %)	(7 %)	(8 %)	(1 %)	(8 %)
750	4.80	5.27	4.95	7.05	5.10	5.16
(PF)	(3 %)	(1 %)	(1 %)	(2 %)	(6 %)	(7 %)
475	1.84	1.15	2.05	1.65	1.87	1.75
(PF)	(7 %)	(1 %)	(13%)	(7 %)	(6 %)	(6 %)
1200	19.20	18.10	13.50	12.92	18.08	19.40
(FF)	(4 %)	(5 %)	(4 %)	(7 %)	(2 %)	(1 %)
750	7.67	7.70	8.20	9.20	8.07	7.60
(FF)	(2 %)	(9 %)	(7 %)	(6 %)	(5 %)	(5 %)
475	1.62	2.42	2.69	3.25	2.12	1.95
(FF)	(4 %)	(13%)	(11%)	(8 %)	(5 %)	(9 %)
	Water Immersion (days)					
		7	15	30	60	90
1200		19.40	16.60	19.40	19.70	18.40
(PF)		(5 %)	(6 %)	(3 %)	(6 %)	(5 %)
750		6.84	6.96	6.40	6.07	5.40
(PF)		(3 %)	(7 %)	(7 %)	(6 %)	(2 %)
475		1.85	1.65	1.60	1.47	1.20
(PF)		(4 %)	(7 %)	(6 %)	(5 %)	(10%)
1200		20.40	20.30	20.10	18.60	19.67
(FF)		(6 %)	(3 %)	(9 %)	(9 %)	(6 %)
750		7.30	7.97	6.70	8.00	5.97
(FF)		(5 %)	(2 %)	(8 %)	(4 %)	(7 %)
475		1.67	2.15	2.37	2.27	2.30
(FF)		(9 %)	(4 %)	(3 %)	(7 %)	(10%)

Note: PF = Plain foams, FF = Fibre-reinforced foams; Three specimens per mix
Values in parentheses are Coefficient of Variation.

Table 6.2: Flexural strength at various stages of sulphate and water immersion

Mix	Flexural Strength [MPa]					
	Sulphate Immersion (Days)					
	0	7	15	30	60	90
1200	0.53	0.22	0.26	0.30	0.30	0.26
(PF)	(10%)	(13%)	(12%)	(16%)	(14%)	(5 %)
750	0.51	0.24	0.23	0.31	0.30	0.36
(PF)	(9 %)	(8 %)	(10%)	(9 %)	(3 %)	(11%)
475	0.11	0.15	0.12	0.24	0.16	0.16
(PF)	(5 %)	(25%)	(3 %)	(10%)	(9 %)	(8 %)
1200	0.76	0.32	0.31	0.40	0.35	0.35
(FF)	(26 %)	(4 %)	(14%)	(4 %)	(4 %)	(12%)
750	0.58	0.44	0.68	0.50	0.40	0.33
(FF)	(12 %)	(8 %)	(12%)	(5 %)	(12%)	(10%)
475	0.29	0.34	0.37	0.48	0.29	0.31
(FF)	(4 %)	(5 %)	(9 %)	(1 %)	(3 %)	(17%)
	Water Immersion (days)					
		7	15	30	60	90
1200		0.52	0.17	0.27	0.33	0.14
(PF)		(11%)	(12%)	(22%)	(15%)	(11%)
750		0.26	0.32	0.22	0.24	0.23
(PF)		(14%)	(15%)	(20%)	(11%)	(12%)
475		0.11	0.09	0.17	0.08	0.08
(PF)		(13%)	(16%)	(16%)	(15%)	(10%)
1200		0.43	0.47	0.40	0.46	0.64
(FF)		(12%)	(9 %)	(6 %)	(17%)	(5 %)
750		0.31	0.30	0.32	0.33	0.28
(FF)		(0.5%)	(3 %)	(17%)	(10%)	(6 %)
475		0.28	0.37	0.31	0.34	0.26
(FF)		(4 %)	(9 %)	(19%)	(10%)	(18%)

Note: PF = Plain foams, FF = Fibre-reinforced foams; Three specimens per mix
Values in parentheses are Coefficient of Variation.

Table 6.3: Flexural toughness factor at various stages of sulphate and water immersion

Mix	Flexural Toughness Factor [kPa]					
	Sulphate Immersion (Days)					
	0	7	15	30	60	90
1200	19.24	4.80	6.41	7.59	5.27	5.89
(PF)	(5 %)	(16%)	(10%)	(27%)	(11%)	(7 %)
750	10.89	8.27	5.71	12.65	11.54	8.46
(PF)	(8 %)	(16%)	(13%)	(14%)	(3 %)	(1 %)
475	7.48	6.06	4.13	12.89	5.26	7.58
(PF)	(9 %)	(12%)	(2 %)	(10%)	(13%)	(11%)
1200	512.5	255.9	242.7	267.2	233.6	209.9
(FF)	(14%)	(3 %)	(14%)	(12%)	(14%)	(14%)
750	260.7	362.4	414.7	357.3	334.9	293.7
(FF)	(12%)	(5 %)	(13%)	(10%)	(12%)	(10%)
475	212.2	274.3	300.2	381.6	226.8	254.9
(FF)	(1 %)	(3 %)	(2 %)	(2 %)	(3 %)	(17%)
	Water Immersion (Days)					
		7	15	30	60	90
1200		33.88	1.52	13.82	38.99	6.30
(PF)		(17%)	(12%)	(12%)	(3 %)	(1 %)
750		9.35	10.98	3.47	10.74	8.36
(PF)		(1 %)	(13%)	(14%)	(12%)	(12%)
475		2.54	2.16	12.60	5.65	3.11
(PF)		(12%)	(23%)	(2 %)	(23%)	(15%)
1200		253.5	384.3	224.5	361.9	431.4
(FF)		(1 %)	(24%)	(14%)	(4 %)	(6 %)
750		266.9	252.9	282.0	286.5	249.8
(FF)		(3 %)	(24%)	(6 %)	(9 %)	(7 %)
475		225.3	301.1	254.32	289.33	217.61
(FF)		(8 %)	(9 %)	(18%)	(9 %)	(24%)

Note: PF = Plain foams, FF = Fibre-reinforced foams; Three specimens per mix
Values in parentheses are Coefficient of Variation.

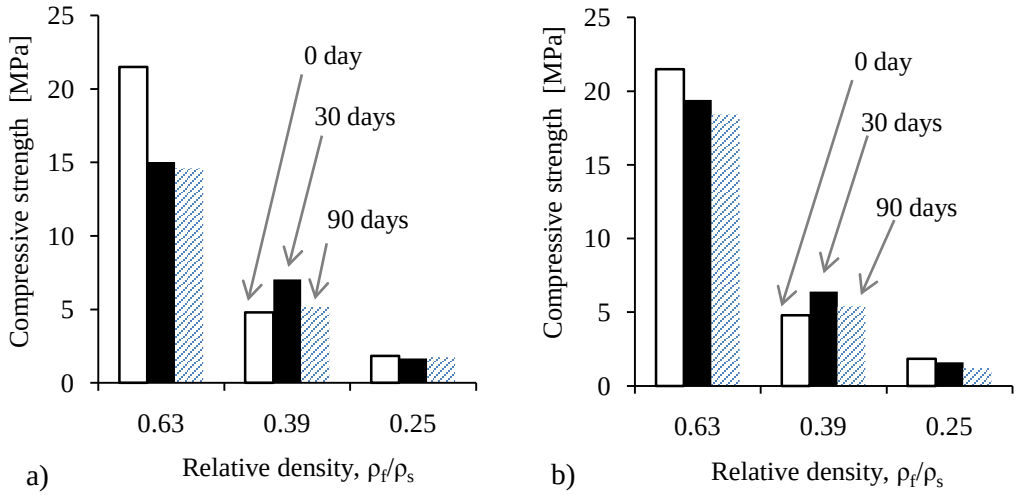

Figure 6.1: Effect of relative density on the compressive strength of **plain** cement-based foams upon (a) sulphate exposure; (b) immersion in water

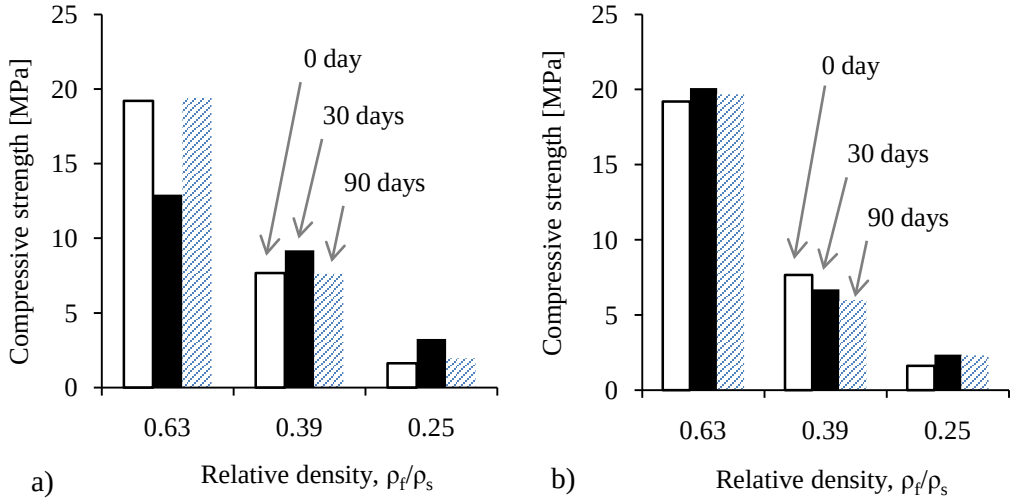

Figure 6.2: Effect of relative density on the compressive strength of **fibre-reinforced** cement-based foams upon (a) sulphate exposure; (b) immersion in water

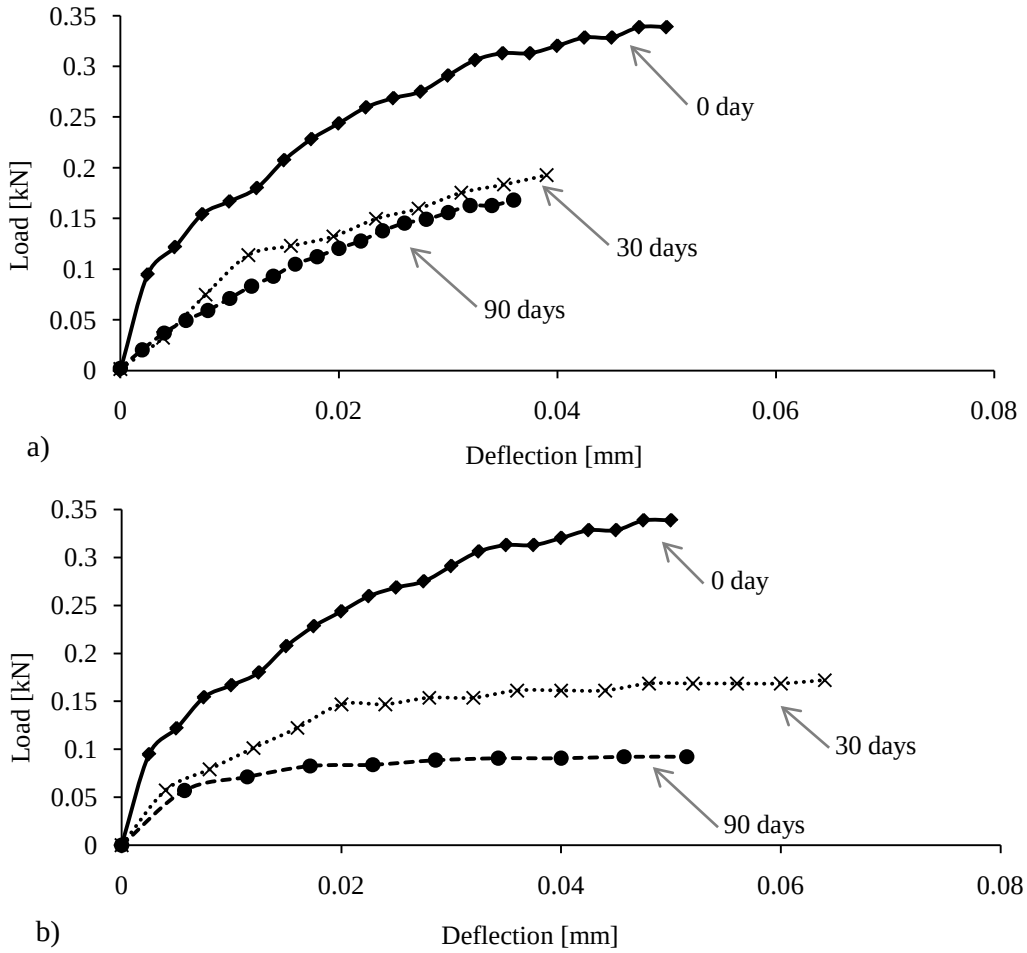

Figure 6.3: Flexural response of **plain** cement-based foams with cast density of 1200 kg/m^3 upon (a) sulphate exposure; (b) immersion in water

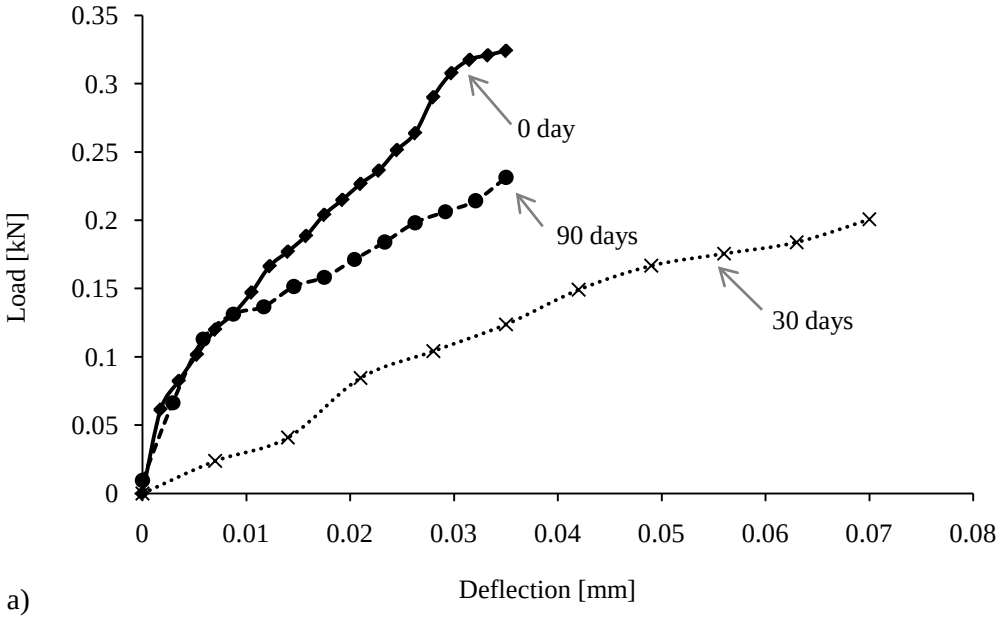

a)

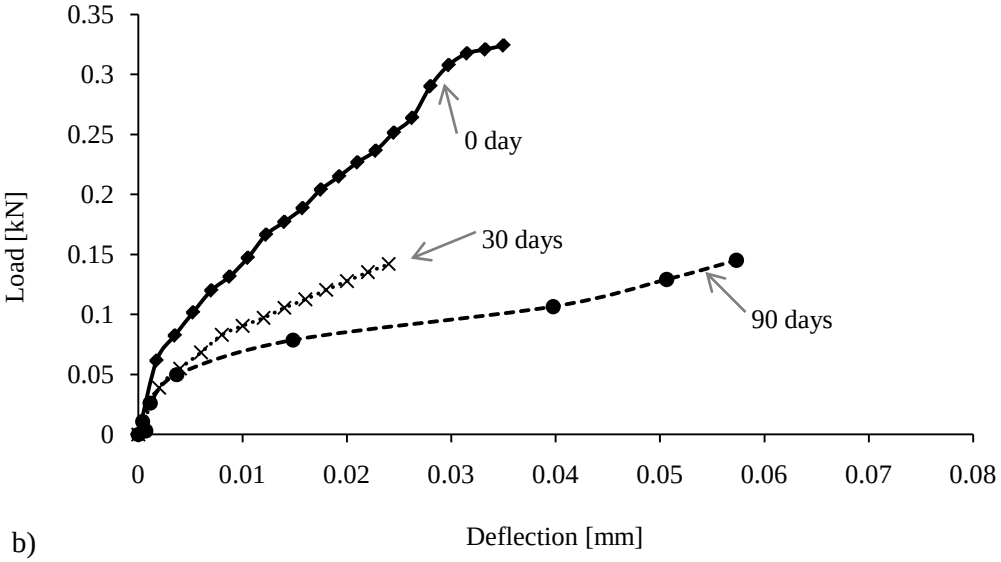

b)

Figure 6.4: Flexural response of **plain** cement-based foams with cast density of 750 kg/m^3 upon (a) sulphate exposure; (b) immersion in water

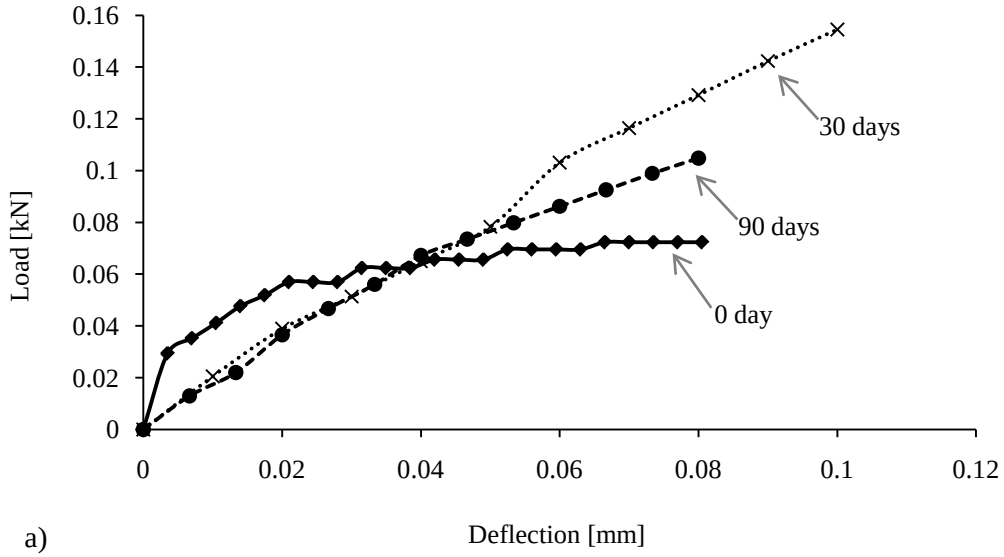

a)

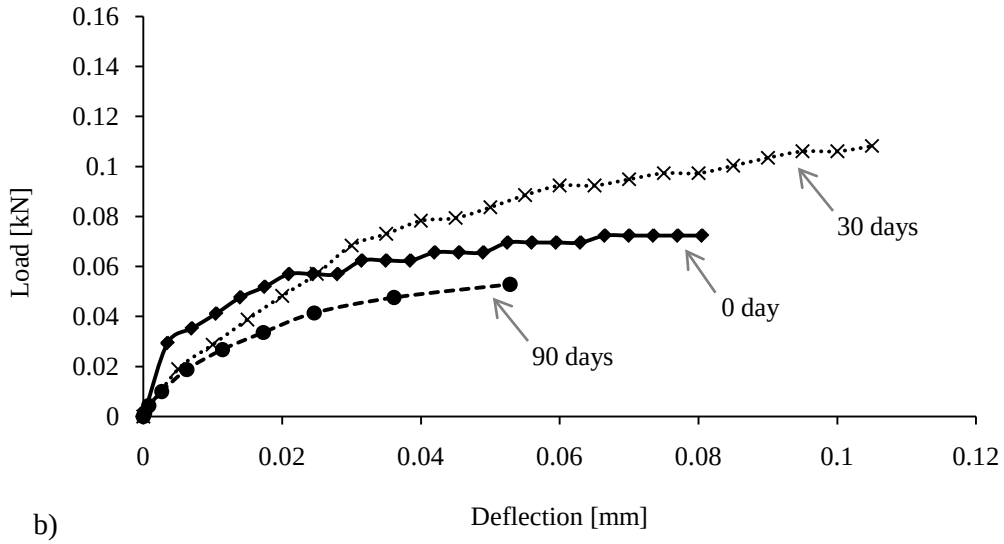

b)

Figure 6.5: Flexural response of **plain** cement-based foams with cast density of 475 kg/m^3 upon (a) sulphate exposure; (b) immersion in water

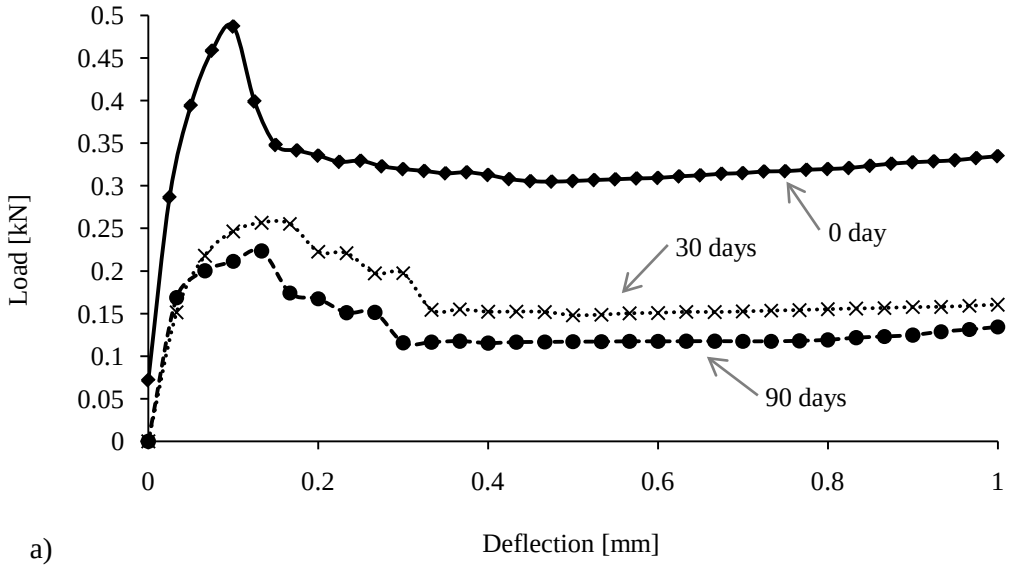

a)

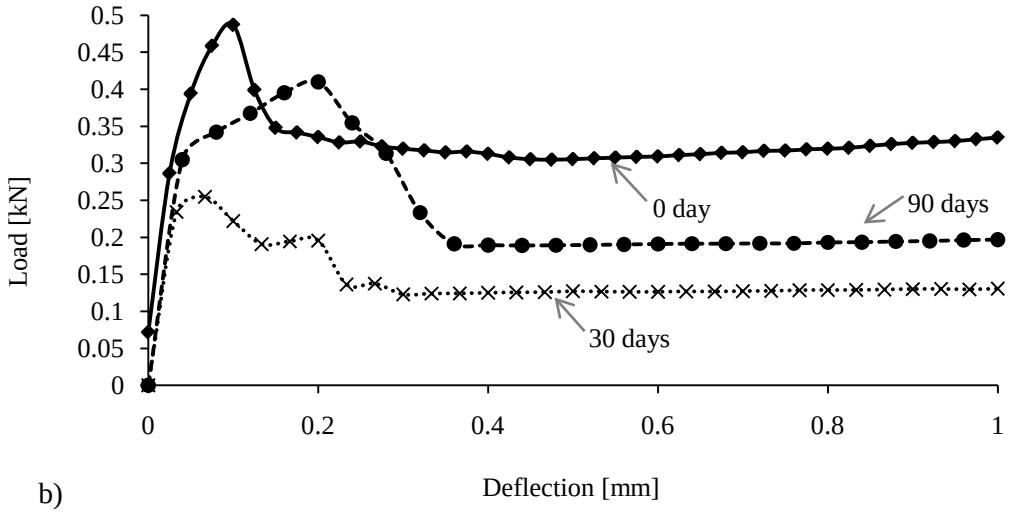

b)

Figure 6.6: Flexural response of **fibre-reinforced** cement-based foams with cast density of 1200 kg/m^3 upon (a) sulphate exposure; (b) immersion in water

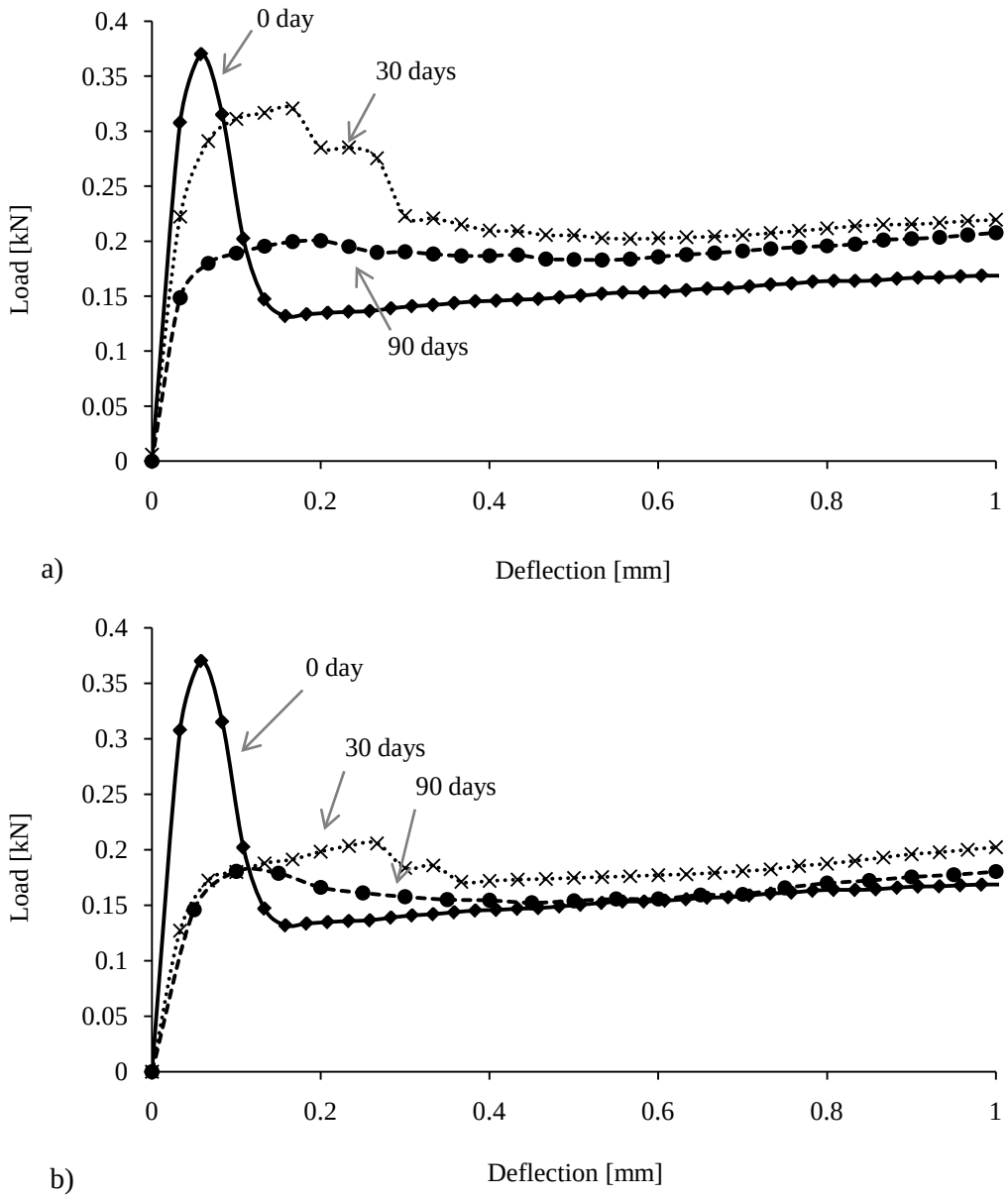

a)

b)

Figure 6.7: Flexural response of **fibre-reinforced** cement-based foams with cast density of 750 kg/m^3 upon (a) sulphate exposure; (b) immersion in water

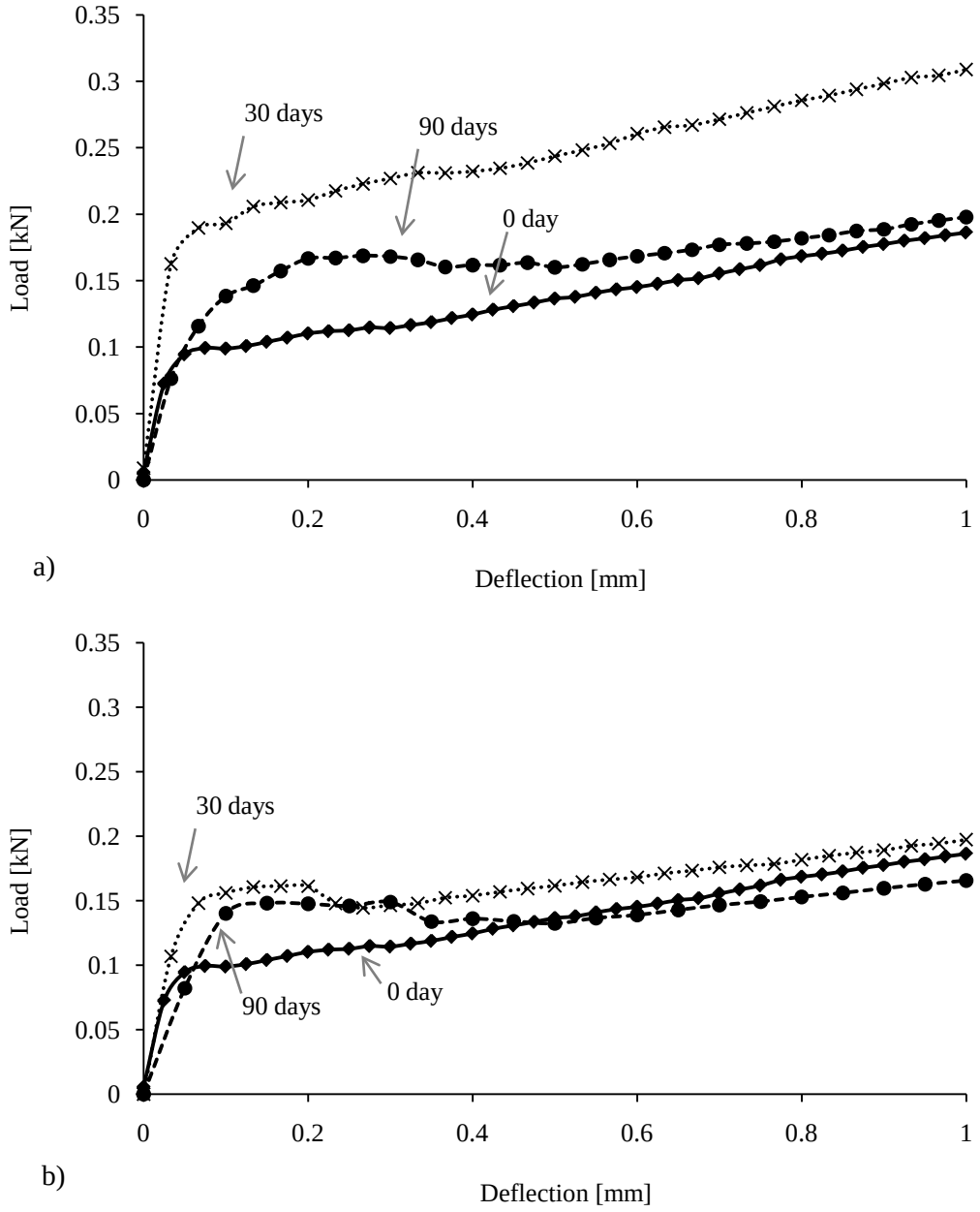

Figure 6.8: Flexural response of **fibre-reinforced** cement-based foams with cast density of 475 kg/m^3 upon (a) sulphate exposure; (b) immersion in water

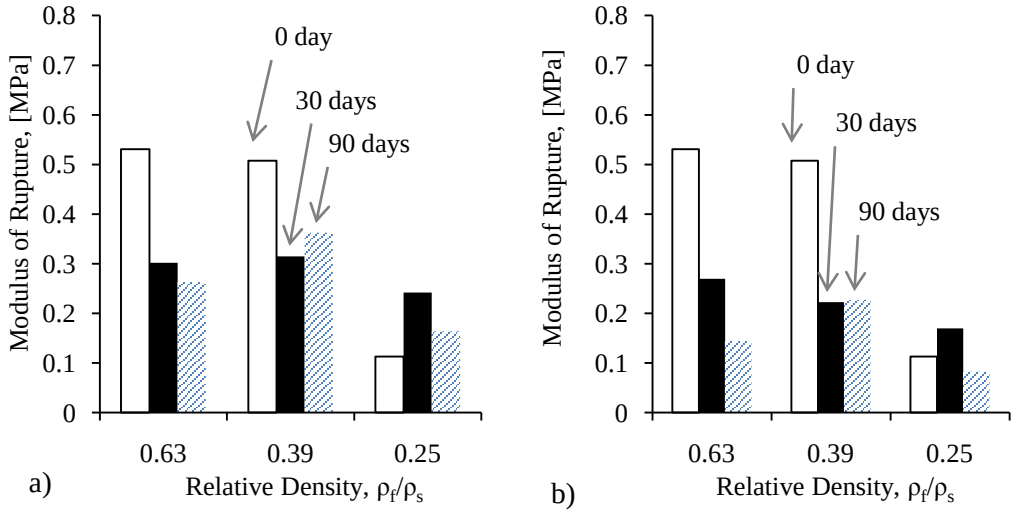

Figure 6.9: Effect of relative density on the modulus of rupture of **plain** cement-based foams upon (a) sulphate exposure; (b) immersion in water

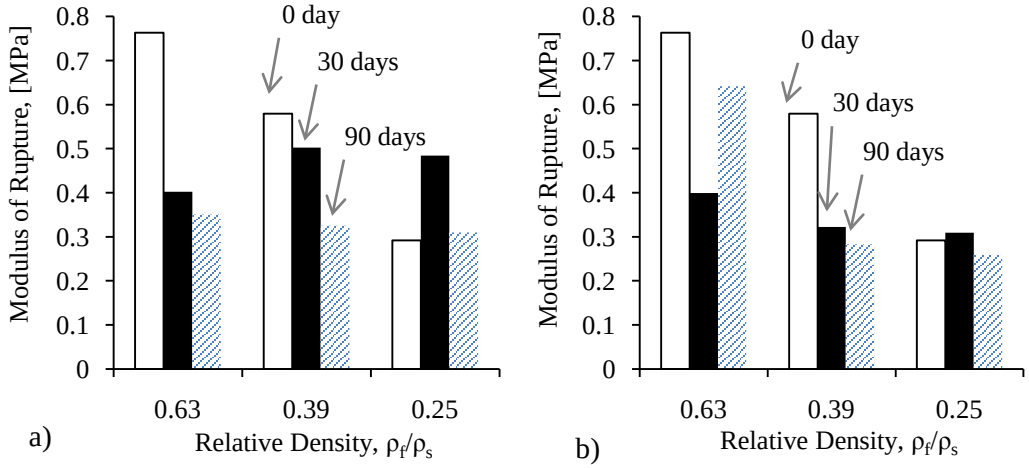

Figure 6.10: Effect of relative density on the modulus of rupture of **fibre-reinforced** cement-based foams upon (a) sulphate exposure; (b) immersion in water

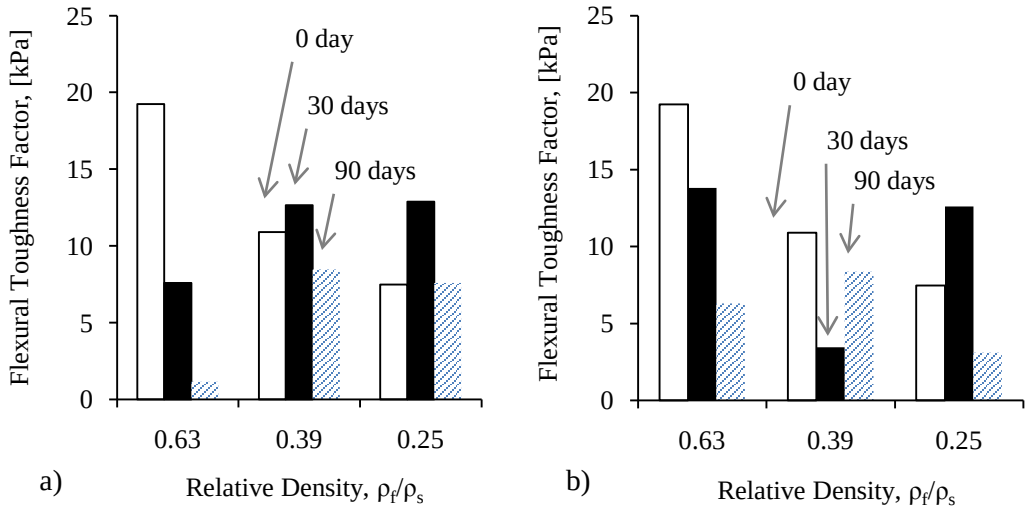

Figure 6.11: Effect of relative density on the flexural toughness factor of **plain** cement-based foams upon (a) sulphate exposure; (b) immersion in water

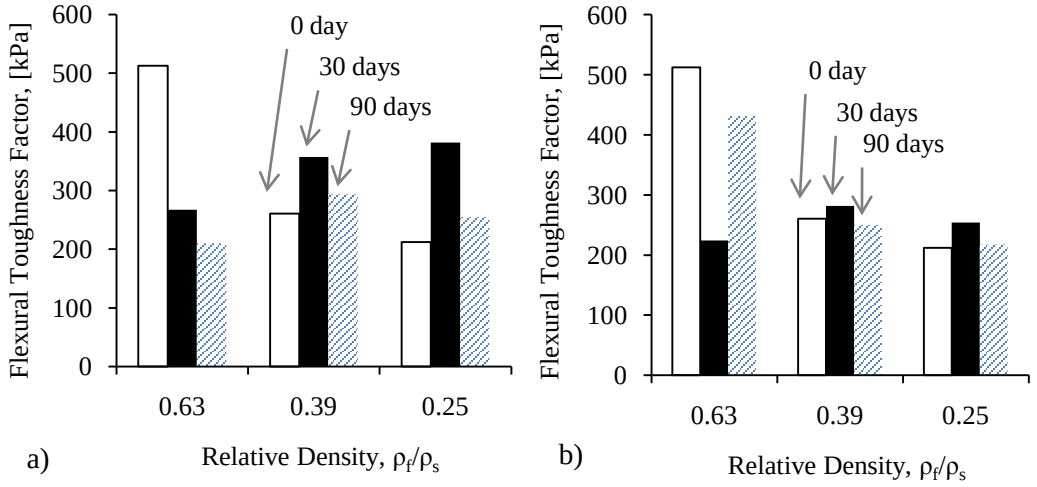

Figure 6.12: Effect of relative density on the flexural toughness factor of **fibre-reinforced** cement-based foams upon (a) sulphate exposure; (b) immersion in water

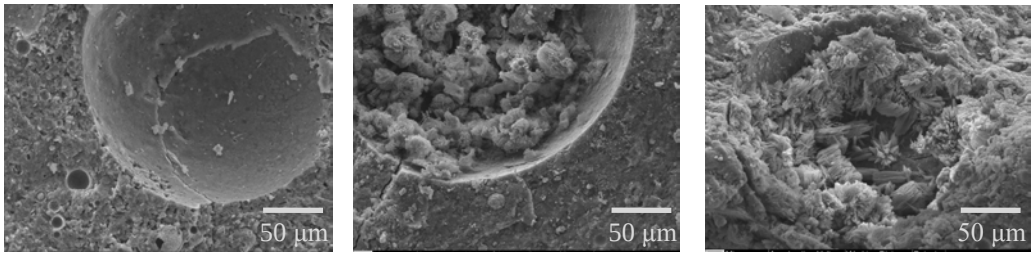

a) b) c)

Figure 6.13: Scanning electron micrograph (1000x) showing the densification in cement-based foams exposed to **sulphate** for cast density of 1200 kg/m^3 (a) 0 day; (b) 30 days; (c) 90 days

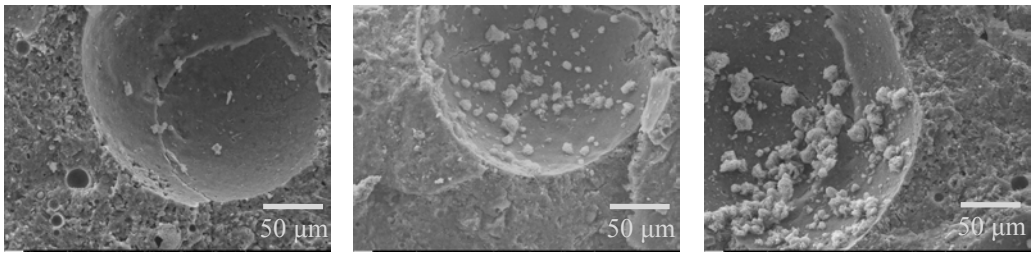

a) b) c)

Figure 6.14: Scanning electron micrograph (1000x) showing the cellular structure in cement-based foams exposed to **water** for cast density of 1200 kg/m^3 (a) 0 day; (b) 30 days; (c) 90 days

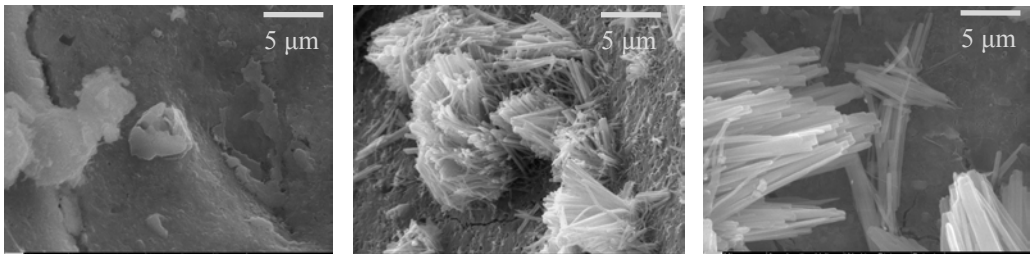

a) b) c)

Figure 6.15: Scanning electron micrograph (10,000x) showing ettringite formation in cement-based foams exposed to **sulphate** for cast density of 1200 kg/m^3 (a) 0 day; (b) 30 days; (c) 90 days

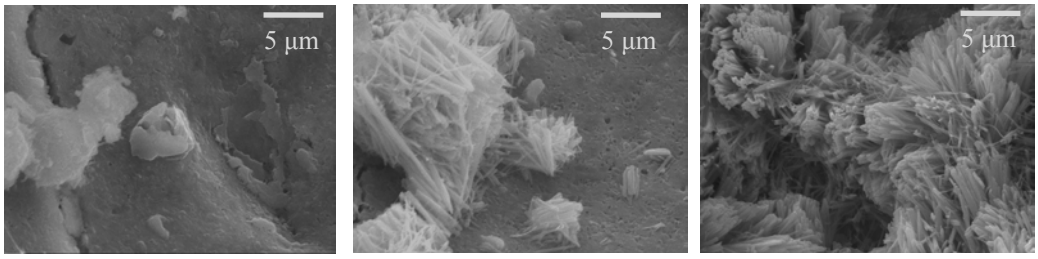

a) b) c)

Figure 6.16: Scanning electron micrograph (10,000x) showing hydration products in cement-based foams exposed to **water** for cast density of 1200 kg/m^3 (a) 0 day; (b) 30 days; (c) 90 days

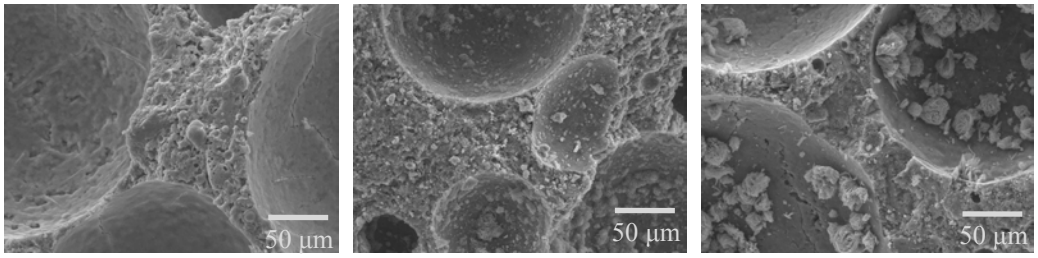

a) b) c)

Figure6.17: Scanning electron micrograph (1000x) showing the densification in cement-based foams exposed to **sulphate** for cast density of 750 kg/m^3 (a) 0 day; (b) 30 days; (c) 90 days

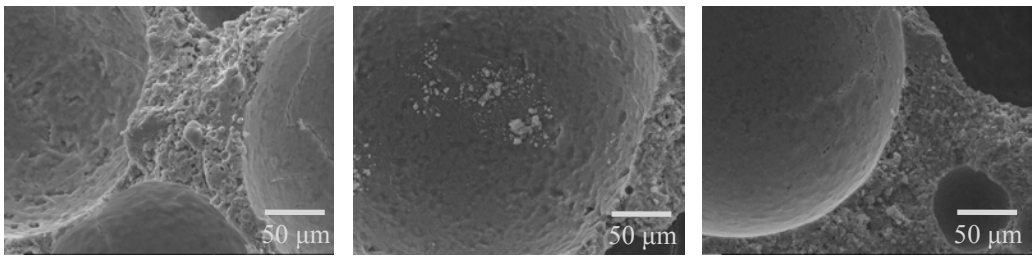

a) b) c)

Figure6.18: Scanning electron micrograph (1000x) showing the cellular structure in cement-based foams exposed to **water** for cast density of 750 kg/m^3 (a) 0 day; (b) 30 days; (c) 90 days

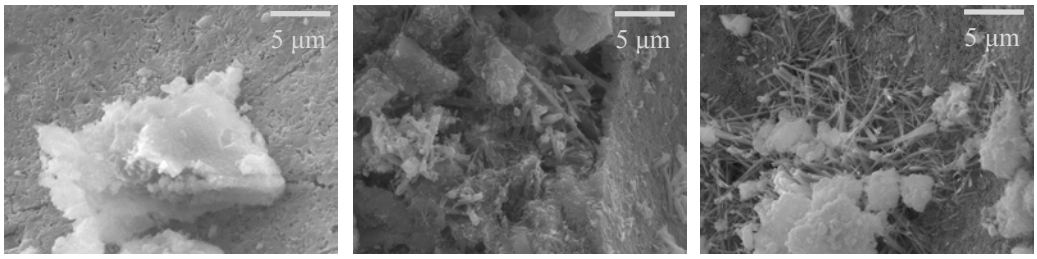

a) b) c)

Figure 6.19: Scanning electron micrograph (10,000x) showing ettringite formation in cement-based foams exposed to **sulphate** for cast density of 750 kg/m^3 (a) 0 day; (b) 30 days; (c) 90 days

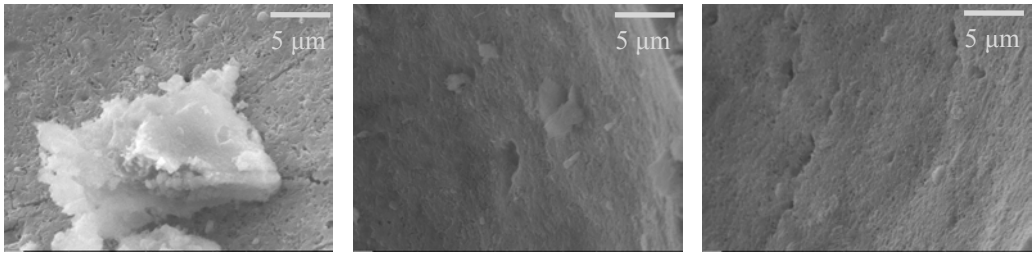

a) b) c)

Figure 6.20: Scanning electron micrograph (10,000x) showing hydration products in cement-based foams exposed to **water** for cast density of 750 kg/m^3 (a) 0 day; (b) 30 days; (c) 90 days

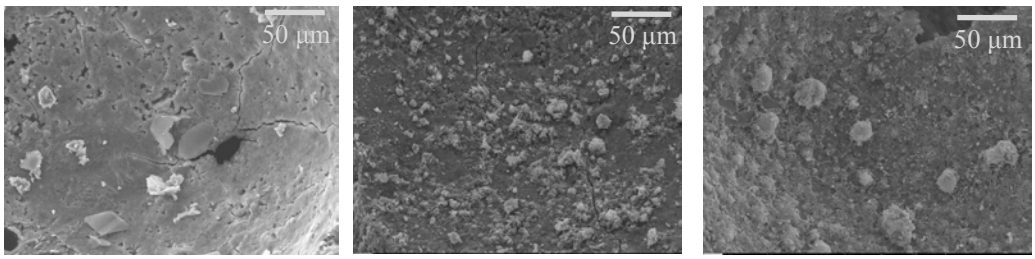

a) b) c)

Figure 6.21: Scanning electron micrograph (1000x) showing the densification in cement-based foams exposed to **sulphate** for cast density of 475 kg/m^3 (a) 0 day; (b) 30 days; (c) 90 days

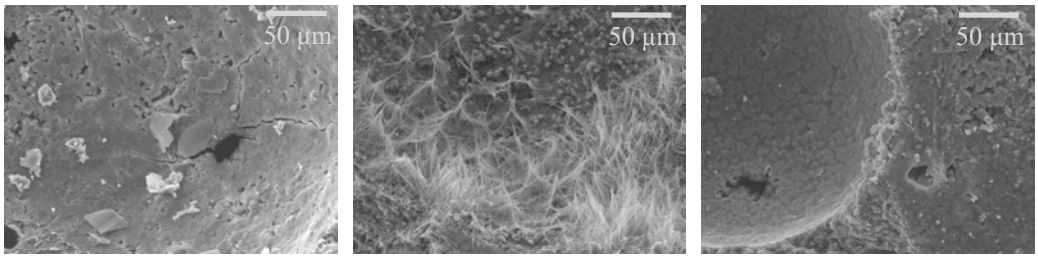

a) b) c)

Figure 6.22: Scanning electron micrograph (1000x) showing the cellular structure in cement-based foams exposed to **water** for cast density of 475 kg/m^3 (a) 0 day; (b) 30 days; (c) 90 days

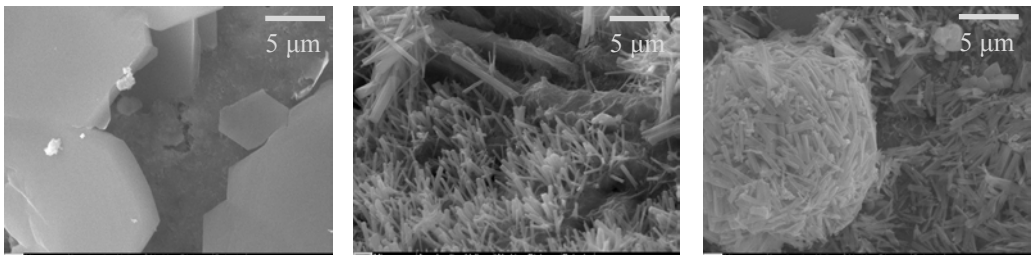

a) b) c)

Figure 6.23: Scanning electron micrograph (10,000x) showing ettringite formation in cement-based foams exposed to **sulphate** for cast density of 475 kg/m^3 (a) 0 day; (b) 30 days; (c) 90 days

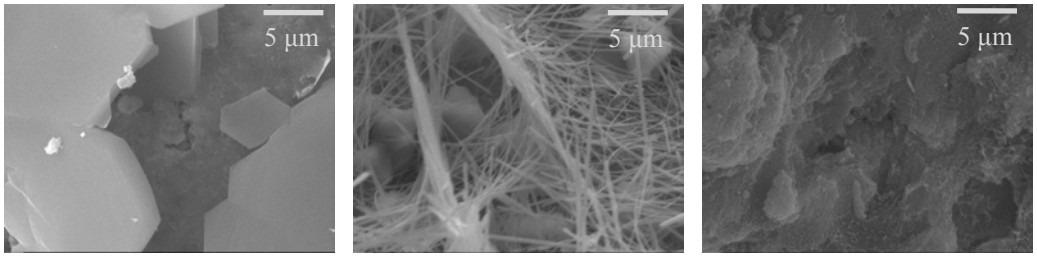

a) b) c)

Figure 6.24: Scanning electron micrograph (10,000x) showing hydration products in cement-based foams exposed to **water** for cast density of 475 kg/m^3 (a) 0 day; (b) 30 days; (c) 90 days

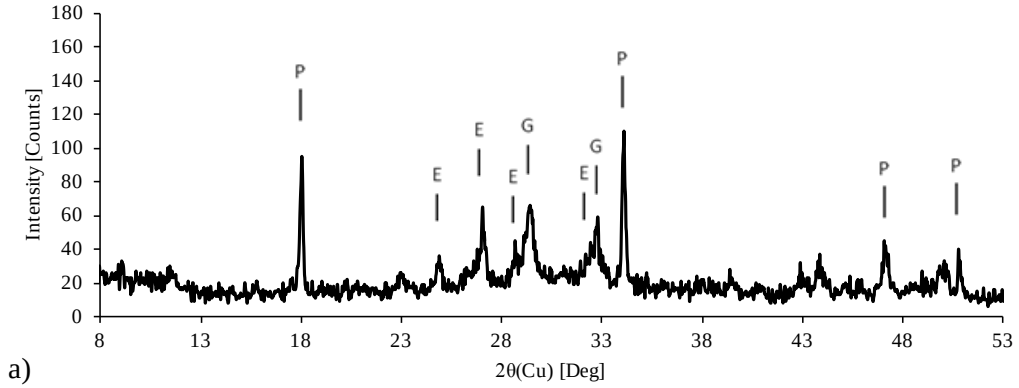

a)

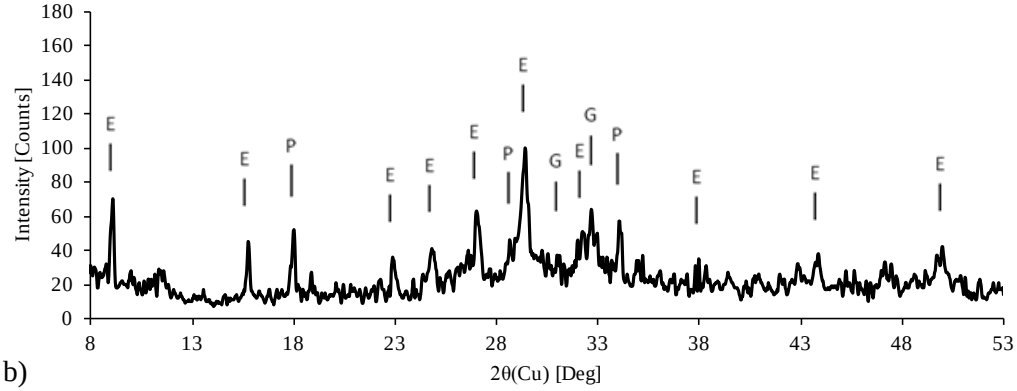

b)

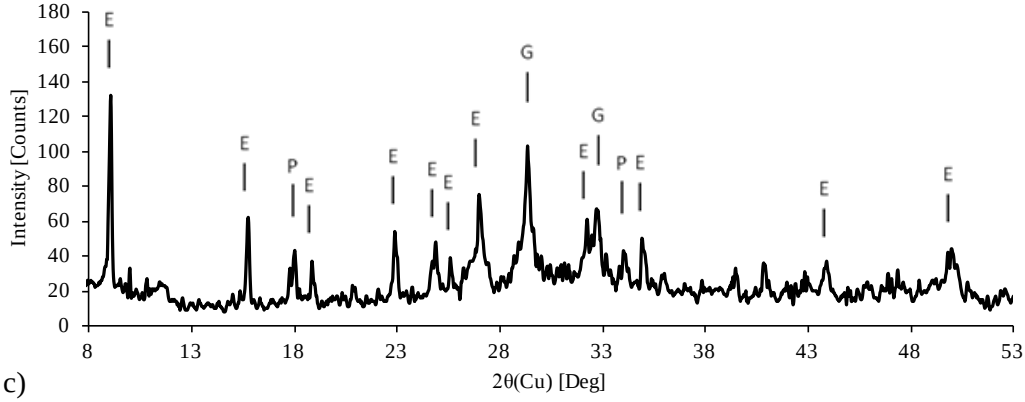

c)

Figure 6.25: X-ray diffraction of cement-based foams exposed to **sulphate** for cast density of 1200 kg/m^3 (a) 0 day; (b) 30 days; (c) 90 days

Note: C ≡ Calcite; E ≡ Ettringite; G ≡ Gypsum; P ≡ Portlandite

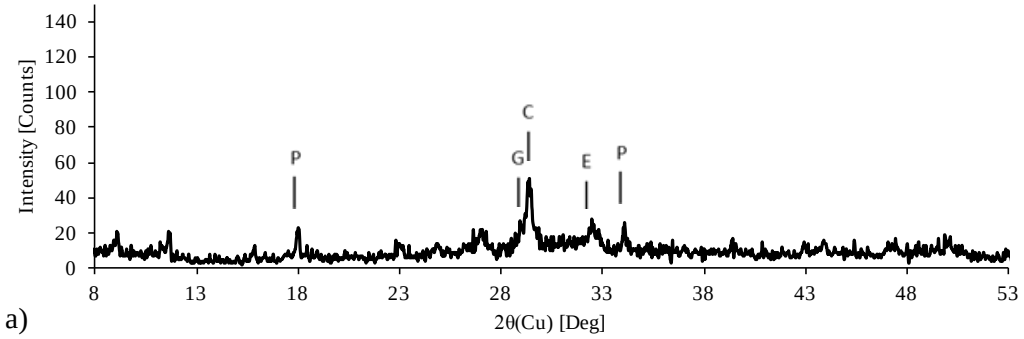

a)

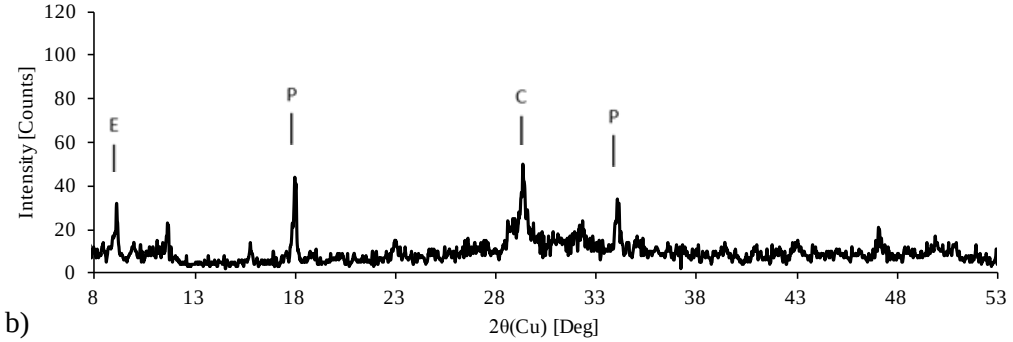

b)

Figure 6.26: X-ray diffraction of cement-based foams exposed to **water** for cast density of 1200 kg/m^3 (a) 30 days; (b) 90 days

Note: C ≡ Calcite; E ≡ Ettringite; G ≡ Gypsum; P ≡ Portlandite

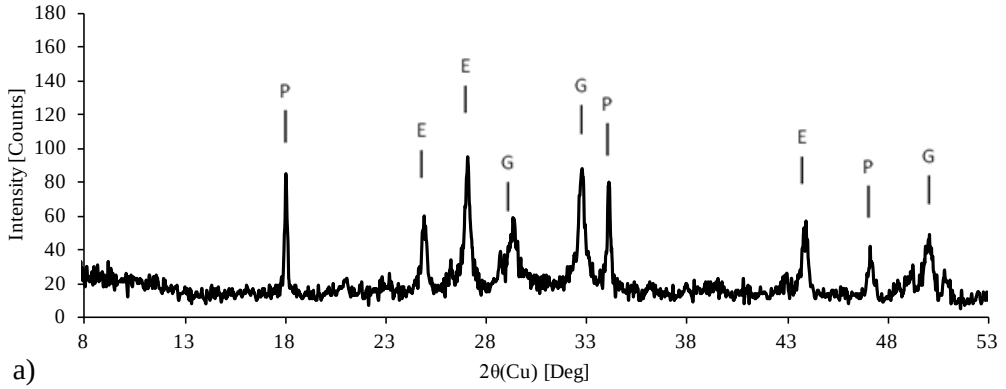

a)

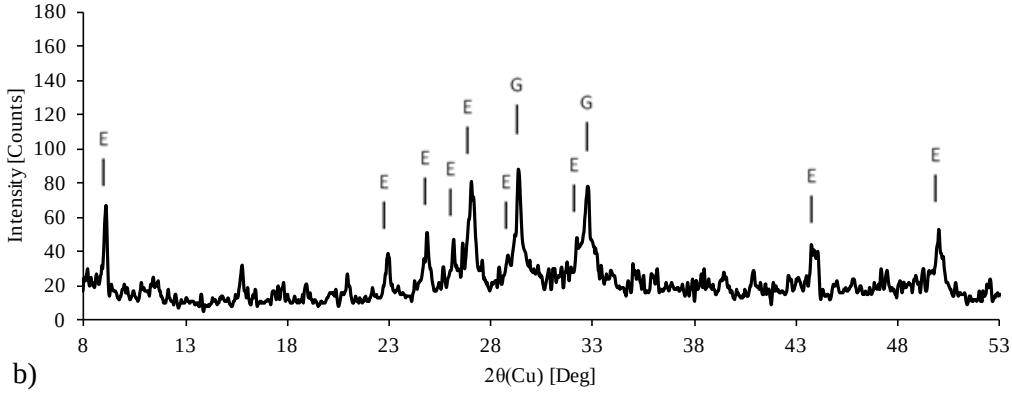

b)

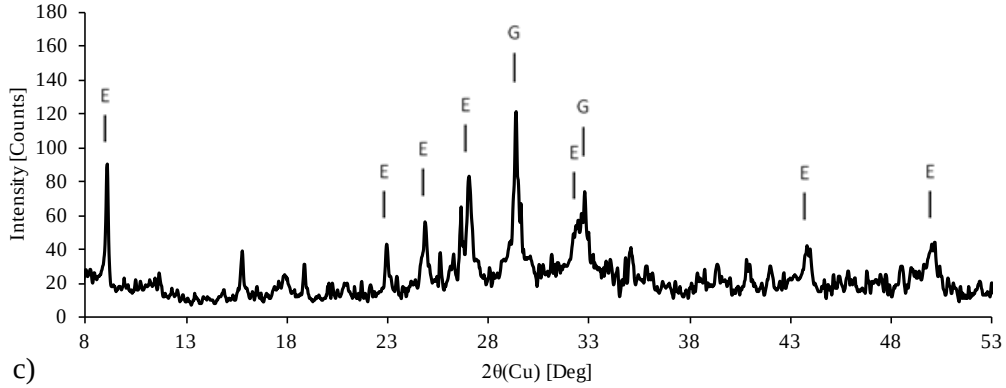

c)

Figure 6.27: X-ray diffraction of cement-based foams exposed to **sulphate** for cast density of 750 kg/m^3 (a) 0 day; (b) 30 days; (c) 90 days

Note: C ≡ Calcite; E ≡ Ettringite; G ≡ Gypsum; P ≡ Portlandite

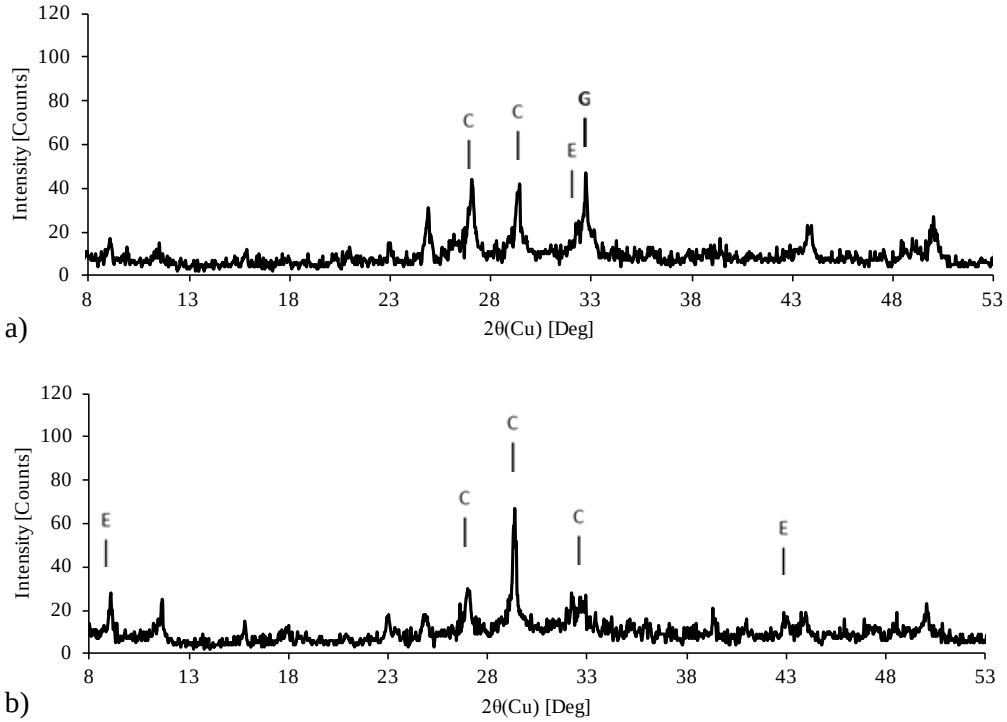

Figure 6.28: X-ray diffraction of cement-based foams exposed to **water** for cast density of 750 kg/m^3 (a) 30 days; (b) 90 days

Note: C ≡ Calcite; E ≡ Ettringite; G ≡ Gypsum; P ≡ Portlandite

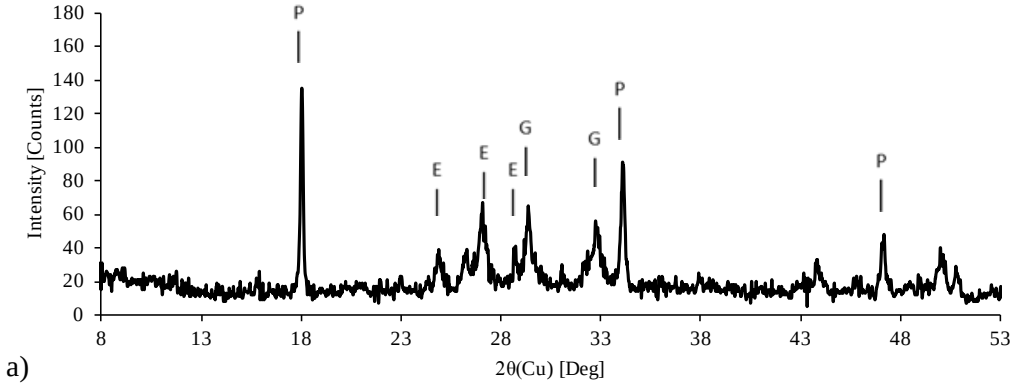

a)

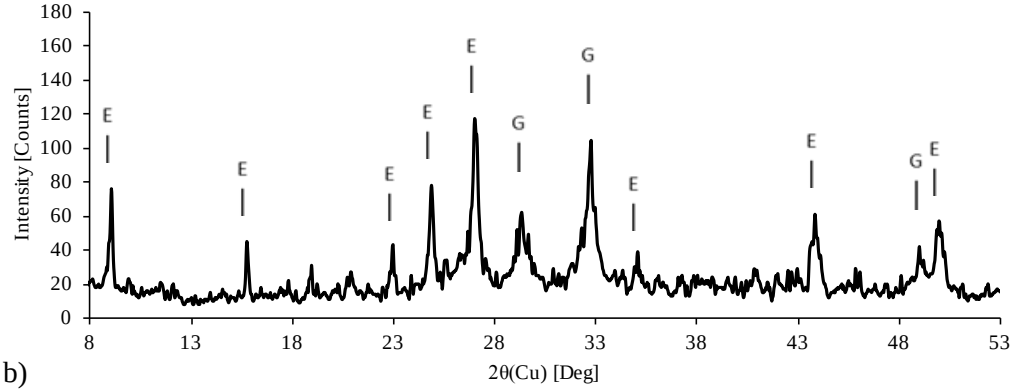

b)

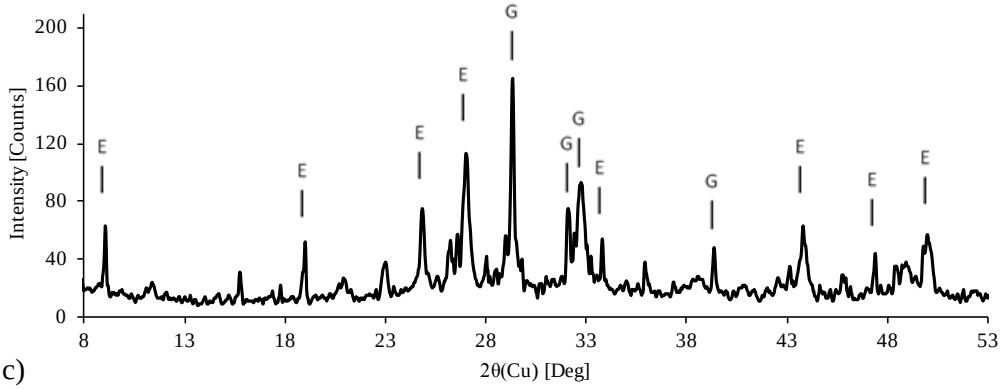

c)

Figure 6.29: X-ray diffraction of cement-based foams exposed to **sulphate** for cast density of 475 kg/m^3 (a) 0 day; (b) 30 days; (c) 90 days

Note: C ≡ Calcite; E ≡ Ettringite; G ≡ Gypsum; P ≡ Portlandite

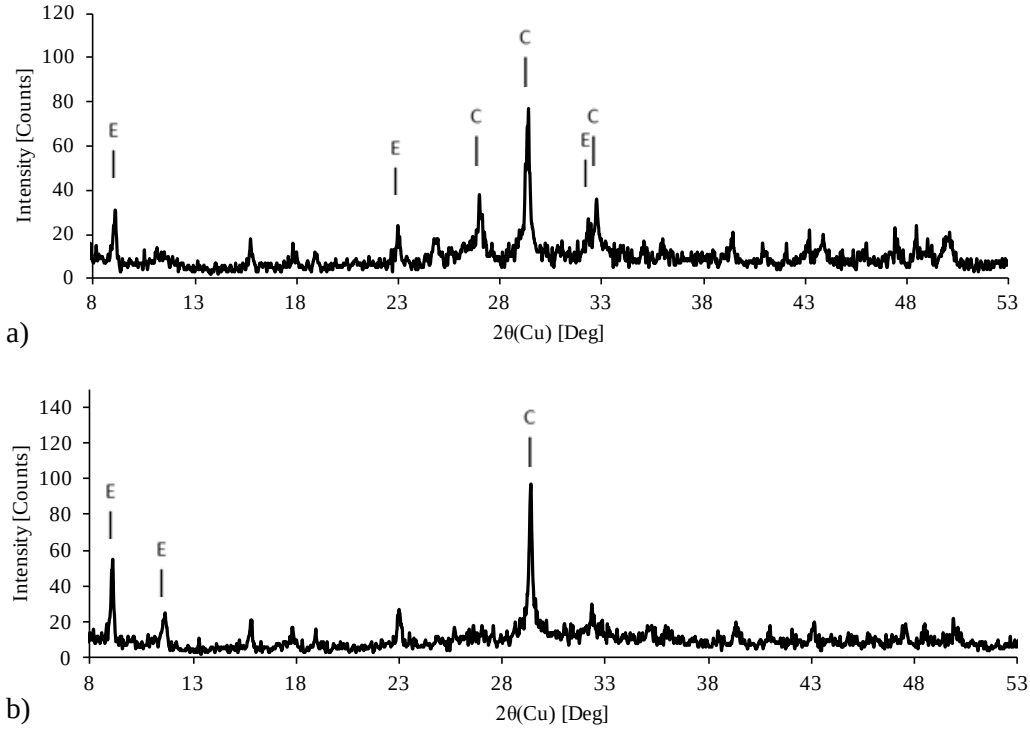

Figure 6.30: X-ray diffraction of cement-based foams exposed to **water** for cast density of 475 kg/m^3 (a) 30 days; (b) 90 days

Note: C ≡ Calcite; E ≡ Ettringite; G ≡ Gypsum; P ≡ Portlandite

a) 0 day

b) 30 days

c) 90 days

Figure 6.31: Photograph of **plain** cement-based foams with cast density of 475 kg/m^3 exposed to sulphate for various duration

a) 0 day

b)30 days

c) 90 days

Figure 6.32: Photograph of **fibre-reinforced** cement-based foams with cast density of 475 kg/m^3 exposed to sulphate for various duration

a) 0 day

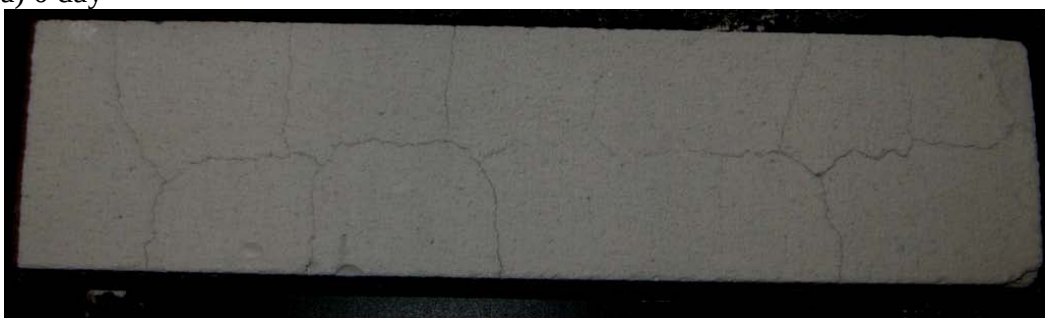

b) 7 days

c) 90 days

Figure 6.33: Photograph of **plain** cement-based foams with cast density of 750 kg/m^3 exposed to sulphate for various duration

a) 0 day

b) 15 days

c) 90 days

Figure 6.34: Photograph of **fibre-reinforced** cement-based foams with cast density of 750 kg/m^3 exposed to sulphate for various duration

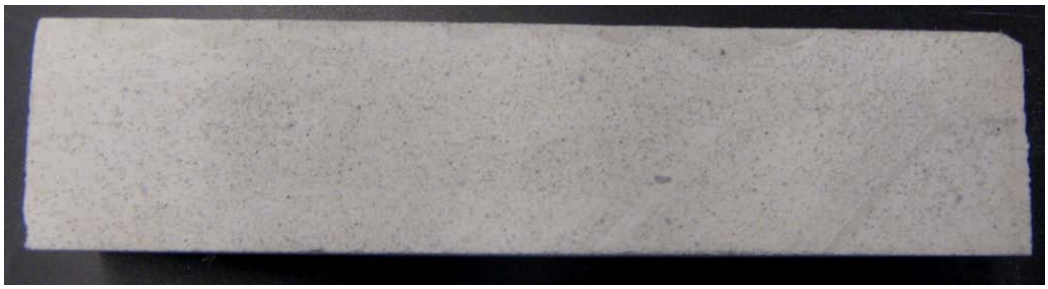

a) 0 day

b) 7 days

c) 90 days

Figure 6.35: Photograph of **plain** cement-based foams with cast density of 1200 kg/m^3 exposed to sulphate for various duration

a) 0 day

b) 7 days

c) 90 days

Figure 6.36: Photograph of **fibre-reinforced** cement-based foams with cast density of 1200 kg/m^3 exposed to sulphate for various duration

Chapter 7

CONCLUSION AND RECOMMENDATIONS

7.1 Summary

Cement-based foam, a controlled low-strength material, is used widely today as a light weight fill and insulation across Canada. Development of techniques to utilize it as crash-cushions and in other shock absorbing application needs technical data regarding the mechanical response especially when subjected to a high strain rate. In geothermal applications, resistance to sulphate attack is a significant concern for this cementitious material. In order to explore the above mentioned areas of interest, a detailed experimental program was carried out.

Altogether, both unreinforced and fibre-reinforced specimens were prepared at three cast densities. Three types of loading configurations were chosen for this study — compression, quasi-static flexure and drop-weight impact. Tests were conducted using available standards or techniques, well documented in the literature. Experimental setups were arranged by choosing appropriate types of test apparatus including a state-of-the-art data acquisition system. Sulphate resistance tests were conducted using a test environment as per an existing ASTM standard. However, changes in the mechanical response were chosen to describe performance instead of the conventional way of reporting length change to describe resistance to sulphate exposure. These were followed by microscopic

imaging and crystallographic techniques to study the internal structure and explain the micromechanical response.

The mechanical response of cement-based foams was discussed in terms of compressive strength, modulus of elasticity, Poisson's ratio, modulus of rupture, flexural toughness, strain-rate sensitivity and stress-rate sensitivity. The resistance to sulphate attack was presented with the help of change in compressive strength, flexural strength and flexural toughness supported by scanning electron micrographs and X-ray diffraction analysis.

7.2 Concluding Remarks

Based on the experiments carried out in this research program the following conclusions can be made:

- The compressive strength of cement-based foams scales exponentially with relative density (defined as the ratio of the cast density to that of the cement paste in the cell wall), with an exponent of around 2.5. This indicates higher sensitivity to the cast density compared to other brittle cellular solids, which scale at an exponent of 1.5.

- Adding polypropylene microfibres leads to an increase in the modulus of rupture under quasi-static as well as impact loading.

- Under quasi-static loading, the modulus of elasticity of plain and fibre-reinforced foams is proportional to the square of the relative density, as is well known for brittle cellular solids.

- The Poisson's ratio of cement-based foams is independent of relative density and was equal to 0.22 for the mixes examined in this study.

- Cement-based foams are strain-rate sensitive in flexure. However, existing rate sensitivity models for the tensile strength of concrete (CEB-FIP) are non-conservative and overestimate the strain rate sensitivity of low-density cement-based foams below a cast density of 800 kg/m^3.

- Cement-based foams are stress-rate sensitive and this sensitivity increases with a decrease in the cast density for material with cast densities below 800 kg/m^3.

- The outcome of sulphate exposure on the compressive strength of cement-based foams is not as significant as the effect on the flexural response. For heavier cast densities, the flexural strength and flexural toughness factor steadily drop with exposure time. On the other hand, the mix with the lowest cast density — 475 kg/m3 — performs better up to 30 days in the sulphate solution before succumbing to the expansive attack.

- Scanning electron micrographs and X-ray diffraction reveal that upon exposure to sulphates, the empty cells are filled with ettringite. While this results in expansive cracking in the heavier composites, it manifests as

self-healing in the lightest mix, which results in higher strength and flexural toughness factors.

- Immersion in water promotes the formation of calcite as noted from X-ray diffraction. However, this was not enough to cause any significant change to the mechanical performance.
- Polypropylene microfibres lead to better post-peak response for the lighter densities in spite of the exposure to sulphate solution.

The mechanical response generated from this study may be utilized to develop predictive models, through suitable numerical analysis for any cement-based foam system. The data from the dynamic tests presented here would be useful to develop crash cushions incorporating cement-based foams. The results gathered on the sulphate resistance establish the fact that while the lighter foams can mechanically withstand a sulphate-rich environment, additional consideration is required regarding its performance as a thermal insulator.

7.3 Recommendations

While working with cement-based foams for their mechanical behaviour and performance under severe chemical exposure, other areas of interest came into consideration for further investigation to get more in depth knowledge about this material. The following points should be noted for further research work:

- The internal cellular structure can be engineered by using a suitable type of surfactant. It is well known for polymeric or metallic cellular materials that mechanical properties differ considerably when different cellular structures such as open-cell and closed-cell are compared. Open-cell structure provides benefits of easy drainage. It has been found that the use of pervious (open-cell structure) foamed concrete is economical and more convenient than regular foamed material with closed-cell structures. Very little is known about the behaviour of open-cell cement-based foams. A comparative study can be undertaken.

- In this research program the strain-rate sensitivity of foamed material was studied under flexure where the underlying idea was to gather technical data to develop shock-absorbing material like sandwiched type semi-structural element. The common use of cementitious foams reflects the fact that they are subjected to direct compression most of the time in their service life. It is certainly worth looking into the rate sensitivity of this material when subjected to a high rate of compressive load.

- The use of cement-based foams in lightweight structural application requires further research. An important aspect to be investigated is the bond between cement-based foams and reinforcing ties.

- A detailed study on the effect of bubble size on the mechanical properties of cement-based foams is recommended in order to provide more insight about

internal cellular structures and their effect on macro-scale engineering behaviour.

- In order to be able to predict behaviour of a material, an appropriate response prediction model is required. It was shown in this study that existing empirical models, which were developed for regular cementitious material, do not work well for cement-based foams. Adaption of modified CEB formulations for strain-rate sensitivity did not reflect the experimental results. Development of models to assess the high strain-rate sensitivity of such low-strength and low-density material would serve as a useful tool.

- It is important to identify the crystalline formation inside cement-based foams. Energy dispersive X-ray spectroscopy (EDX) would be a more suitable technique (in contrast to X-ray diffraction) to get a thorough understanding of the crystalline formation due to the exposure to sulphate and water.

- One of the most popular applications of this material is in thermal insulation. The efficient use of cellular cementitious material requires a thermal model. A thermal model would help in understanding its behaviour dynamically with change in input variables. Once heat-flow characteristics are known, a more economical proportioning on a case by case basis can be employed.

- One of the outcomes of this study indicates that internal void space in cement-based foam gets filled up with ettringite crystals over the time when

exposed to a sulphate-rich environment. The consequences on the performance of this material as a thermal insulator must be researched. A detailed study regarding the change in thermal resistance due to change in the chemical environment over time should be conducted so that appropriate measures may be taken for continued use of this material effectively in insulation.

REFERENCES

ACI 213R, 2003. Guide for structural lightweight-aggregate concrete. American Concrete Institute, Farmington Hills, MI.

ACI 318, 2005. Building Code Requirements for Structural Concrete and Commentary. American Concrete Institute, Farmington Hills, MI.

ACI 523.1R, 1996. Guide for Cast-in-Place Low-Density Cellular Concrete. American Concrete Institute, Farmington Hills, MI.

ACI 523.3R, 1993. Guide for Cellular Concretes Above 50 pcf, and for Aggregate Concretes Above 50 pcf with Compressive Strengths Less Than 2500 psi. American Concrete Institute, Farmington Hills, MI.

ACI 523.3R, 2010. Guide for Cellular Concretes Above 50 pcf, and for Aggregate Concretes Above 50 pcf with Compressive Strengths Less Than 2500 psi (A draft document). American Concrete Institute, Farmington Hills, MI.

Aldrige, D., 2005. Introduction to Foamed Concrete: What, Why, How?. Proceedings: International Conference on the Use of Foamed Concrete in Construction, University of Dundee, Scotland, July 5, pp. 1–14.

Alexander, K. M., 1980. Comments on 'An Unsolved Mystery in Concrete Technology'. Concrete (UK), 14(4): 28-29.

ASTM C1012, 2004. Standard Test Method for Length Change of Hydraulic-Cement Mortars Exposed to a Sulfate Solution. ASTM International, West Conshohocken, PA.

ASTM C109, 2008. Standard Test Method for Compressive Strength of Hydraulic Cement Mortars (Using 2-in. or [50-mm] Cube Specimens). ASTM International, West Conshohocken, PA.

ASTM C1609-07, 2007. Standard Test Method for Flexural Performance of Fibre-Reinforced Concrete (using beam with third point loading). ASTM International, West Conshohocken, PA.

ASTM C39, 2009. Standard Test Method for Compressive Strength of Cylindrical Concrete Specimens. ASTM International, West Conshohocken, PA.

ASTM C42, 2004. Standard Test Method for Obtaining and Testing Drilled Cores and Sawed Beams of Concrete. ASTM International, West Conshohocken, PA.

ASTM C452, 2006. Standard Test Method for Potential Expansion of Portland-Cement Mortars Exposed to Sulfate. ASTM International, West Conshohocken, PA.

ASTM C469, 2002. Standard Test Method for Static Modulus of Elasticity and Poisson's Ratio of Concrete in Compression. ASTM International, West Conshohocken, PA.

ASTM C617, 2009. Standard Practice for Capping Cylindrical Concrete Specimens. ASTM International, West Conshohocken, PA.

ASTM C618, 2008. Standard Specification for Coal Fly Ash and Raw or Calcined Natural Pozzolan for Use in Concrete. ASTM International, West Conshohocken, PA.

ASTM STP 563, 1973. Instrumented impact testing, Philadelphia, Jun 24-29.

Babu, D.S., Wee, T-H and Tamilselvan, T., 2005. Mechanical Properties of Foamed Concrete with and without Aggregates. Proceedings (CD-ROM): ConMat '05 and Mindess Symposium, Vancouver, August 2005.

Banthia, N. and Trottier, J-F., 1995. Test Methods for flexural toughness characterization of fiber-reinforced concrete: Some concerns and a Proposition. ACI Materials Journal, 92(1): 48-57.

Banthia, N., P., Mindess, S., Bentur, A. and Pigeon, M., 1989. Impact testing of concrete using a drop-weight impact machine. Experimental Mechanics, 29(1): 63-39.

Batool, F., 2010. Thermal Conductivity in Cement-based Foams. Private Communication, PhD candidate, University of Alberta.

Beningfield, N., Gaimster, R., and Griffin P., 2005. Investigation into the Air Void Characteristics of Foamed Concrete. Proceedings of International

Conference on the Use of Foamed Concrete in Construction, University of Dundee, Scotland, July 5, pp. 51–60.

Bindiganavile, V., 2003. Dynamic Fracture Toughness of Fibre Reinforced Concrete, Ph.D Thesis, The University of British Columbia, Vancouver.

Bindiganavile, V., and Banthia, N., 2005. Impact response of the fiber-matrix bond in concrete. Canadian Journal of Civil Engineering, 32(5): 924-933.

Bindiganavile, V. and Hoseini, M., 2008. Foamed concrete. In: Mindess, S., ed., Developments in the formulation and reinforcement of concrete, CRC Press, Cambridge, England.

Bischoff, P. H. and Perry, S. H., 1991. Compressive behaviour of concrete at high strain rates. Materials and structures, 24(6): 425-450.

British Cement Association, 1994. Foamed Concrete: Compositions and Properties. Cambery, UK.

Comite Euro-International du Beton (CEB), 1993. CEB-FIP Model Code 1990, Redwood Books, Trowbridge, Wiltshire, UK.

Cotterell, B., 1962. Fracture toughness and the Charpy V-notch impact tests. British Welding Journal, 9(2): 83-90.

Cowell, W. L., 1966. Dynamic Properties of Portland Cement Concrete. Technical Report R447, Naval Civil Engineering Laboratory, Port Hueneme, Calif., 46.

Fagerlund, G., 1973. Strength and Porosity of the Concrete, Proceedings of the International Symposium RILEM/IUPAC on Pore Structure and Properties of Materials, Prague, D51-D141.

Fouad, F.H., 2006.Cellular concrete. Significance of Tests and Properties of Concrete and Concrete-making materials. ASTM STP 169D, pp. 558-566.

Gibson, L. J. and Ashby, M. F., 1999. Cellular Solids : Structure and Properties. Cambridge Univ. Press.

Gopalaratnam, V. S., Shah, S. P. and Rcji, J., 1984. A modfied instrumented Othrpy test for cement based composites. Experimental Mechanics,24(2): 102-111.

Hamidah, M.S., Azmi, I., Ruslan, M.R.A., Kartini, K., and Fadhil, N.M., 2005. Optimization of Foamed Concrete Mix of Different Sand-Cement Ratio and Curing Conditions. Proceedings of International Conference on the Use of Foamed Concrete in Construction, University of Dundee, Scotland, July 5, pp. 37–44.

Hoff, G.C., 1972. Porosity-Strength Considerations for Cellular Concrete. Cement and Concrete Research, 2(1): 91–100.

Jones, M.R. and McCarthy, A., 2004. Utilising unprocessed low-lime coal fly ash in foamed concrete. Fuel, 84(11): 1398-1409.

Jones, M.R. and McCarthy, A., 2005. Behavior and Assessment of Foamed Concrete for Construction Application. Proceedings of International Conference on the Use of Foamed Concrete in Construction, University of Dundee, Scotland, July 5, pp. 61–88.

Jones, M.R. and McCarthy, A., 2005. Preliminary Views on the Potential of Foamed Concrete as a Structural Material. Magazine of Concrete Research, 57(1): 21–31.

Jones, M.R. and McCarthy, A., 2006. Heat of Hydration in Foamed Concrete: Effect of Mix Constituents and Plastic Density. Cement and Concrete Research, 36(6): 1032–1041.

Jones, P.G., and Richart, F.E., 1936. The Effect of Testing Speed on. Strength and Elastic Properties of Concrete, ASTM Proc., 36(2): 380-391

JSCE G-552, 1999. Test Method for Bending Strength and Bending Toughness of Steel Fiber Reinforced Concrete, Standard specification for concrete structures, test methods and specifications, Japanese Society of Civil Engineers.

Kearsley, E. P. and Mostert, H. F. 2003. The Effect of Fibre Reinforcing on Foamed Concrete Behaviour. Role of concrete in sustainable development, Thomas Telford, London, pp. 557-566.

Kearsley, E.P. and Mostert, H.F., 2005. Designing Mix Composition of Foamed Concrete with Fly Ash Contents. Proceedings of International Conference on the Use of Foamed Concrete in Construction, University of Dundee, Scotland, July 5, pp. 29–36.

Kearsley, E.P. and Mostert, H.F., 2005. Opportunities for Expanding the Use of Foamed Concrete in the Construction Industry. Proceedings of International Conference on the Use of Foamed Concrete in Construction, University of Dundee, Scotland, July 5, pp. 143–154.

Kearsley, E.P. and Wainwright, P.J., 2001. The Effect of High Fly Ash Content on the Compressive Strength of Foamed Concrete. Cement and Concrete Research, 31(1): 105–112.

Kearsley, E.P. and Wainwright, P.J., 2002. Ash Content for Optimum Strength of Foamed Concrete. Cement and Concrete Research, 32(2): 241–246.

Kearsley, E.P. and Wainwright, P.J., 2002. The Effect of Porosity on the Strength of Foamed Concrete. Cement and Concrete Research, 32(2): 233–239.

Kearsley, E.P., 1999. Just Foamed Concrete: An Overview. Proceedings of International Conference on Specialist Techniques and Materials for Concrete Construction, University of Dundee, Scotland, September 8–10, pp. 227–237.

Kolsky, H., 1949. An investigation of the mechanical properties of materials at very high strain rates of loading. Proc. Phys. Soc. B, 62: 676-699.

Krivenko, P.V., Kovalchuk, G.Y., and Kovalchuk, O.Y., 2005. Heat Resistant Cellular Concrete Based on Alkaline Cements. Proceedings of International Conference on the Use of Foamed Concrete in Construction, University of Dundee, Scotland, July 5, pp. 97–104.

Lacey, R.M, 1965. Response of Several Materials at Intermediate Strain Rates. Fifth International Symposium on High Speed Testing, Boston, Massachusetts.

Lee, H. K., Lee, K. M. and Kim, B. G., 2003. Autogenous Shrinkage of High-Performance Concrete Containing Fly Ash. Magazine of Concrete Research, 55(6): 507-515.

Lee, Y.L. and Hung, Y.T., 2005. Exploitation of Solid Wastes in Foamed Concrete: Challenges Ahead. Proceedings of International Conference on the Use of Foamed Concrete in Construction, University of Dundee, Scotland, July 5, pp. 15–22.

Legatski, L. A., 1994. Cellular concrete. Significance of Tests and Properties of Concrete and Concrete-making materials. ASTM STP 169C, pp. 530-536.

Li, G. and Muthyala, V.D., 2008. A Cement Based Syntactic Foam, Materials Science & Engineering: A, 478(1-2): 77-86.

Malvar, L. J. and Ross, C. A., 1998. Review of strain rate effects for concrete in tension. ACI Materials Journal, 95(6): 735-773.

Mehta, P. K. and Monteiro, P. J. M., 1993. Concrete : Structure, Properties, and Materials.2nd edition, Prentice Hall.

Mirza, W.H. and Al-Noury, S.I., 1986. Utilisation of Saudi sands for aerated concrete production. International Journal of Cement Composites and Lightweight Concrete. 8(2): 81-85.

Nadeau, J. S., Bennett, R. and Fuller, E. R. (Jr), 1982. An explanation for the rate-of- loading and the duration-of-load effects in wood in terms of fracture mechanics. Journal of Materials Science, 17(10): 283 1-2840.

Nambiar, E. K. and Ramamurthy, K., 2008. Fresh State Characteristics of Foam Concrete, Journal of Materials in Civil Engineering, 20(2): 11-117.

Nambiar, E.K.K. and Ramamurthy, K., 2006. Influence of Filler Type on the Properties of Foam Concrete. Cement & Concrete Composites, 28(5): 475–480.

Nambiar, E.K.K. and Ramamurthy, K., 2007. Air-Void Characterization of Foam Concrete. Cement and Concrete Research, 37(2): 221–230.

Nehdi, M., Djebbar, Y., and Khan, A., 2001. Neural Network Model for Preformed-Foam Cellular Concrete. ACI Materials Journal, 98(5): 402–409.

Nehdi, M., Khan, A., and Lo, K.Y., 2003. Development of Deformable Protective System for Underground Infrastructure using Cellular Grouts. ACI Materials Journal, 99(5): 490–498.

Odler, I. and Abdul-Maula, S., 1987. Investigations on the Relationship between Porosity Structure and Strength of Hydrated Portland Cement Pastes. III. Effect of Clinker Composition and Gypsum Addition, Cement and Concrete Research, 1987, 17(1): 22-30.

Ouellet, S., D. Cronin, and M. Worswick. 2006. Compressive response of polymeric foams under quasi-static, medium and high strain rate conditions. Polymer Testing, 25 (6): 731-743.

Papayianni, I. and Milud, I.A., 2005. Production of Foamed Concrete with High Calcium Fly Ash. Proceedings of International Conference on the Use of Foamed Concrete in Construction, University of Dundee, Scotland, July 5, pp. 23–28.

Rachel C. and Bindiganavile V., 2010. Toughness of fibre reinforced hydraulic lime mortar, Part 2: Dynamic response, Materials and Structures (RILEM). Available Online 14th April 2010 at DOI: 10.1617/s11527-010-9599-3.

Raphael JM, 1984. The tensile strength of concrete. ACI Journal, 81(2): 158–165

Reinhardt, H. W., 1982. Concrete under Impact Loading: Tensile Strength and Bond. HERON, 27(3).

Rinde, J. A. and Hoge, K. G., 1971. Time and Temperature Dependence of the Mechanical Properties of Polystyrene Bead Foam, Journal of Applied Polymer Science, 15: 1377-1395.

Rossi, P., 1991. A Physical Phenomenon which can Explain the Mechanical Behaviour of Concrete under High Strain Rates, Materials & Structures (RILEM), 24(6): 422-424.

Steiger, R. W. and Hurd, M. K., 1978. Lightweight Insulating Concrete for Floors and Roof Decks. Publication #C780411, The Aberdeen Group.

TEMA, 2009. Excerpts from Image Systems [Website] [Cited July 2010], Available from url: <http://www.imagesystems.se/ImageSystems/TEMAAutomotiveProduct.html>

Tikalsky, P.J., Pospisil, J., and MacDonald, W., 2004. A Method for Assessment of the Freeze–Thaw Resistance of Preformed Foam Cellular Concrete. Cement and Concrete Research, 34(5): 889–893.

Tyler, C. J. and Ashby, M. F., 1986. Project Report. Cambridge University Engineering Department.

Valore, R. C., Jr., 1954. Cellular Concretes. ACI Journal, Proceedings, 50(9): 773–796.

Wee, T-H, Babu, D.S., Tamilselvan, T., and Lim, H-S, 2006. Air-Void System of Foamed Concrete and its Effect on Mechanical Properties. ACI Material Journal, 103(1): 45–52.

Wild, S., J. M. Khatib, and M. O'Farrell, 1997. Sulphate Resistance of Mortar, Containing Ground Brick Clay Calcined at Different Temperatures. Cement and Concrete research. 27 (5): 697-710.

Wimpenny, D.E., 1996. Some aspects of the design and production of foamed concrete, Appropriate Concrete Technology. Proceedings from the international conference 'Concrete in the service of mankind', London, pp. 245-254.

Zollo, R.F. and Hays, C.D., 1998. Engineering Material Properties of a Fiber Reinforced Cellular Concrete. ACI Material Journal, 95(5): 631–635.

APPENDIX

A1. Calibration chart for LLOYD test frame (screw-type machine)

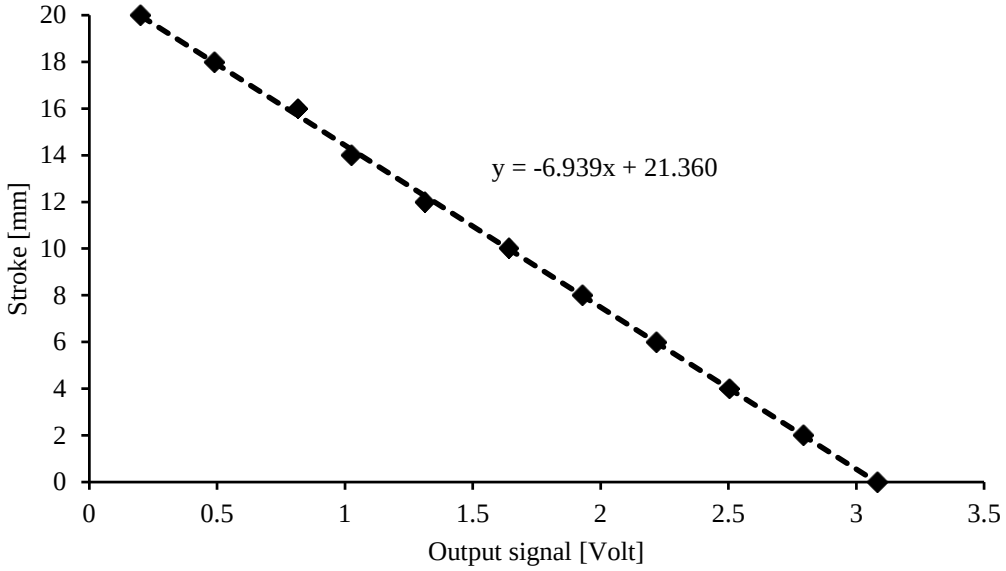

Figure A1.1: Stroke calibration chart for LLOYD test frame

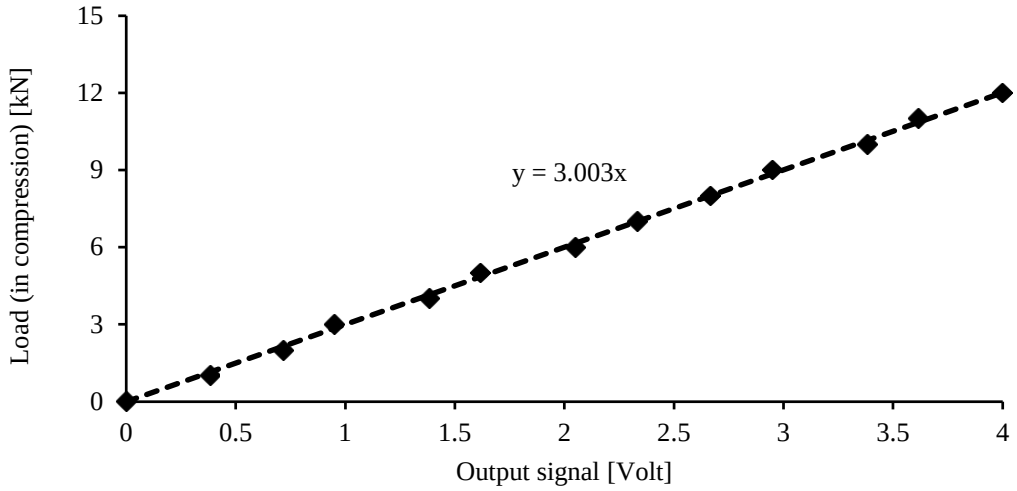

Figure A1.2: Load calibration chart for LLOYD test frame

A2. Calibration chart for MTS 2600 (servo-hydraulic machine)

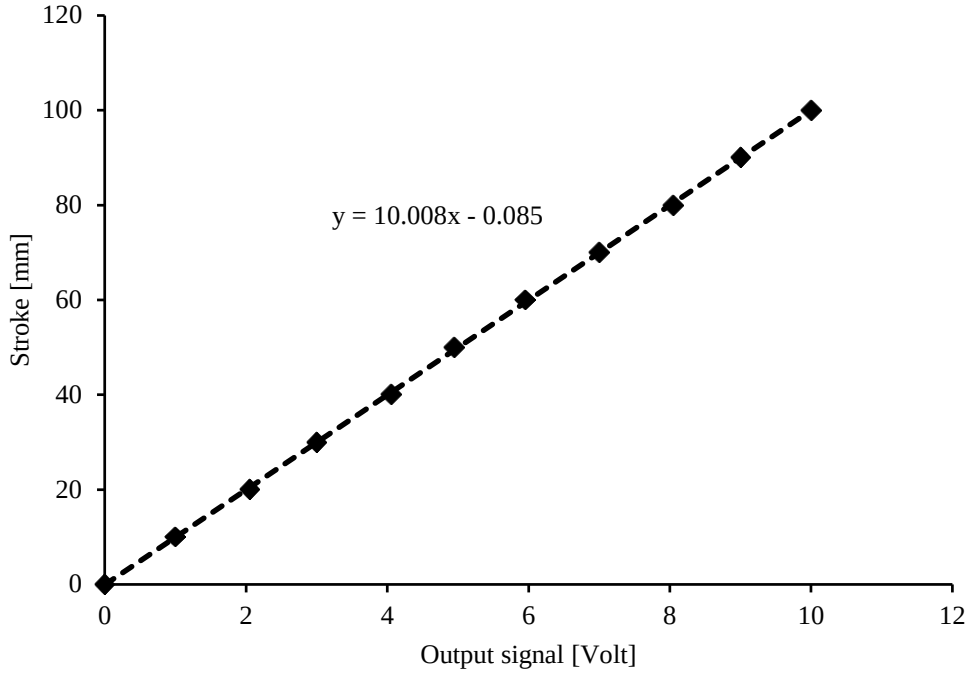

Figure A2.1: Stroke calibration chart for MTS 2600

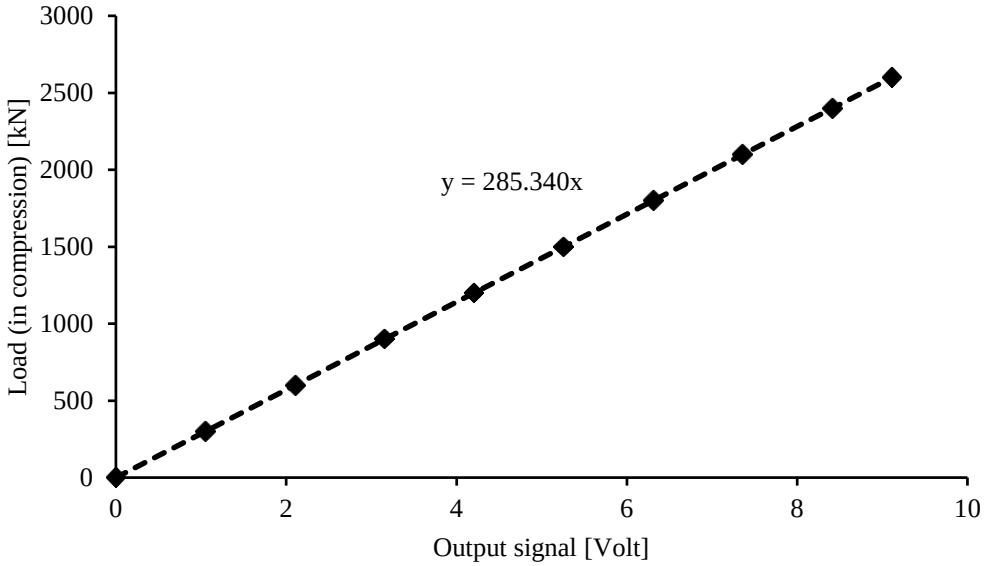

Figure A2.2: Load calibration chart for MTS 2600

A3. Calibration chart for impact system (drop-weight machine)

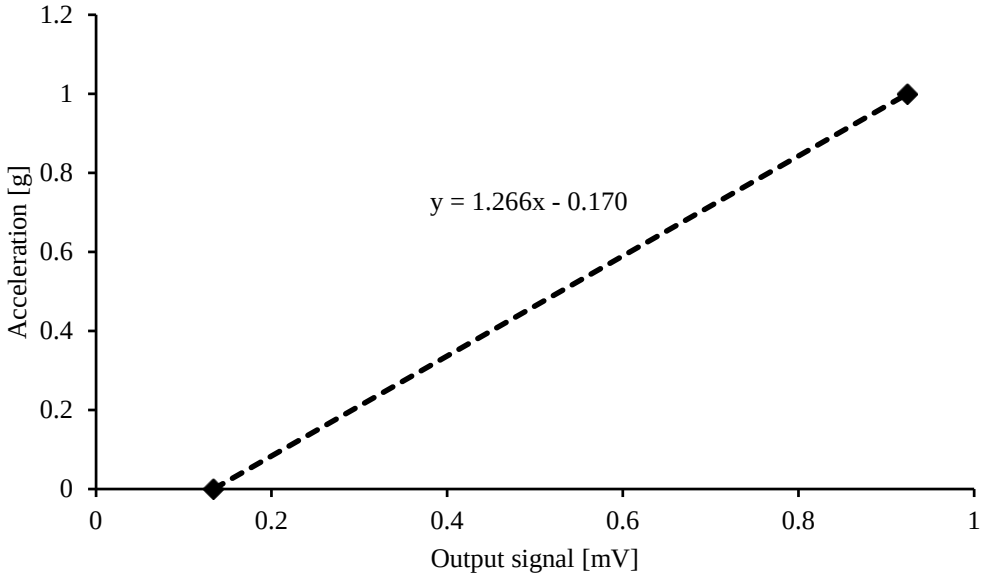

Figure A3.1: Acceleration calibration chart for accelerometer

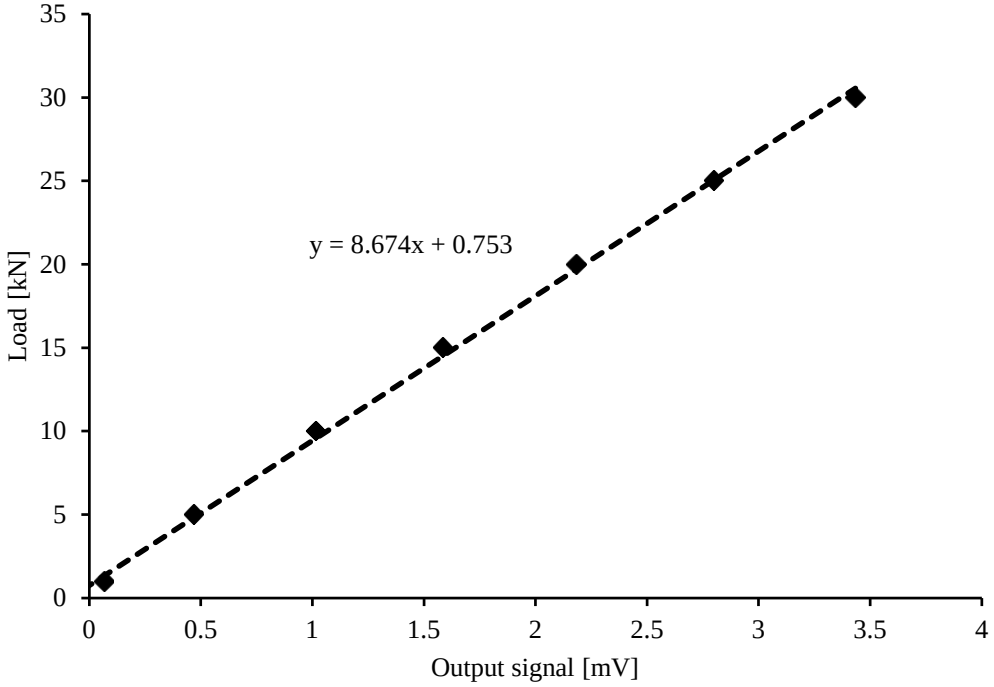

Figure A3.2: Load calibration chart for Blade cell (bridge type)